SEISMOTECTONICS AND VELOCITY STRUCTURE

OF THE SOUTHEASTERN HAWAIIAN RIDGE

A DISSERTATION SUBMITTED TO THE GRADUATE DIVISION OF THE
UNIVERSITY OF HAWAII IN PARTIAL FULFILLMENT
OF THE REQUIREMENTS FOR THE DEGREE OF

DOCTOR OF PHILOSOPHY

IN GEOLOGY AND GEOPHYSICS

MAY 1979

By

Robert E. Estill

Dissertation Committee:

Frederick K. Duennebier, Chairman
James E. Andrews
Eduard Berg
Murli H. Manghnani
Michael P. Ryan

How are earthquake depths determined?

What are some experiments that might shed light on the origin of the Hawaiian Ridge?

ACKNOWLEDGMENTS

The OBS data discussed in this paper was collected by the crew and scientific staff of the R/V Kana Keoki, Hawaii Institute of Geophysics. Clyde Nishimura and Bill Kempner reduced most of the OBS analog data. Special thanks to Bob Koyanagi, Fred Klein and Elliot Endo of the U.S.G.S. who provided valuable historical HVO seismicity records and focal mechanisms.

I would like to express sincere appreciation to my committee especially Fred Duennebier and Mark Odegard for their guidance and forbearance. Elsie and Larry Wipperman, Pat and Gerard Fryer, Pat and Chris Cooper, Karen Mansfield and Rich Halada provided refreshing honesty and humor during my tenure at HIG. Madame Pele (Volcano Goddess), Akua Pa'ani (Pipeline Surfing God), Bob Samarzea (Lightning Bolt Pies), Tor Kamaka and Dr. Orgasto made my experience in Hawaii no ka oi.

This work was sponsored by the National Science Foundation under grants No. EAR 77-20255, OCE 76-82056, OCE 76-82156 and by the Office of Ocean Science and Technology of the Office of Naval Research.

ABSTRACT

Five separate offshore earthquake surveys have been conducted by the Hawaii Institute of Geophysics deploying forty-three ocean bottom seismographs (OBS) along the southeastern Hawaiian Ridge during 1976-1977. Regional seismicity has been determined from 11,173 events with $M_L \geq 2.0$ using both OBS and historical Hawaii Volcano Observatory (HVO) epicenters. Seismicity results indicate: (1) a south-southwestward trend of events offshore the island of Hawaii with the major concentration near Loihi seamount; (2) a spectacular concentration of events 25 to 40 km below Kilauea trending southward at depth; (3) a region of high activity appearing to connect the summit of Mauna Loa to the region below Kilauea; (4) a large number of events at 10 km depth beneath the island of Hawaii indicating a zone of tension due to both island loading and magmatic intrusion from below 10 km depth; (5) shallow sparse activity along the Kilauea east rift terminating offshore and deeper events between 30 and 60 km beneath the Kilauea southwest rift zone; (6) scattered offshore seismicity near Oahu, Maui and Molokai islands due to probable submarine slumping; (7) the b-value determined for the Hawaiian Ridge is $0.93 \pm .10$; (8) focal mechanisms from this study show general south to southeastern and vertical compression along the Kilauea south flank as evidenced by high angle normal and low angle reverse faulting; (9) focal mechanisms determined using both the OBS and land arrays indicate near vertical pressure axes and horizontal tension axes for

offshore upper mantle events, especially near Loihi seamount; (10) the data presented in this paper indicate southeastern evolution of the Hawaiian Ridge with active formation of seamounts through oceanic crust.

The Tau Inversion method has been used to invert earthquake travel times from the Hawaiian Ridge to determine velocity structure with limits. The inversion gives a velocity model showing a rapid increase in velocity from 5.9 km/sec to 7.2 km/sec between 4-km and 7.5-km depth, a monotonic increase to 7.5 km/sec near 11 km, and Moho velocity of 8.0 km/sec at 15-km depth. Three prominent travel time delays, indicating heterogeneous velocity structure, are shown to correspond to the major volcanoes on Hawaii: Kilauea, Mauna Loa and Mauna Kea. Also from the Moho depth determined by Tau Inversion we infer that previous estimates of crustal flexure for the Hawaiian Ridge, based on deeper Moho depths (> 15 km), are too large. The Tau method is shown to be useful in delineating heterogeneous velocity structure and determining limits on velocity depth models from local earthquake travel time data.

TABLE OF CONTENTS

TABLE OF CONTENTS (Continued)

LIST OF TABLES

LIST OF ILLUSTRATIONS

LIST OF ILLUSTRATIONS (Continued)

LIST OF ILLUSTRATIONS (Continued)

LIST OF ILLUSTRATIONS (Continued)

LIST OF ILLUSTRATIONS (Continued)

LIST OF ILLUSTRATIONS (Continued)

1. SEISMICITY AND TECTONICS OF THE HAWAIIAN RIDGE

1.1 Introduction

In this dissertation, two major problems are undertaken: (1) the seismicity and contemporary tectonics of the Hawaiian Ridge; (2) the velocity structure of the southeastern Hawaiian Ridge. This dissertation seeks to combine seismicity and tectonic data in order to infer active processes for the formation of the Hawaiian Ridge.

The dissertation is basically divided into three parts. Chapter 1 contains the analysis of Hawaiian Ridge seismicity data. Chapter 2 describes the results of applying the Tau Inversion algorithms to Hawaiian Ridge travel time data. Chapter 3 was not written as a filler for the dissertation but at the request of others, hopefully to serve as a package of earthquake programs for OBS data reduction at HIG.

The southeastern Hawaiian Ridge (Fig. 1.1) consists primarily of eight major volcanic islands in the central Pacific built on Cretaceous sea floor. The major Hawaiian islands are composed almost entirely of tholeiitic basalt and range in age from early quaternary at the northwest (Kauai) to recent at Kilauea Volcano on the island of Hawaii. In order to determine constraints for the origin and evolution of the Hawaiian Ridge, a joint effort by the Hawaii Institute of Geophysics (HIG) and the Hawaiian Volcano Observatory (HVO) has been undertaken using seismicity and tectonic data. Five separate offshore earthquake surveys were conducted by the Hawaii

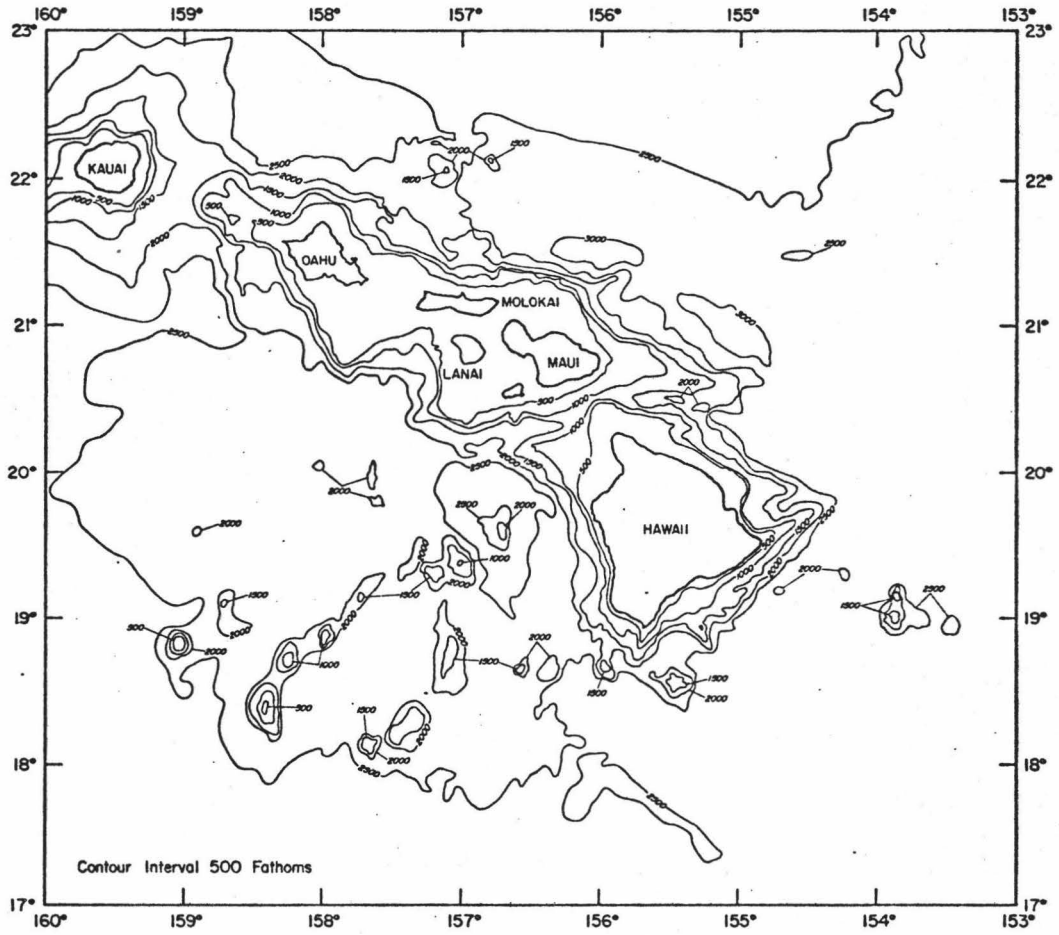

Figure 1.1 Map of the southeastern Hawaiian Ridge showing major islands and seamounts. Data taken from HIG, U. S. Naval Oceanographic Office and U. S. Coast and Geodetic Survey contoured on mercator projection.

Institute of Geophysics deploying POP-UP ocean bottom seismographs (OBS) from the R/V Kana Keoki along the southeastern Hawaiian Ridge during 1976-77 as shown in Figure 1.2 and Table 1.1. The OBS seismic data have been combined with recent and historical HVO data from U.S.G.S. seismographs (Table 1.2) to determine regional seismicity and source mechanisms for the Hawaiian Ridge in order to constrain present geotectonic models for the formation of the Hawaiian Ridge.

In 1963, J. Tuzo Wilson (1963) proposed that the Hawaiian islands were formed as the Pacific Plate moved northwestward over a fixed "hot spot". Morgan (1972a) proposed mantle convection plumes flowing upward in narrow bands from a core-mantle heat source to explain hot spots. Morgan (1972b) postulated values for the diameter and plume flow velocity of 150 km and 2 m/yr, respectively, yet the cause of mantle convection and plume formation remains uncertain.

Anderson (1975) has proposed chemical plumes in which concentrations of uranium and thorium in an originally chemical heterogeneous mantle provides the heat necessary to start plume formation from convection in the lower mantle. Convection bumps at the lower lithosphere boundary would cause fracturing and magmatism. Parmentier et al. (1975) has shown by experiments on steady state thermal convection in a cylindrical geometry that only base heated flows exhibit plume-like flow patterns and that plumes are considered to be a mode of upper mantle convection in which a magma reservoir inflates until a sufficient hydrostatic head is reached giving rise to lithospheric fracture and volcanism. Ringwood (1975), in basic agree-

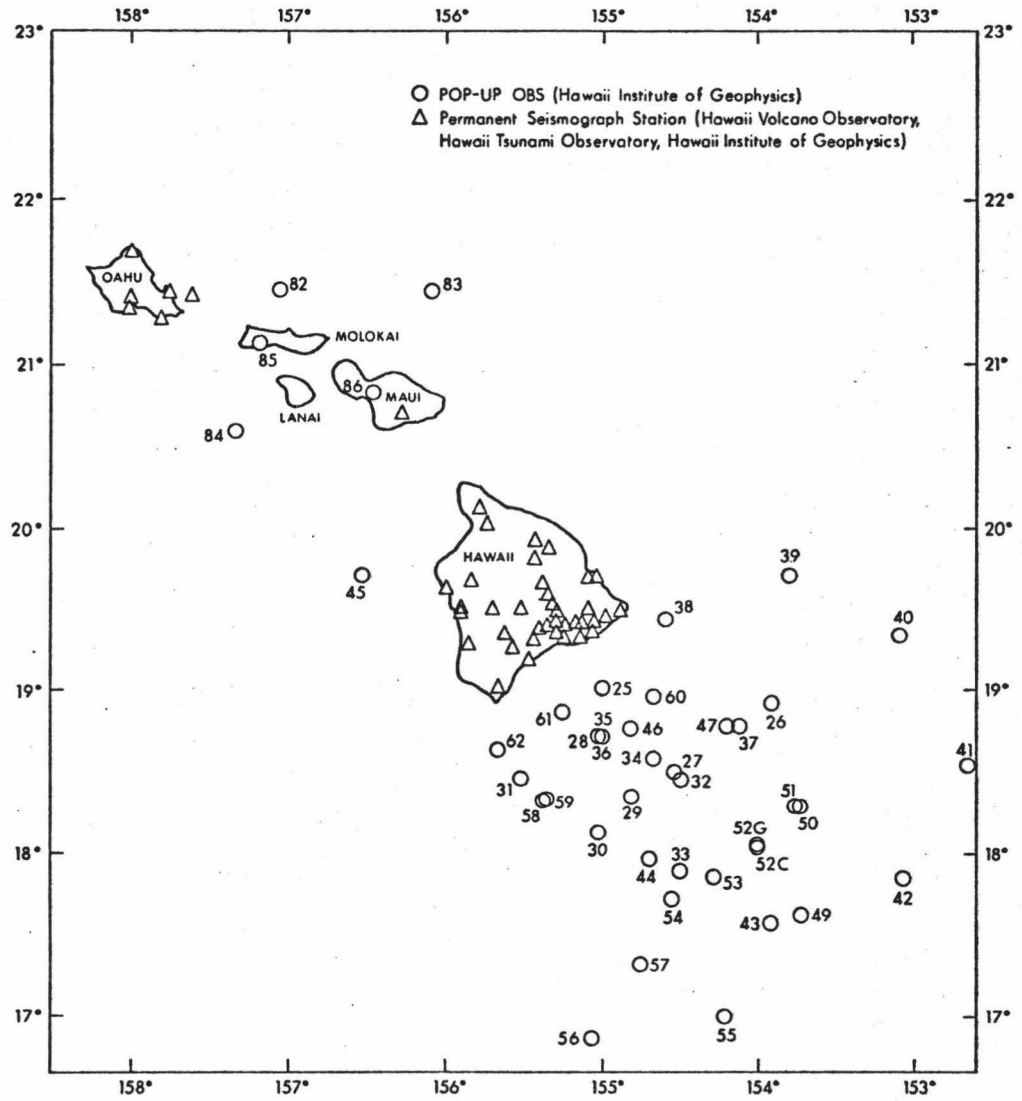

Figure 1.2 Map of OBS's (circles) and permanent land station (triangles) seismographs along Hawaiian Ridge. OBS's were deployed for up to three week intervals during five separate cruises from 10 October 1976 to November 1977.

TABLE 1.1

HAWAIIAN RIDGE POP-UP OBS DEPLOYMENTS

Cruise	OBS	Location		Depth (meters)
KK 76-10-10	RAT ISLAND (25)	19°00.98'N	155°02.06'W	3430
	TOKYO (26)	18°54.97'N	154°55.97'W	5013
	KRAKATOA (27)	18°32.01'N	154°34.98'W	5260
KK 77-02-20	TOKYO-23 (28)	18°43.40'N	155°03.80'W	5175
	DEHRA-4 (29)	18°19.50'N	154°54.40'W	5180
	BIHAR-2 (30)	18°07.00'N	155°02.00'W	5160
	AWATERE-1 (31)	18°28.00'N	155°30.00'W	4630
	KRAKATOA-65 (32)	18°25.90'N	154°30.00'W	5230
	CUTCH-3 (33)	17°52.80'N	154°30.60'W	5010
KK 77-03-17 (Leg 6)	AWATERE (34)	18°35.96'N	155°40.10'W	3964
	BIHAR (35)	18°43.01'N	154°59.81'W	5200
	CUTCH (36)	18°43.01'N	154°59.79'W	5200
	DEHRA DUN (37)	18°45.99'N	154°08.98'W	5275
	ERZINCAN (38)	19°25.66'N	154°36.75'W	3650
	FUKUI (39)	19°42.01'N	153°48.99'W	5333
	GIFU (40)	19°19.52'N	153°05.88'W	5015
	HAWKS BAY (41)	18°35.01'N	152°41.01'W	5037
	IZU (42)	17°50.83'N	153°06.99'W	4983
	JAN MAYAN (43)	17°33.12'N	153°55.00'W	5080
	LOCRIS (44)	17°56.00'N	154°42.98'W	5019
KK 77-08-15	*KERN (45)	19°44.46'N	156°30.31'W	4788
	AWATERE (46)	18°44.00'N	154°48.00'W	5290
	BIHAR (47)	18°46.27'N	154°10.80'W	5283
	(48)	STATION ABANDONED		
	*DEHRA DUN (40)	17°37.86'N	153°43.28'W	5020
	*ERZINCAN (50)	18°16.00'N	153°44.92'W	5016
	FUKUI (51)	18°16.05'N	153°44.91'W	5016
	CUTCH (52-C)	18°02.45'N	154°01.71'W	5055
	GIFU (52-G)	18°03.87'N	154°01.04'W	5055
	*HAWKS BAY (53)	17°52.87'N	154°18.20'W	5025
	ISU (54)	17°42.97'N	154°34.04'W	4987
	JAN MAYEN (55)	16°57.96'N	154°12.98'W	5077
	GIFU (56)	16°49.99'N	155°04.12'W	5070
	ERZINCAN (57)	17°17.99'N	154°45.98'W	4875
	LOCRIS (58)	18°20.06'N	155°21.96'W	4545
	CUTCH (59)	18°20.05'N	155°21.95'W	4538
	MANNIX (60)	18°57.94'N	154°41.08'W	5351
	NANKAIDO (61)	18°52.11'N	155°14.40'W	2390
	CUTCH (62)	18°38.15'N	155°39.71'W	4130

TABLE 1.1 (Continued)
HAWAIIAN RIDGE POP-UP OBS DEPLOYMENTS

Cruise	OBS	Location		Depth (meters)
KK 77-10-06	CUTCH (82)	21°29.50'N	157°05.50'W	3850
	*RIMA (83)	21°28.00'N	156°00.00'W	5725
	IZU (84)	20°40.50'N	157°21.30'W	3000
	**AWATERE (85)	21°08.10'N	157°10.75'W	402
	**MAUI (86)	20°52.90'N	156°31.10'W	279

*Lost of no data

**Land Stations

TABLE 1.2

PERMANENT SEISMOGRAPH STATIONS IN THE STATE OF HAWAII

Hawaii Volcano Observatory (HVO)

Station Code	Latitude	Longitude	Elevation (meters)
AHU	19°22.40'N	155°15.90'W	1070
AIN	19°22.50'N	155°27.62'W	1524
CAC	19°29.29'N	155°55.09'W	323
CPK	19°23.70'N	155°19.70'W	1038
DAN	19°21.42'N	155°40.04'W	3003
DES	19°20.20'N	155°23.30'W	815
ESR	19°24.68'N	155°14.33'W	1177
HAE	20°46.00'N	156°15.00'W	2090
HAL	20°46.00'N	156°15.00'W	2090
HAN	20°46.00'N	156°15.00'W	2090
HIE	19°43.20'N	155°05.30'W	20
HIL	19°43.20'N	155°05.30'W	20
HIN	19°43.20'N	155°05.30'W	20
HLP	19°17.96'N	155°18.63'W	707
HPU	19°46.85'N	155°27.50'W	3396
HSS	19°36.31'N	155°29.13'W	2445
HUA	19°41.25'N	155°50.32'W	2189
HUL	19°25.13'N	154°58.72'W	369
KAA	19°15.98'N	155°52.28'W	524
KAE	19°17.35'N	155°07.95'W	37
KHU	19°14.90'N	155°37.10'W	1939
KII	19°30.56'N	155°45.90'W	1841
KIP	21°25.40'N	158°00.90'W	76
KOH	20°07.69'N	155°46.77'W	1166
KKU	19°53.39'N	155°20.58'W	1863
KPN	19°20.10'N	155°17.40'W	924
KPR	19°16.40'N	155°26.70'W	610
LUA	19°24.55'N	155°04.25'W	622
MLO	19°29.80'N	155°23.30'W	2010
MLX	19°27.60'N	155°20.70'W	1475
MOK	19°29.28'N	155°34.98'W	4000
MPR	19°22.10'N	155°09.80'W	881
MTV	19°30.25'N	155°03.75'W	409
NAG	19°42.12'N	155°01.72'W	18
NPT	19°24.90'N	155°17.00'W	1115
OTL	19°23.40'N	155°16.80'W	1084
PAU	19°22.62'N	155°13.10'W	994
PHO	19°28.90'N	154°53.40'W	215
PLA	19°23.00'N	155°27.67'W	2992
POL	19°17.02'N	155°13.47'W	169
PPL	19°09.50'N	155°27.87'W	35

TABLE 1.2 (Continued) PERMANENT SEISMOGRAPH STATIONS IN THE STATE OF HAWAII

Station Code	Latitude	Longitude	Elevation (meters)
Hawaii Volcano Observatory (HVO)			
RIM	19°23.90'N	155°16.60'W	1128
SCA	19°28.20'N	155°35.08'W	4048
SPT	18°58.91'N	155°39.92'W	244
SWR	19°27.26'N	155°36.30'W	4048
TAN	19°27.70'N	154°58.51'W	351
USE	19°25.40'N	155°17.60'W	1240
USZ	19°25.40'N	155°17.60'W	1240
UWE	19°25.60'N	155°17.60'W	1240
WHA	19°19.90'N	155°02.92'W	29
WIL	19°28.15'N	155°35.02'W	4037
WLG	19°25.49'N	155°15.69'W	1067
Honolulu Tsunami Observatory (HTO)			
HKL	20°42.70'N	156°15.30'W	3050
HON	21°19.30'N	158°00.50'W	2
KHUE	19°14.90'N	155°37.10'W	1940
KIPE	21°25.40'N	158°00.90'W	70
KKH	19°39.85'N	156°00.53'W	5
MKH	19°49.60'N	155°28.35'W	4200
MOKE	21°27.39'N	157°44.19'W	90
OPA	21°41.43'N	158°00.72'W	150
PAH	19°29.70'N	154°56.80'W	205
Hawaii Institute of Geophysics (HIG)			
DHV	21°15.90'N	157°48.20'W	76
MOBH	21°23.53'N	157°37.10'W	-600
MOBV	21°23.53'N	157°37.10'W	-600

ment with Parmentier et al. (1975) believes that the source region for hot spot formation is from 150 to 200 km and long term, stable, hot spot evolution from the lower mantle is unlikely. A sub-lithospheric Rayleigh-Benard convection mechanism has been postulated for hot spot formation by Richter (1973), Richter and Parsons (1975) and McKenzie and Weiss (1975). These authors believe that convection cells become extended and aligned parallel to the motion of the overlying lithosphere producing lines of weakness in the lower lithosphere which controls the formation of linear volcanic chains.

Another major hypothesis for the formation of the Hawaiian chain is the idea of a propagating fracture mechanism. Propagating fracture systems have been proposed by Menard (1964), Walcott (1976), Turcotte and Oxburgh (1973) and McDougall (1971). Menard (1964) attributes the formation of the Hawaiian chain primarily to the development of new volcanoes where the load-produced arch intersects a major fault, in basic agreement with the island load fracturing system of Walcott (1976) and McDougall (1971) who proposed that the Hawaiian islands are the result of a propagating tensional fracture that is due to a greater than normal concentration of heat producing elements beneath the lithosphere. Further, Turcotte and Oxburgh (1973) show that the lithosphere could be subjected to tensional stress due to the movement of the lithosphere over the nonspherical earth, and Menard (1973) has proposed asthenospheric bumps for lithospheric fracture. Also, Jackson and Shaw (1975) suggest that the Hawaiian chain was formed as a series of en echelon volcanoes in response to changes in the

northwest-southeast stress field of the Pacific lithosphere parallel to the maximum principal stress over the last 70-100 m.y. An alternative hypothesis to the propagating fracture and hot spot models in the thermal feedback (gravitational anchor) model proposed by Shaw and Jackson (1973). The thermal feedback model is based on the idea that a viscous medium is heated under the shear stress generated at the lithosphere-asthenosphere boundary. This shearing stress causes a temperature increase and viscosity decrease until a surface eruption occurs after which temperature decreases, viscosity increases and a new thermal feedback cycle begins.

Whichever model is adapted to explain the origin of the Hawaiian Chain the petrology of the islands must also fit the tectonic model. To this end, the results of Moore's (1969), Figure 1.3, offshore Hawaii dredging and underwater photography have important implications for Hawaiian tectonic evolution. Fresh pillow basalts and slightly altered pillows occur along the offshore extension of the volcanic rift zones of the island of Hawaii. Similar fresh and altered basalts are observed at Bushnell seamount to the southeast. Although Loihi seamount shows weathered basalt in Moore's (1969) paper, recent dredging results indicate fresh, glassy pillow basalt at Loihi. If Loihi, Bushnell, and other seamounts in the area are active volcanoes, then they are most likely extensions of the Hawaiian Ridge. Further, analysis of recent seamount swarm seismicity may correlate with submarine eruptions.

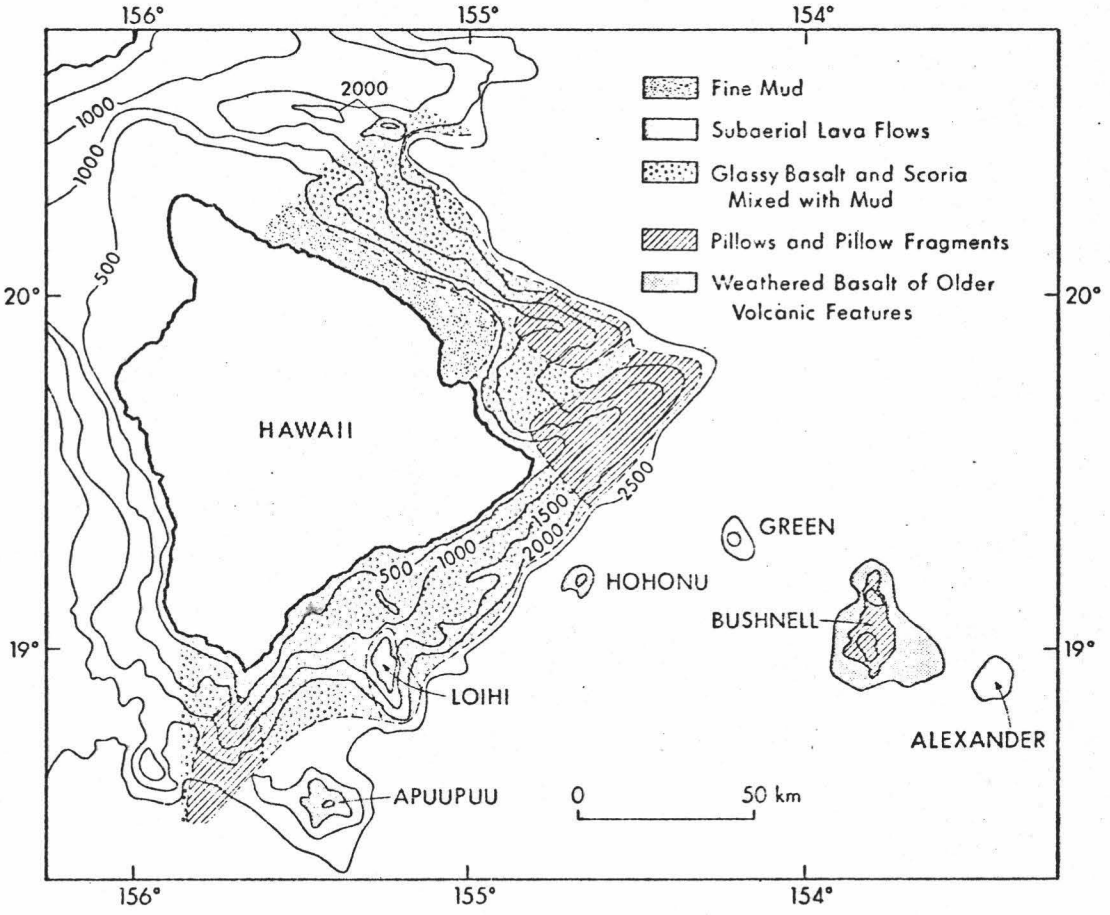

Figure 1.3 Offshore dredging and underwater photography results near Hawaii. Redrawn from Moore (1969). Contour intervals given in meters. Names correspond to offshore seamounts.

1.2 Data and Instrumentation

Five separate research cruises aboard the R/V Kana Keoki were undertaken in which a total of forty-three deployments of Hawaii Institute of Geophysics OBS's were made for up to three weeks intervals along the Hawaiian Ridge (Fig. 1.2 and Table 1.1). The HIG POBS has been described in detail by Sutton et al., 1977. OBS data are recorded on 4-track AM cassette magnetic tapes. Filtering and automatic time code decoding made playback and arrival time picking routine. The primary purpose of these OBS deployments was an earthquake reconnaissance survey of offshore Hawaiian Ridge areas especially south of the island of Hawaii near the presumed location of the Hawaiian hot spot. The telemetered HVO seismometer network operated by the U. S. Geological Survey on the island of Hawaii was also utilized in this study and historical seismicity data from the Hawaiian Volcano Observatory, Coast and Geodetic Survey and Hawaii Institute of Geophysics were obtained up to August, 1977.

Eleven thousand one hundred and seventy (11,173) events with $M_L \geq 2.0$, were compiled from the above sources, spanning historical times through 1977. Data quality has varied due to array changes and improvements but the majority of epicenters, hypocenters and magnitudes are taken from 1962 and later when HVO expanded its seismograph array. Nonetheless, large but poorly located historical events have been included in the epicenter maps in this paper. Earthquake locations became much more reliable in the late 60's and 70's as a result of the application of iterative least squares methods for

epicenter determinations as described by Lee and Lahr, 1972. Three hundred and eighty-four (384) events recorded on both OBS's and land stations were located using HYPO71 (Lee and Lahr, 1972) with RMS residuals less than 0.5 seconds. The Tau velocity model for the Hawaiian Ridge, Figure 2.5, as determined by Estill and Odegard (1978) was used for epicenter determinations.

The HIG OBS data, combined with historical events along the Hawaiian Ridge, have been used to study the contemporary tectonics of the Hawaiian Ridge. The vast majority of the data set was recorded and processed by HVO (USGS). Large historical events, whose magnitudes and epicenters were poorly determined (RMS ≥ 0.5 sec) and events ($M_L \geq 2.0$) from 1952 to present have been included. A discussion of Hawaiian Ridge seismicity and tectonics follows and is divided into three major geographic regions: (1) offshore southeastern Hawaii; (2) island of Hawaii; (3) offshore Oahu, Molokai, Maui and western offshore Hawaii. Reference maps of the Hawaiian Ridge and the island of Hawaii are shown in Figures 1.1, 1.3 and 1.4.

1.3 Offshore Southeastern Hawaii

Epicenter maps for different source depths, Figure 1.5 through Figure 1.8, display the offshore seismicity off the southeastern coast of Hawaii near the presumed location of the Hawaiian hot spot. A striking feature is the concentration of seismicity southward of Kilauea near Loihi seamount, Figure 1.3, especially at shallow depths. Historical records and the OBS surveys indicate sporadic small magnitude earthquakes south of Hawaii with major historical swarm

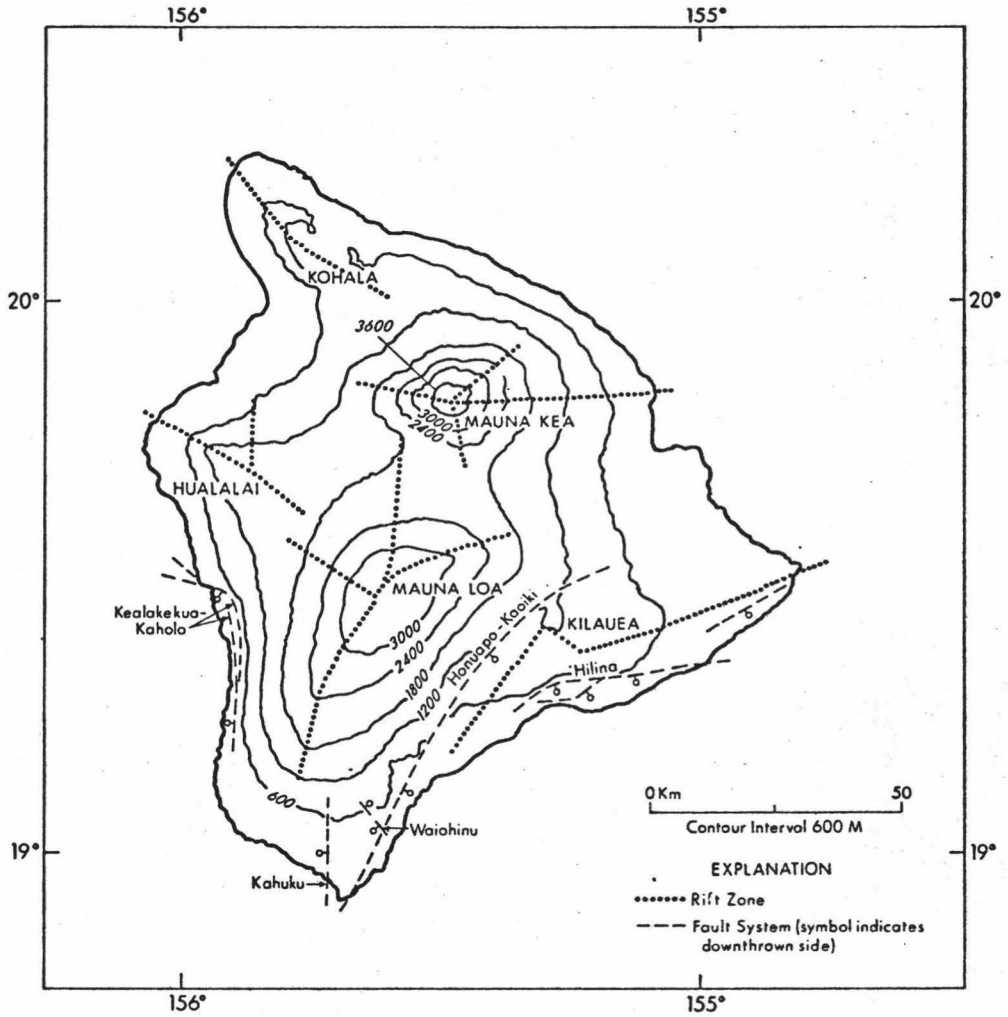

Figure 1.4 Map of the island of Hawaii showing major rift zones and fault systems, redrawn after Macdonald (1970). Each of the major volcanoes have rift zones (solid dots) which are denoted by their orientation. For example, Kilauea Southwest Rift and Mauna Loa Northeast Rift.

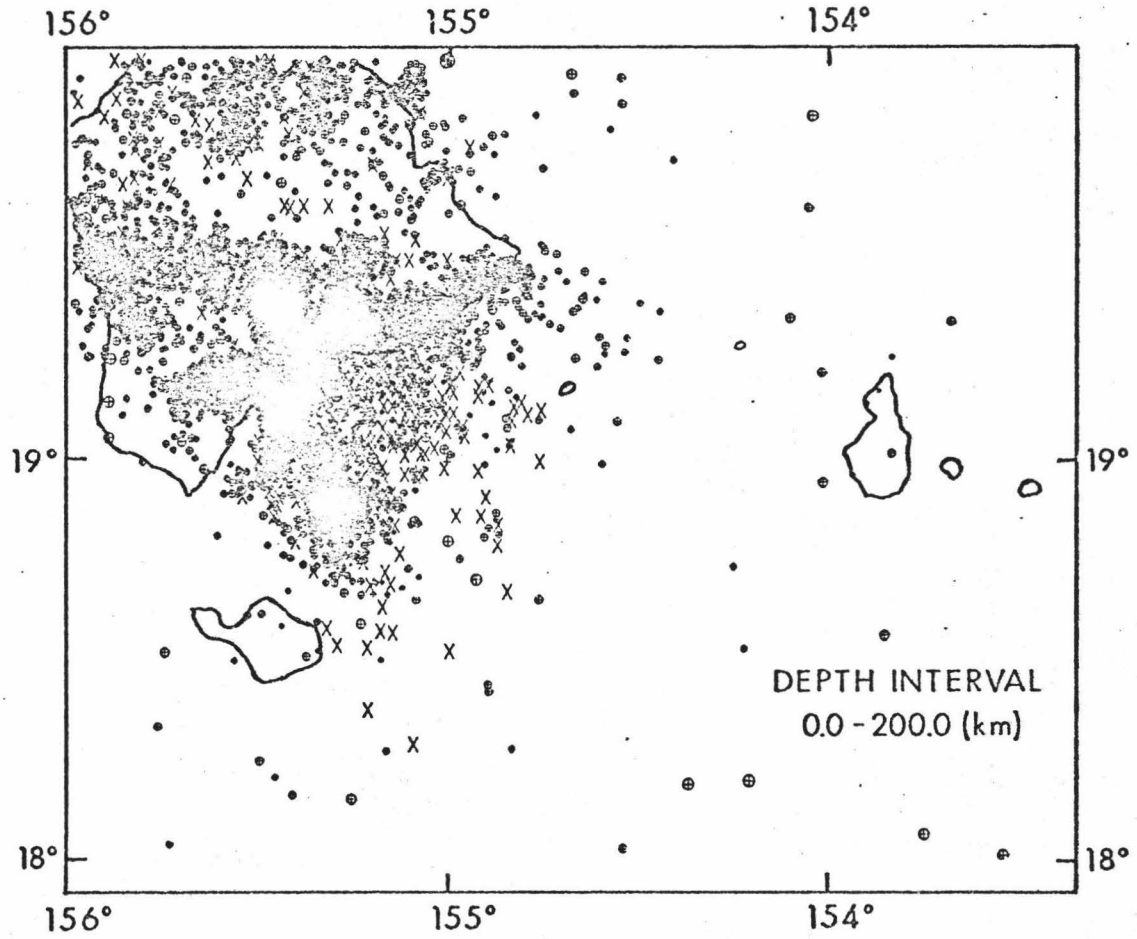

Figure 1.5 Epicenter map of southeastern Hawaii and offshore seamounts in the depth interval 0.0 to 200.0 km including events of $M_L \geq 2.0$. Open circles and X's represent epicenters; the circles showing better magnitude or hypocenter determination (RMS < 0.5 sec) than the X's. Event magnitude is proportional to symbol size for circles. The 4000 m depth contour is shown for Bushnell and Apuupuu seamounts. This symbol convention is used in all following epicenter and hypocenter maps in this paper.

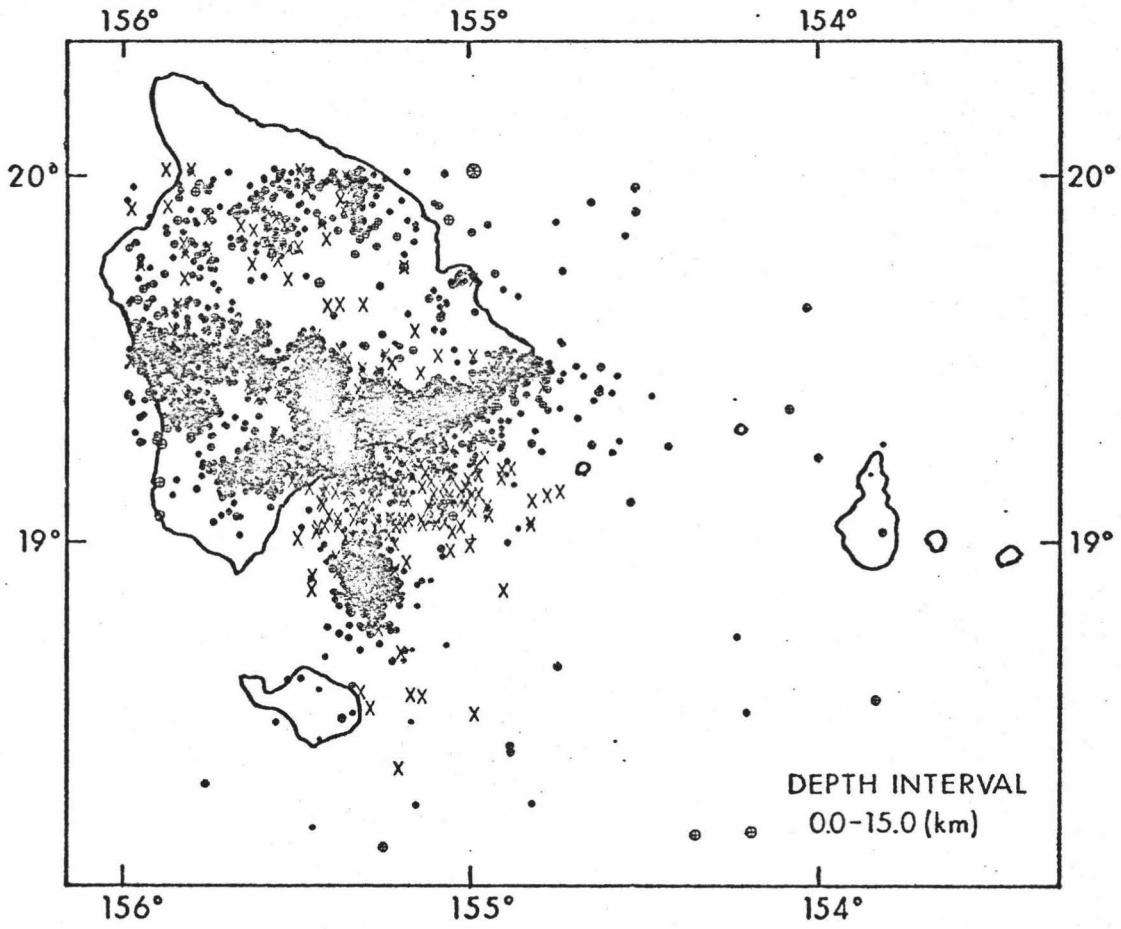

Figure 1.6 Epicenter map for Hawaii and southeastern offshore seamounts showing crustal events (0.0-15.0 km depth). Note concentration of shallow events offshore at Loihi seamount.

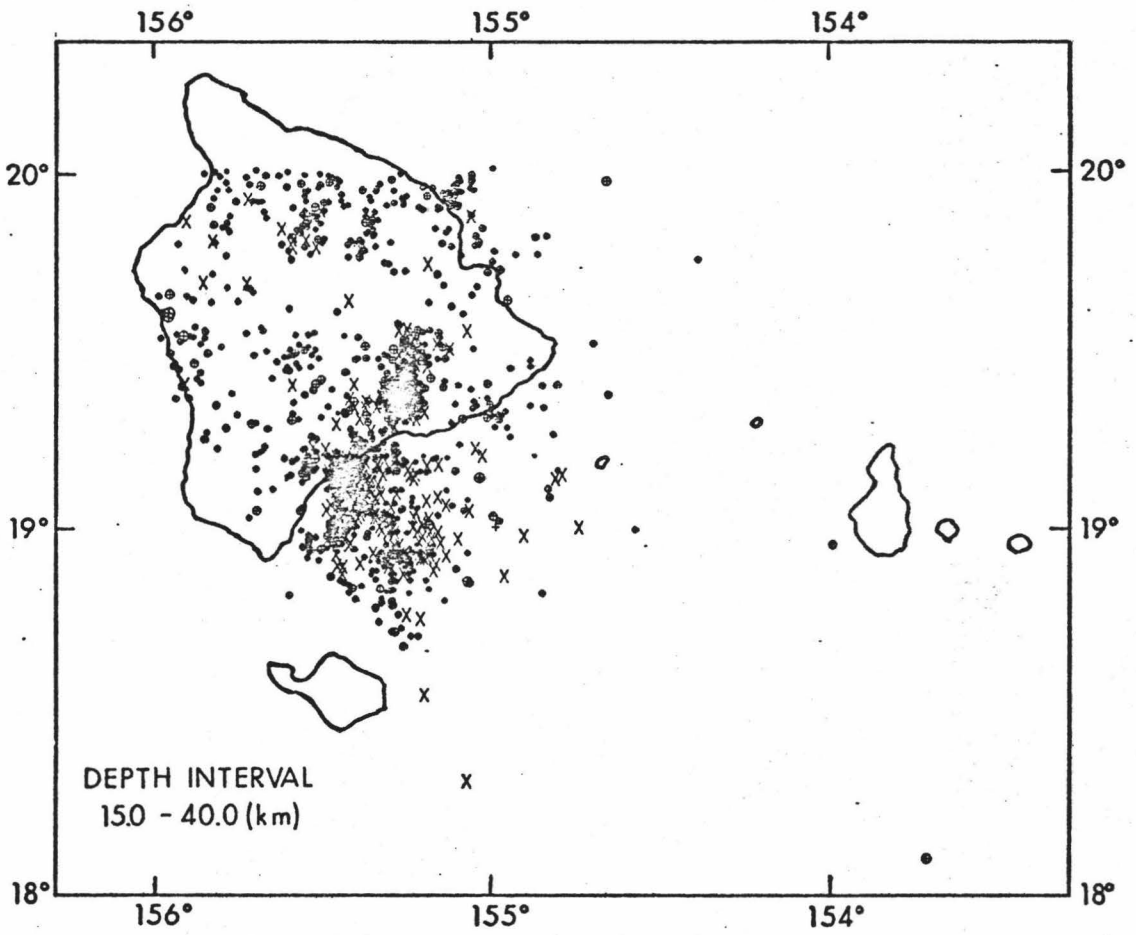

Figure 1.7 Epicenter map for Hawaii and southeastern offshore seamounts showing upper mantle events (15.0-40.00 km depth). Note concentration of offshore events along extension of Kilauea southwest rift and near Loihi seamount.

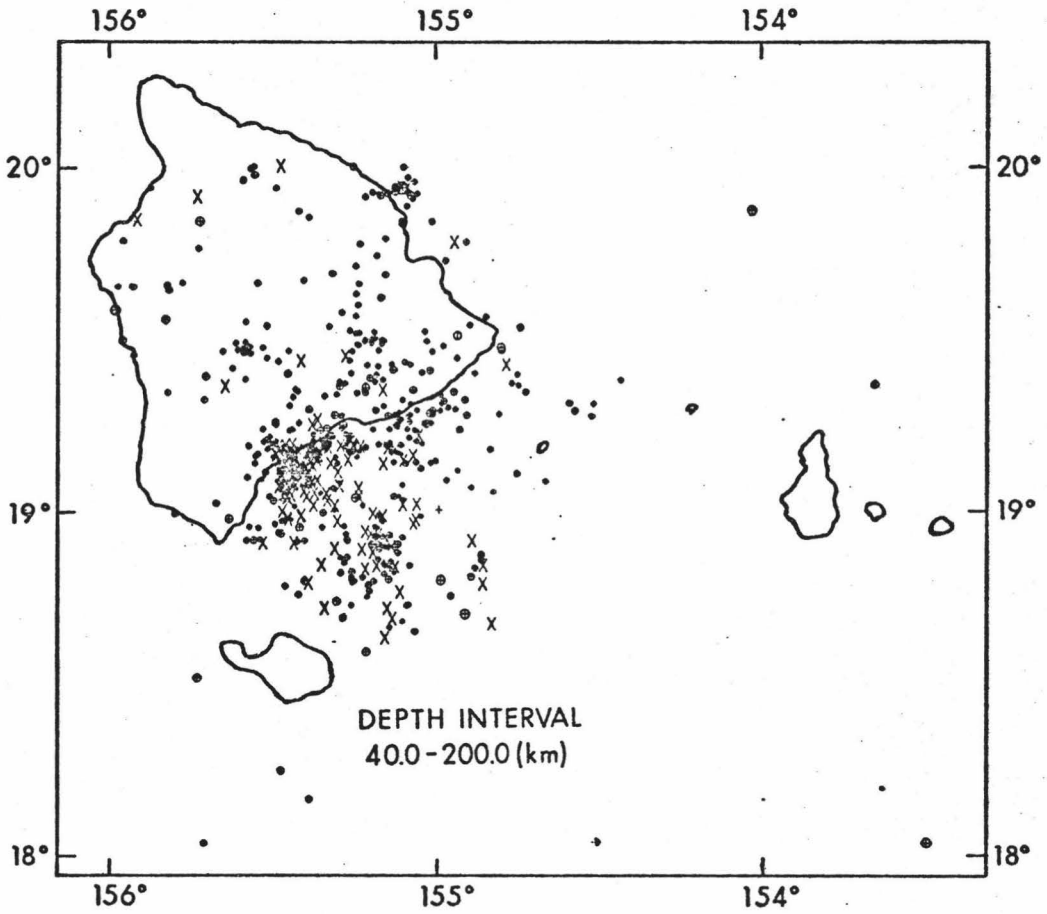

Figure 1.8 Epicenter map for Hawaii and southeastern offshore seamounts showing mantle events (40.0-200.0 km depth). Concentration of offshore events marked by X's are events with poor magnitude and depth determinations. Loihi seamount area is still seismically active at these mantle depths.

activity near Loihi seamount. It appears that recent events represent seamount slumping and local shallow faulting between periods of swarm activity and possible submarine volcanism. Also prominent are the events, X's, corresponding to the offshore extension of the Kilauea southwest rift zone.

Cross sections of this offshore seismicity are plotted in Figures 1.9 and 1.10. The large number of offshore events at about 10 km depth, Figure 1.9, correspond to the Loihi seamount area. Noteworthy is the northward dipping layer of hypocenters. Although the dip may be caused by systematic mis-location of hypocenters, the sharpness of the layer indicates a minimum depth for these events, possibly due to Loihi was also the site of a probable 1971 submarine volcanic eruption that produced over 13,000 events (as indicated by Koyanagi et al. (1976)). The northward dipping layer of hypocenters may indicate an active submarine rift zone or sill injection.

The Loihi seismic events are in most part due to the 1971 swarm and from recent dredging results, Sec. 1.1, Loihi is probably an active volcano. The dredging of Bushnell by Moore (1969), farther to the south of Loihi, also indicates recent volcanic eruption. The petrogenesis of these two seamounts is uncertain. If a common magma source exists for the seamounts, then the source must be at depths greater than 50 km since large scale lateral magma migration from Loihi to Bushnell is unlikely. Also, from hypocenters in Figure 1.9, there appears to be no obvious connection between Loihi and Kilauea magma sources. Perhaps aseismic partial melting and magma migration

Figure 1.9 Hypocenter cross section from Kilauea Volcano on the island of Hawaii to Loihi seamount offshore area. All events within area of box are projected along A-A' plane. Dark area (0.0-15.0 km depth), beneath Kilauea represents crustal events. Note cutoff at about 12 to 15 km depth corresponding to base of crust. Numerous events at 25 to 40 km depth beneath Kilauea believed to be a major zone of stress due to magmatic intrusion. Concentration of offshore events at 8 to 13 km represent Loihi seamount area.

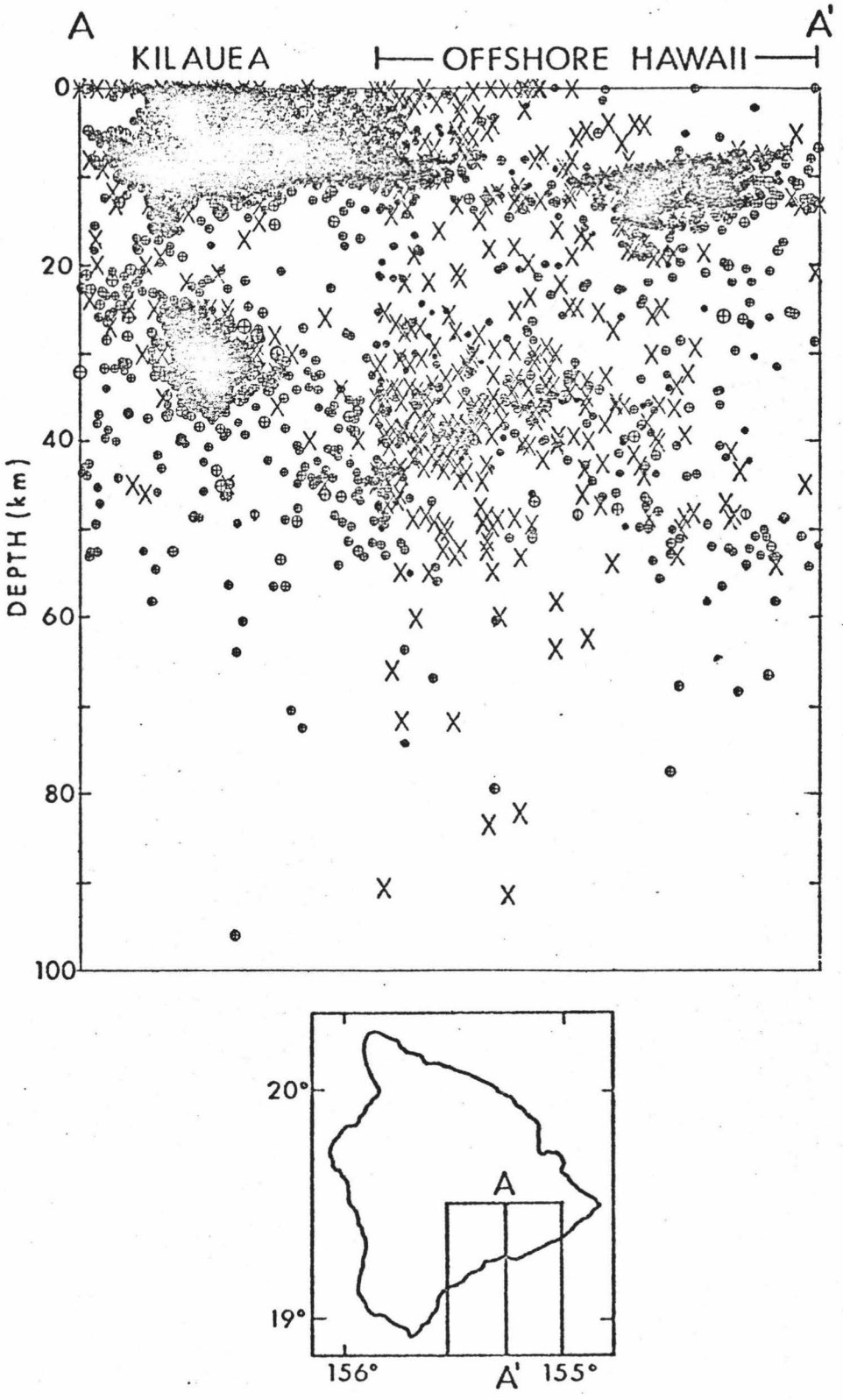
A
A'
KILAUEA
OFFSHORE HAWAII
0
20
40
60
80
100
DEPTH (km)
20°
19°
156°
155°
A
A'

Figure 1.10 Hypocenter cross section from Kilauea Volcano on the island of Hawaii along the Kilauea southwest rift zone offshore. All events within area of box are projected along A-A' plane. Dark area above 12 km represents crustal events beneath the island of Hawaii. Note the ~ 12 km seismicity cutoff at the base of the crust. The major zone of stress beneath Kilauea due to magma intrusion in the upper mantle is shown by the numerous events at 25 to 40 km depth. The large number of X's at 25 to 50 km depth below SW Rift may be due both to magmatic pressure at depth and poor hypocenter determinations.

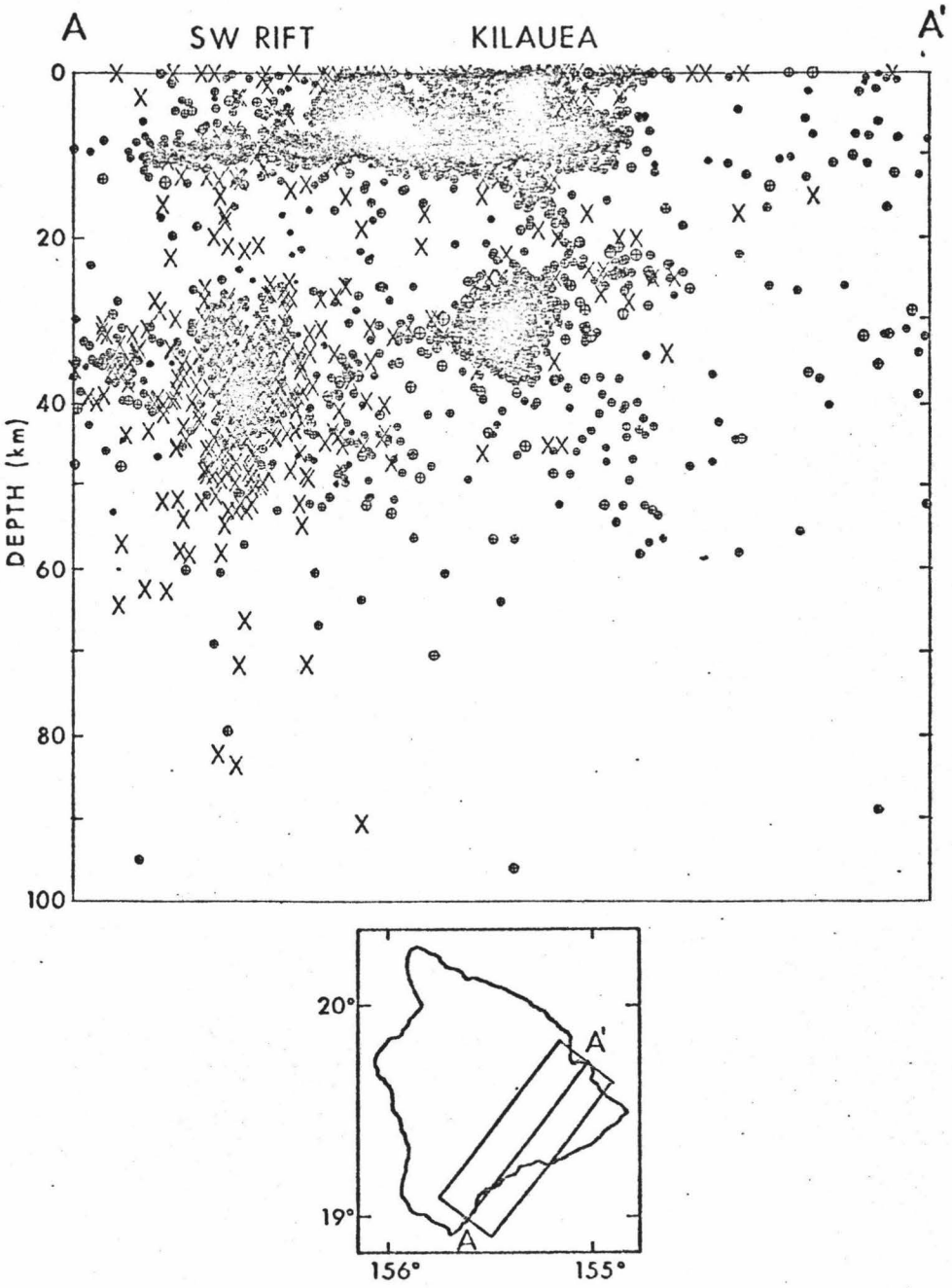
A
SW RIFT
KILAUEA
A'
0
20
40
60
80
100
DEPTH (km)
20°
19°
156°
155°
A
A'

at depths greater than 50 km connect the two magma source regions. From the seismicity and petrologic data Loihi is likely to be the next volcano to surface as part of the Hawaiian Ridge island chain.

Also in Figure 1.9, a seismic-aseismic boundary appears to exist from about 10 to 12 km beneath the island of Hawaii deepening offshore to 12 to 15 km beneath Loihi seamount. I believe that in part, this boundary represents the boundary of the crust. Events above this boundary are due both to crustal loading and eruption events. Further, this boundary may represent the top of a seismic low velocity zone with crustal loading from above and magmatic pressure from below. The island wide occurrence of this boundary is discussed in Section 1.4.

Figure 1.10 shows a cross section from Kilauea along the southwest rift zone offshore. The deeper events beneath the southwest rift between 30 and 50 km may be due to magmatic pressure at depth. The poor solutions indicated in the figure are due to uncertain magnitude and hypocentral estimates during an early period of sparser seismograph coverage. The infrequent events which occur offshore southeastern Hawaii and not associated with seamounts imply both inadequate station coverage and low scale-magnitude seismicity. Further OBS seismicity surveys ~~need to be deployed~~ are needed in these offshore areas.

1.4 Island of Hawaii

Hawaii island epicenters have been plotted in Figures 1.11 through 1.13. Most crustal earthquakes in Hawaii,

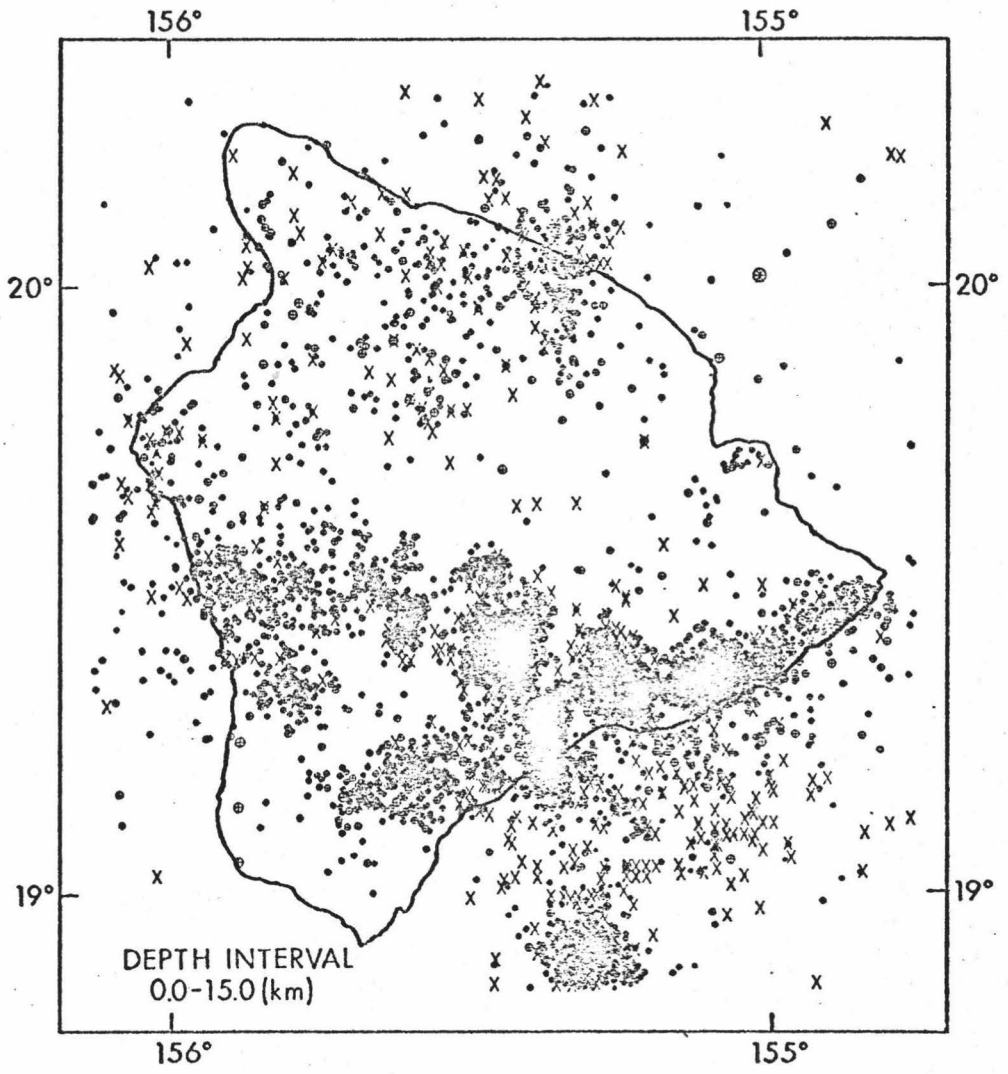

Figure 1.11 Epicenter map of the island of Hawaii for crustal events (0.0-15.0 km depth) with island outline shown for reference. See (Fig. 1.4) for reference to faults rift zones and volcanoes. Major seismic activity near Mauna Loa and Kilauea summit and rift zone regions.

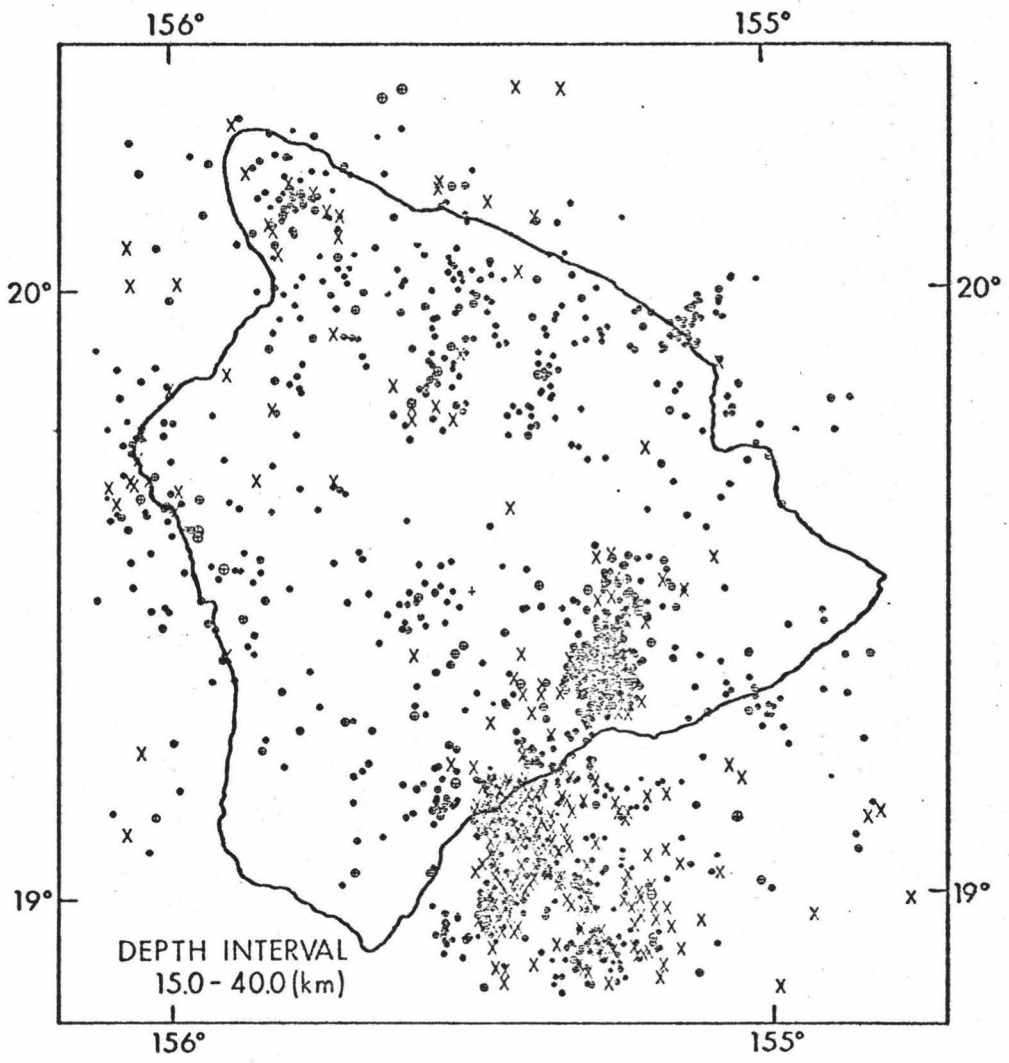

Figure 1.12 Epicenter map of the island of Hawaii for upper mantle (15.0-40.0 km depth) events with island outline shown for reference. Major activity near Kilauea summit.

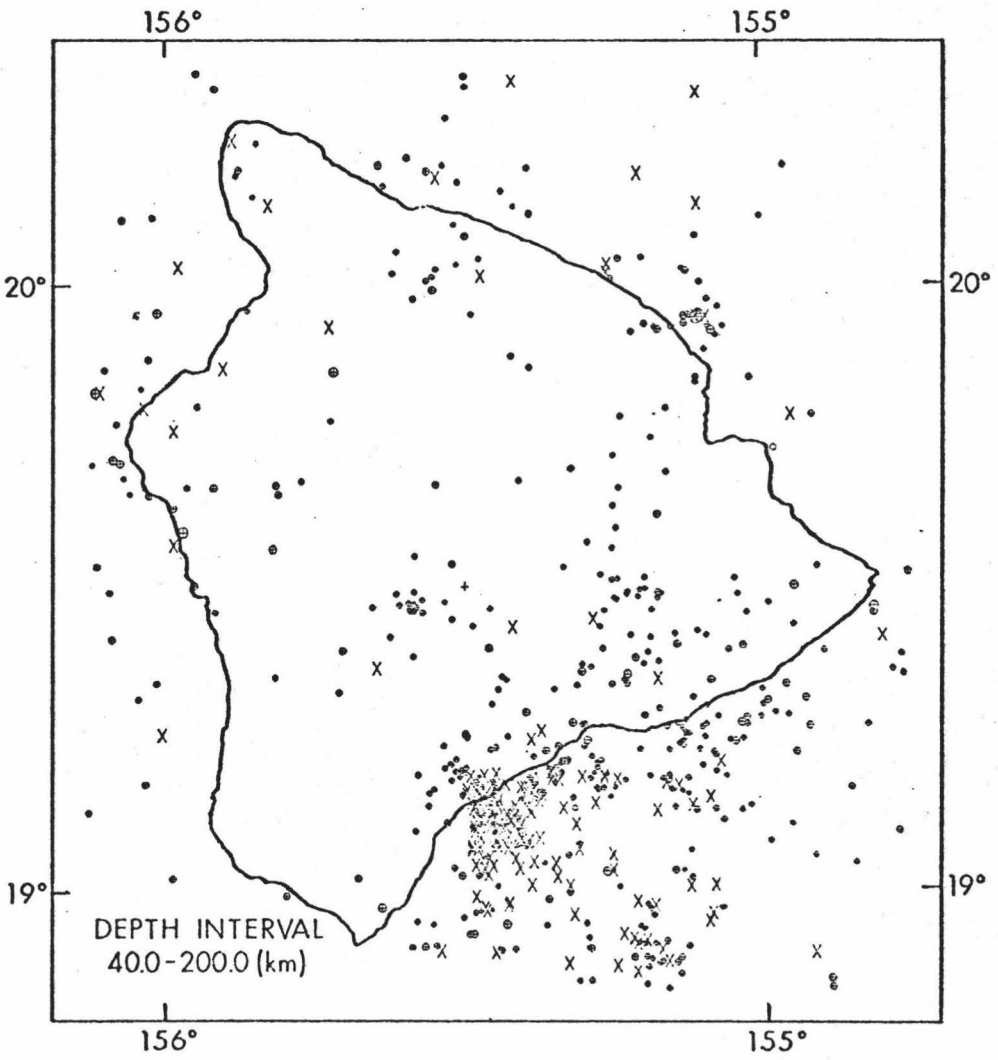

Figure 1.13 Epicenter map of the island of Hawaii for mantle events (40.0-200.0 km depth).

Figure 1.11, occur around Kilauea volcano under the summit area and on the shoreward side of the rift zones, and along the Kaoiki fault zone between Kilauea and Mauna Loa. Stearns and Macdonald (1946) note that displacements on the Hilina fault system (Fig. 1.4) total more than 450 meters with blocks on the seaward side downthrown. This fault system is considered to be due to seaward gravity sliding in response to inflation and deflation of the east rift. The distribution of crustal earthquakes related to the mobility of south flank Kilauea has been summarized by Koyanagi et al. (1972). They observe that (1) earthquakes outside the summit area of Kilauea generally take place along or seaward of the rift zones and the Koae fault system; (2) many of these earthquakes are related in space and time to magmatic events, either extrusive or intrusive; (3) most earthquakes during the early stage of a magmatic event are located along the rifts or along the Koae fault system at depths of 5 km or less; (4) many of the earthquakes during the later stages of or immediately after a magmatic event are located seaward of the initial activity at depths of as much as 10 km; (5) aftershocks of "tectonic" earthquakes not immediately related to magmatic events show a different pattern of occurrence than "magmatic" earthquakes; (6) maximum stress axes of most south flank earthquakes plunge gently seaward and are oriented within 20^{o} of a normal to the trend of east-rift fissures and Koae faults. Finite element models for Kilauea as determined by Dieterich and Decker (1975) support the conclusion that the east rift is a series of dikes and fracture that dip southward and that dike injection

pressures cause opening of the rift zone. The Kalapana earthquake of November 29, 1975 (M_L ~ 7.1) and crustal tectonics of the Kilauea south flank have been discussed by Rogers (1978). He indicates that the south flank of Kilauea is being wedged seaward by forceful injection of magma into the rift zones, in basic agreement with Swanson et al. (1976). Further, the shallow fault systems (1 to 3 km) along the south coast of Hawaii are a secondary feature of south flank movement. Rogers (1978) concludes that the large Kalapana main-shock event was associated with seaward movement of the south flank with a near vertical aftershock zone. Ando (1977) shows that normal faulting also took place to the south of the after shock area.

The majority of the remaining crustal events occur along the Kaoiki fault zone between Kilauea and Mauna Loa volcanoes, and the shield area of Mauna Loa and the western Kealakekua Fault system. The Kaoiki fault was the site of (M_L ~ 6.1) earthquake on June 17, 1962 described by Koyanagi et al. (1966). The quadrant distribution of compressions and rarefactions that was observed could have been produced by either (1) right lateral strike slip movement on a fault trending N25°E, roughly parallel to the Kaoiki fault trace, or (2) left lateral strike slip movement on a fault trending N65°W. The north-eastern edge of Kealakekua Bay is a scarp formed by a fault along which the lower slope of Mauna Loa has been moving downward in relation to the major part of the Mauna Loa Shield. The Kona earth-quake of August 21, 1951 has been discussed by Macdonald and Wentworth (1951) and may be related in some way to either an increase

of pressure under Mauna Loa and resulting rise of the central part of the volcano, or a readjustment resulting from the lava extrusion in June, 1950. Focal mechanisms from my study, indicate high angle normal faulting along the Honuapo-Kaoiki fault system and slumping on the Kealakekua-Kaholo faults.

Earthquakes in the mantle in Hawaii, Figures 1.12 and 1.13, are primarily concentrated in the three zones that lie roughly along a NNE trending line. The highest and most continuous activity is under Kilauea volcano where the earthquakes outline a roughly cylindrical zone extending from depths of 60 km (Eaton, 1962) up into the crust. With the advent of a denser seismograph array most mantle earthquakes have been located at depth of 30 to 40 km. A second center of activity, around Loihi Seamount, which was especially active in late 1971 and early 1972, is located 40 km south of the island. The third center of activity is on the northeast coast of the island of Hawaii; this zone was active during an aftershock sequence of a magnitude 6.2 earthquake that occurred at about 45 km depth on April 26, 1973, causing considerable damage in the town of Hilo, 20 km to the southeast (Unger and Ward, 1974). First motions from this earthquake indicate a strike slip focal mechanism. The data are insufficient to conclusively determine the fault plane but the alternate possibilities are (1) a left lateral movement along one nodal plane strike about N70^{o}W and (2) a right lateral movement along a nodal plane strike about N30^{o}E.

The island of Hawaii and the southeastern area in particular are the most seismically active regions of the entire Hawaiian Ridge. The majority of activity is beneath Kilauea but significant activity occurs along the Kilauea southwest and east rift zones. Although Kilauea and the rift zones account for much of the seismic activity at shallow depths, a large number of deeper events occur offshore directly south and southwestward of Kilauea. Examination of hypocenters shown in Figure 1.14 shows a spectacular concentration of events 25 to 40 km below Kilauea, trending southward at depth. I believe that this concentration of events represents a major zone of stress caused by magma intrusion to Kilauea, the east rift zone, and possibly Mauna Loa. The large number of events at about 10 km depth beneath the island may indicate a zone of tension due to both island loading and intrusion of magma from below 10 km. It is interesting to note that Crosson (1976) has determined from inversion of local earthquake travel time data, a pronounced low velocity zone of up to several km thickness at the base of the crust (10 km depth), for the island of Hawaii. Although this low velocity zone beneath Hawaii is not pronounced in the Tau inversion velocity model for the Hawaiian ridge as determined by Estill and Odegard (1978), it may not have been resolved due to the coarse travel time sampling and averaging of the Tau data. The drop in seismicity below about 12 km indicates a gross change in the stress distribution at this depth. Also noteworthy is the shallow aseismic region between Kilauea and Mauna Loa volcanoes. The aseismic region at about 2 to 7 km beneath Kilauea

Figure 1.14 Hypocenter cross-section beneath the island of Hawaii from Kohala at northwest to offshore at the southeast. All events within area of box are projected along A-A' plane. Spectacular concentration of events 25 to 40 km below Kilauea trending southward at depth represent a major zone of stress caused by magma intrusion to Kilauea. The large number of events at about 10 km beneath the island may indicate a zone of tension due to both island loading and intrusion of magma from below 10 km. Noteworthy is the shallow aseismic region between Kilauea and Mauna Loa volcanoes. Also, a region of high activity appears to connect Kilauea to Mauna Loa.

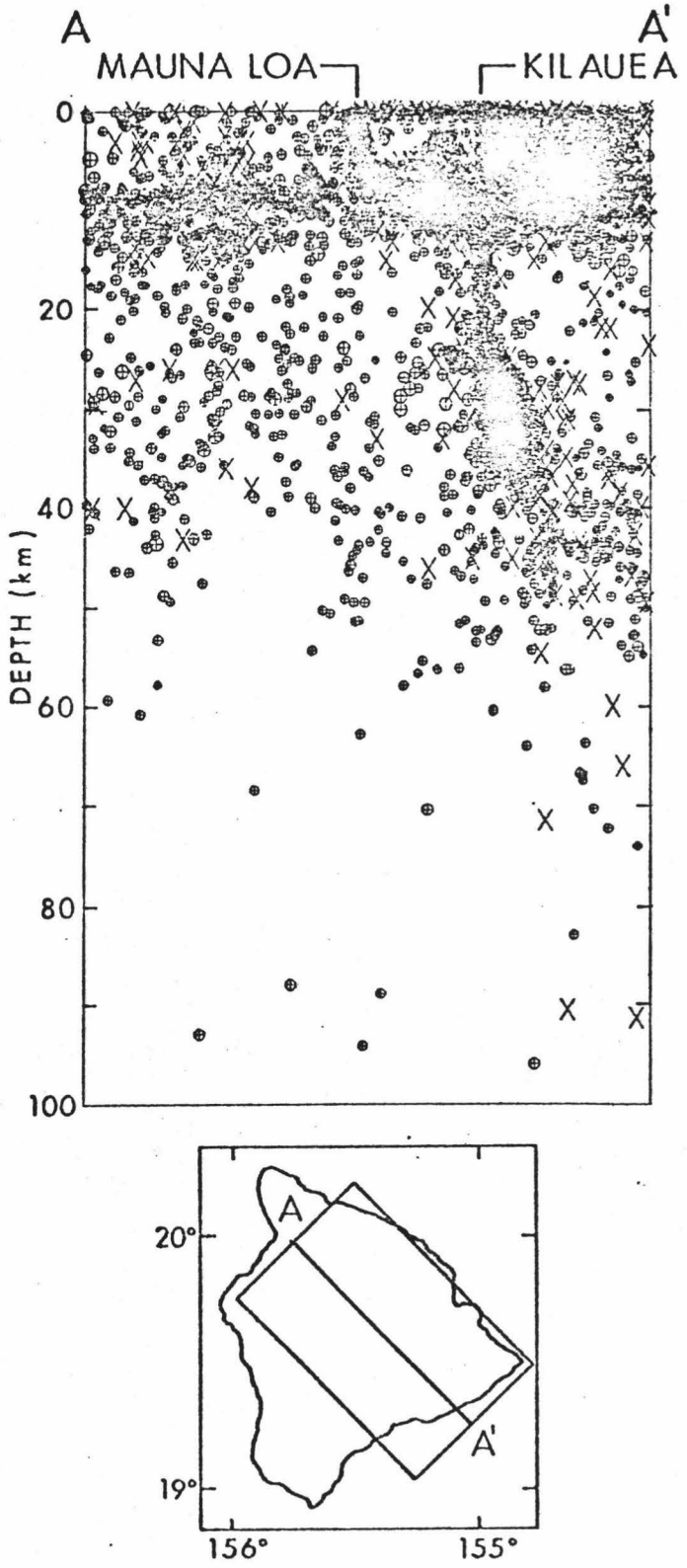
A
A'
MAUNA LOA
KILAUEA
0
20
40
60
80
100
DEPTH (km)
A
A'
20°
19°
156°
155°

described by Koyanagi et al. (1976) is believed to be a shallow magma chamber. A region of high activity appears to connect Mauna Loa to the region below Kilauea. If this seismic activity is indicative of magma movement then Kilauea and Mauna Loa appear to be connected to the same source although their activity cycles do not appear to be closely related.

Koyanagi (1968) believes that the spasmodic tremor (5 Hz) and harmonic tremor (1 to 2 Hz) observed frequently during eruptions represent direct evidence of magma movement. Eaton (1962) noted that between August 14 and 19, 1959, a great swarm of deep earthquakes and associated spasmodic tremor emanated from a zone 55 km below Kilauea, indicating magma movement from deep conduits to the surface. Harmonic tremor corresponding to source depths of 30 km or greater has also been observed by Shimozura et al. (1966) under Kilauea and by Koyanagi (personal communication) for the 1971 Loihi seamount earthquake swarms. These results indicate that magma transfer occurs from depths greater than 30 km to shallow magma reservoirs. The close association of tremor and swarms suggests that magma is present in the focal region of the deep swarms.

Ellsworth and Koyanagi (1977) note that the concentration of deep earthquakes and associated deep tremor 35 km south-southwest of Kilauea caldera delineates a region of current magmatic movement with uncertain temporal association to eruptive processes on either Kilauea or Mauna Loa. Ellsworth and Koyanagi (1977), considering three-

dimensional lateral velocity structure and mantle earthquake distribution, suggest that the center of contemporary magmatic production extends offshore to the south of the active volcanic vents.

The relation of shallow microearthquakes to the mechanics of Kilauea's eruptions has been discussed by Koyanagi et al. (1976). Detailed first motion studies of shallow summit and rift swarm in May 1970 indicate stresses induced by the forceful intrusion of magma from the summit of Kilauea into the upper east rift zone, Endo (1971). Such swarms seem to clearly mark the movement of magma in the upper few kilometers of the volcano. The microearthquake swarms occur predominantly in the upper few kilometers beneath the Halemaumau area. Long Period (L-P) earthquakes, events with emergent onsets and higher-frequency waves preceding or superimposed on the predominant low frequency waves or phases, occur predominantly below 6-km depth; these events seem to delimit a conduit through which magma might be expected to rise from depth.

In general, there exists a relation between seismic activity and corresponding eruptive activity as discussed by Koyanagi and Endo (1971): (1) initial phase--summit deflation, shallow rift quakes, shallow caldera quakes, lava fountains and strong tremor; (2) interim phase--summit inflation, weak tremor, long period caldera quakes, continual summit inflation, weak tremor near eruptive fissure, shallow caldera quakes; (3) secondary phase--summit deflation, occasional shallow rift quakes, lava fountains, moderate tremor. Dieterich and Decker (1975) suggest that for flank eruptions a vertical supply of

magma is supplied to a shallow summit reservoir followed by lateral transport of magma to the flank by dikes that make up the rift zone.

In an attempt to determine migration of seismic events (> 10 km) prior to volcanic eruptions, six recent eruptions were examined: (1) November 5, 1967, Kilauea; (2) May 24, 1969, Kilauea East Rift; (3) December 12, 1973, Kilauea East Rift; (4) September 19, 1974, Kilauea East Rift; (5) December 31, 1974, Kilauea Southwest Rift; (6) July 5, 1975, Mauna Loa. Located events of local magnitude 2.0 or greater were included, yet no obvious seismicity migration paths were evident. The migration patterns may be complicated by the formation of secondary aseismic magma conduits or chambers prior to eruption. Examination of smaller magnitude events ($M_L \leq 2.0$) may provide more conclusive evidence for pre-eruption seismic migration paths at shallow depths as discussed by Koyanagi et al. (1976).

An examination of a cross section from Kilauea along the east rift zone (Fig. 1.15) shows shallow (< 15 km) seismicity beneath the East Rift terminating offshore. The lack of deep activity beneath the East Rift and seismic migration patterns indicate that magma rises from beneath Kilauea and moves out along the east rift prior to and during eruptions. The Mauna Kea-Mauna Loa cross section, Figure 1.16, shows scattered events at depth, indicating lithospheric fracture, but no obvious magma conduits. Nonetheless, both the East Rift (Fig. 1.15) and Mauna Kea-Mauna Loa (Fig. 1.16) cross sections show the 10-12 km zone of high seismicity.

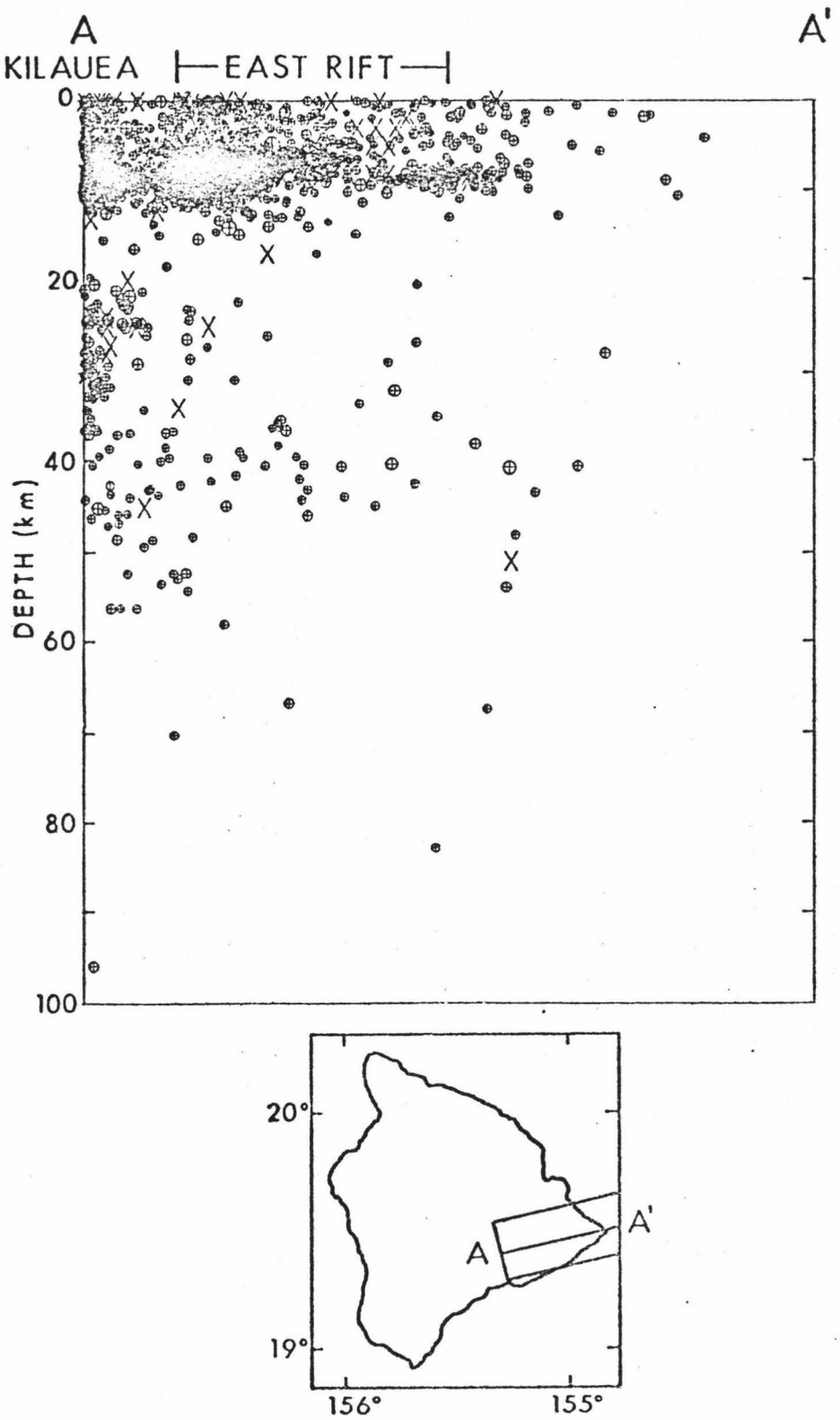

Figure 1.15 Hypocenter cross section from Kilauea along the East Rift zone. All events within area of box are projected along A-A' plane. Note shallow events (~ 12 km) along rift zone with little activity below.

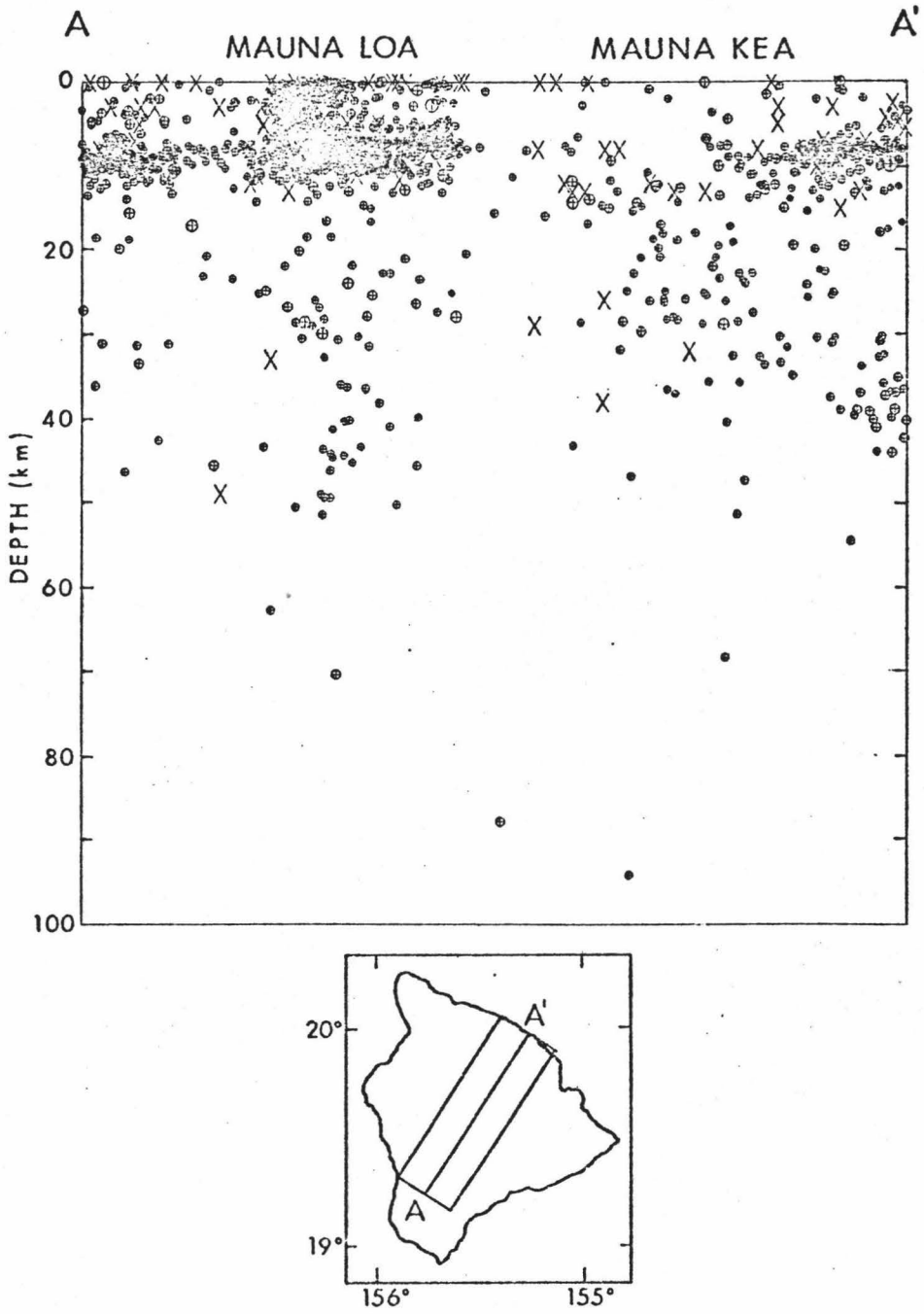

Figure 1.16 Hypocenter cross section from Mauna Loa to Mauna Kea. All events within area of box are projected along A-A' plane. Note shallow events (< 12 km) corresponding to island wide zone at 10 to 12 km depth. No obvious magma conduits apparent from hypocenters for Mauna Loa or Mauna Kea.

1.5 Western Offshore Hawaii Island and Offshore Oahu, Molokai and Maui

Events to the west of Hawaii, Figure 1.17, have much poorer epicenter resolution due to seismograph stations being entirely to the north and west. Nevertheless, significant activity occurs along the Kealakekua fault zone and along offshore slump fault scarps. Noteworthy are the earthquake swarm of 1929 beneath the north flank of Hualalai Volcano and the 1801 volcanic eruption of Hualalai which indicates either remanant magma chambers, multiple shallow magmatic sources or common source at depth. Seamounts off the west coast have been dredged by Moore (1965) and been found to be composed of altered basalt, highly vesicular and extruded in water depths less than 600 m. The northern seamount region has a relatively thick sedimentary section whereas the southern area is flat and appears devoid of all but possibly a thin veneer of sediment (Kroenke, 1965). The ages of these seamounts are unknown.

Epicenters near the islands of Oahu, Molokai, Lanai, Maui and Kahoolawe are shown in Figure 1.18. The concentration of events near the lower right corner are offshore northwestern Hawaii island events and, along with the events south of Lanai and Kahoolawe probably represent oceanward slumping along offshore fault scarps. Four particular areas of interest are (1) north of Molokai; (2) north of Maui; (3) between Molokai and Lanai; (4) east of Oahu. The events north of Molokai and Maui may be related to the Molokai fracture zone although it is generally believed that the fracture zone is older than the Hawaiian Ridge itself and inactive. Moore (1964) indicates

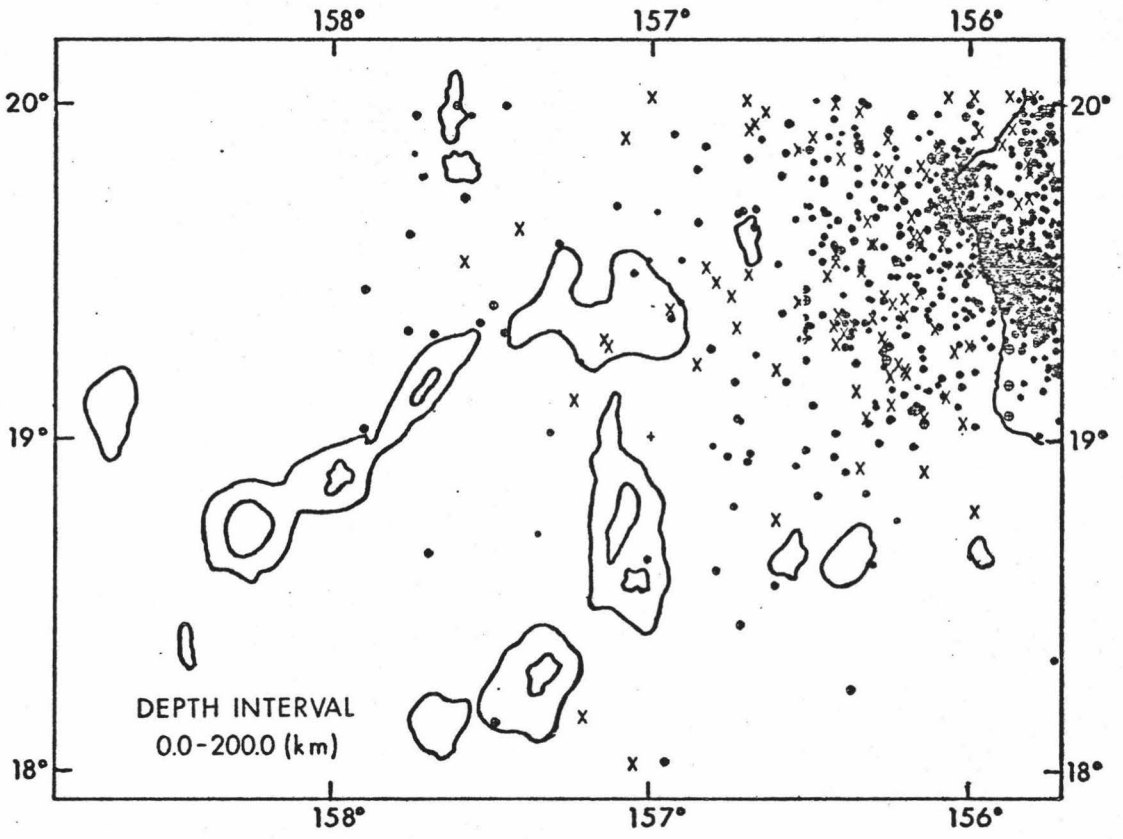

Figure 1.17 Epicenter map of western offshore Hawaii for all events (0.0-200.0 km depth) with $M_L \geq 2.0$. West coast island outline is shown including offshore seamounts (4000 meter contour interval). Major activity along Kealakekua fault system and offshore fault scarps.

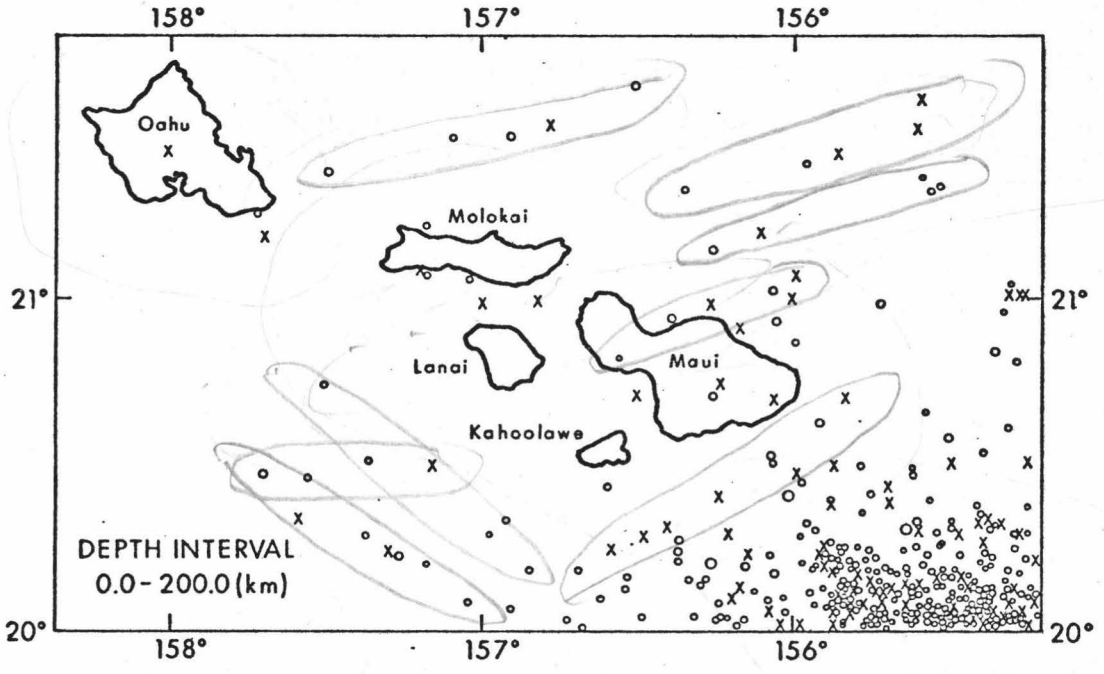

Figure 1.18 Epicenter map of events (0.0-200.0 km depth) near Oahu, Molokai, Lanai, Maui and Kahoolawe islands. Island outlines are shown.

that the area north of Molokai represents an area of large scale submarine landslides. These events may simply represent the downward movement of the northern oceanward side in relation to the upward landward side. Several of the events just north-eastward of Maui are deep (> 20 km) and may be related to the same fault that caused the Maui earthquake of 1938, which had its epicenter 25 km north of Maui. The events between Molokai and Lanai indicate slumping which may be in part due to submarine erosion. Although these earthquakes are generally considered as fault scarp, submarine slumping, part of the seismic activity may be due to offshore extension of submarine rift zones.

An overlooked aspect of the tectonics of the central and northern Hawaiian Ridge has been the occurrence of very recent volcanic eruptions. As discussed by Macdonald (1970), Haleakala volcano on Maui erupted about 1790 and poured lava into the ocean at Makena. Submarine eruptions have also occurred along the central and northern Hawaiian Ridge: (1) on May 22, 1956 between Oahu and Kauai when floating pumice and sulfurous odor were reported (Macdonald (1959)); (2) about August 20, 1955, about 55 miles N85^{o}E of Necker Island when airline passengers observed steam, turbulent water, and several thousand square yards of dry land or probable pumice (Macdonald, 1970). These eruptions may be posterosional eruptions from shallow relic magma chambers. Jarrard and Clague (1977) state that the detailed geometry and timing of volcanism within island chains may reflect an interaction of a large (220 km or more) hot spot with

local crustal-stresses and/or lines of weakness which could account for small scale departures from a uniform age progression along the Hawaiian Ridge.

1.6 Focal Mechanisms

In order to infer the principal stress orientation at the southeastern Hawaiian Ridge, 36 lower hemisphere focal mechanisms were determined from local P-wave first arrivals using both OBS and land seismographs (Table 1.3). No composite focal solutions are in the data set and orthogonal nodal plane solutions were assumed. These OBS-HVO focal mechanisms were combined with previous work as discussed below.

Focal mechanisms for 60 upper mantle earthquakes for Hawaii have been determined by Endo and Rogers (1978). The relative orientations of stress axes from these events have been used to suggest crustal loading as an important mechanism for generation of upper mantle events in Hawaii. Ward and Gregersen (1973) have determined focal mechanisms for 6 upper mantle events and indicate: (1) high angle normal faulting for upper mantle Kilauea events with northeastern tension axes, southwestern pressure axes and low angle dips; and (2) northwestern low angle pressure axes and vertical tension axes for an upper mantle event southwest of the Kaoiki fault system.

Rogers (1978), Koyanagi et al. (1972), Endo and Rogers (1978) and Ward and Gregersen (1973) have published several important focal mechanism solutions including Kalapana, Kilauea South Flank and mantle events for Hawaii. Important results of these focal mechanisms

Table 1.3: FOCAL MECHANISM SOLUTIONS

No.	Date	Origin Time (HST)	Location N Lat	Location W Long	Depth (km)	Mag	Nodal Plane 1 Azimuth	Nodal Plane 1 Dip	Nodal Plane 2 Azimuth	Nodal Plane 2 Dip	T-Axis Azimuth	T-Axis Plunge	P-Axis Azimuth	P-Axis Plunge
1	761015	00:20:38.5	19°19.7'	155°14.1'	6.7	2.5	N20°E	42°SE	N44°E	48°NW	S18°W	77°SW	N56°W	13°NW
2	761017	08:12:22.5	19°19.9'	155°12.9'	10.1	2.5	N42°E	50°SE	N10°E	40°NW	N11°E	74°NE	S69°E	16°SE
3	761019	02:05:45.7	19°25.3'	154°56.7'	8.3	2.7	N03°W	51°NE	N12°E	39°NW	S28°W	90°SW	S84°E	10°SE
4	761019	23:11:50.2	19°20.4'	155°08.1'	9.1	2.7	N13°W	60°NE	N00°E	40°W	S37°W	89°SW	N83°E	11°NE
5	761022	12:42:48.9	19°19.5'	155°12.5'	9.4	2.7	N60°W	80°SW	N65°W	10°NE	N25°E	54°NE	S28°W	36°SW
6	761105	02:58:29.4	19°21.6'	155°09.1'	8.4	2.8	N40°E	34°SE	N50°E	56°NW	N45°W	10°NW	S20°E	80°SE
7	761106	23:40:46.9	19°23.5'	155°25.2'	9.8	3.3	N07°E	41°NW	N12°E	49°SE	N17°W	85°NW	S79°E	05°SE
8	761108	19:51:05.5	19°22.2'	155°06.5'	7.9	2.9	N46°E	29°SE	N47°E	61°NW	N42°W	14°NW	S44°E	86°SE
9	761110	12:05:27.9	19°05.5'	155°24.0'	28.5	2.6	N54°E	59°SE	N44°E	31°NW	N16°W	74°NW	S39°E	16°SE
10	761112	16:54:46.2	19°21.3'	155°03.7'	7.1	3.5	N40°E	48°SE	N32°E	52°NW	N00°E	82°NW	S55°E	08°SE
11	761121	20:46:43.7	19°23.2'	155°05.8'	7.8	2.6	N64°E	50°SE	N57°E	40°NW	S29°E	06°SE	N02°E	84°NE
12	761207	23:40:21.6	19°24.2'	155°17.1'	3.3	2.8	N50°E	40°NW	N56°E	50°SE	S36°E	05°SE	N72°W	85°NW
13	761210	08:48:45.3	19°23.2'	155°05.1'	8.4	2.9	N00°W	38°W	N47°E	52°SE	N02°W	62°NE	S64°E	28°SE
14	761214	04:06:22.5	19°22.4'	154°59.0'	5.9	2.6	N76°E	29°SE	N77°E	61°NE	N14°W	12°NW	S09°E	78°SE
15	761218	04:01:00.3	19°20.1'	155°07.7'	9.9	4.8	N05°E	34°NW	N10°W	56°NE	S52°W	86°SW	N86°E	14°NE
16	761225	07:01:15.1	19°37.5'	155°59.9'	8.2	3.3	N24°W	70°SW	N24°W	20°NW	N62°E	75°NE	S66°W	25°SW
17	761226	23:43:08.6	19°45.9'	155°58.7'	7.8	2.9	N49°W	70°SW	N49°W	20°NE	N36°E	62°NE	S42°W	28°SW
18	761227	12:13:53.5	19°12.7'	155°35.6'	10.1	3.1	N06°E	70°NW	N06°E	20°SE	N84°W	26°NW	S85°E	64°SE
19	761228	07:33:50.6	19°21.4'	155°29.8'	9.1	2.8	N05°E	49°NW	N05°E	41°SE	N92°W	06°NW	S85°E	84°SE
20	761229	18:10:00.5	19°23.4'	155°05.2'	9.5	3.2	N63°E	41°SE	N54°E	49°NW	N36°W	03°NW	N85°E	87°E
21	770101	04:26:34.9	19°19.7'	155°07.4'	6.7	3.3	N15°W	39°SW	N17°W	51°NE	S70°W	87°SW	N76°E	03°NE
22	770104	14:25:12.7	19°23.4'	155°15.2'	6.4	3.4	N86°W	51°SW	N88°E	39°NE	N01°E	02°N	N02°E	88°NE
23	770120	02:20:27.7	19°19.6'	155°11.5'	7.8	2.7	N50°E	62°SE	N08°W	28°SW	N01°E	58°NE	S58°E	32°SE
24	770122	07:32:42.4	19°21.7'	155°13.6'	9.0	3.2	N76°W	88°S	N66°E	02°NE	N22°E	46°NE	S23°W	44°SW
25	770129	11:25:43.2	19°21.0'	155°06.7'	7.9	3.1	N08°W	37°SW	N15°W	53°NE	S70°W	80°SW	N80°E	10°NE
26	770129	22:48:49.5	19°21.9'	155°05.9'	7.5	2.7	N23°W	39°SW	N10°E	51°SE	N30°W	76°NW	S84°E	14°SE
27	770201	07:22:00.8	19°24.0'	155°15.4'	6.7	2.5	N49°E	49°E	N64°E	41°NW	S35°E	11°SE	S88°W	79°SW
28	770220	22:36:56.4	20°02.4'	155°30.3'	15.2	2.9	N12°W	15°SW	N39°E	75°SE	S65°E	38°SE	N35°W	52°NW
29	770226	19:42:28.6	18°31.8'	155°19.5'	11.2	3.1	N10°E	48°NW	N40°W	42°NE	N89°W	12°NW	S32°E	78°SE
30	770302	14:36:00.8	18°49.3'	155°15.1'	31.6	3.2	N42°E	70°SE	N42°E	20°NW	S48°E	25°SE	N44°W	65°NW
31	770302	15:44:37.8	18°51.9'	155°16.1'	43.4	3.1	N62°W	65°SW	N59°E	25°NW	S17°W	28°SW	N43°E	62°NE
32	770305	09:24:22.6	19°19.6'	155°12.4'	8.8	3.1	N78°E	54°SE	N26°E	36°NW	N34°E	76°NE	S44°E	14°SE
33	770309	10:46:21.1	18°58.5'	155°18.2'	38.9	3.2	N80°W	10°SW	N55°E	80°NW	N34°W	38°NW	S38°E	52°SE
34	770310	03:17:15.4	19°20.5'	155°13.9'	7.8	3.4	N50°W	31°SW	N83°E	59°NE	N12°E	22°NE	S50°E	68°SE
35	770326	03:50:02.6	19°19.9'	155°12.1'	7.5	3.2	N68°W	58°SW	N48°W	32°NE	N04°W	74°NW	S30°W	16°SW
36	770719	08:19:36.3	18°35.5'	154°45.3'	8.3	3.1	N52°W	20°SW	N32°W	70°NE	N50°E	25°NE	S80°W	65°SW

for shallow events (< 10 km) on the south flank of Hawaii are: (1) southeastward maximum stress axes normal to the Kilauea east rift zone (Koyanagi et al., 1972); (2) pressure and tension axes nearly horizontal and the tension axes perpendicular to the east rift (Endo, 1972); (3) south to southeastern pressure axes at the east end of Koae fault zone dipping seaward with northeasterly horizontal tension axes, north-south horizontal pressure axes and horizontal east-west tension axes, near the western end of the south flank) east-west horizontal pressure axes and north-south horizontal tension axes on the Kaoiki fault system (Endo unpublished); (4) northeastern horizontal pressure axes and near vertical tension axes for crustal Kilauea southwest rift events and south-southwest near horizontal pressure axes and northeastern low angle tension axes for shallow Kilauea south flank events, Ward and Gregersen (1973). Rogers (1978) determined fault plane solutions for the Kalapana November 29, 1975 mainshock and largest foreshock using local data and Ando (1977) determined the focal mechanism using teleseismic data. The locally determined mechanisms gave southeastern-horizontal pressure axes and vertical tension axes while the teleseismically determined mechanisms and field evidence indicate that faulting for both the mainshock and foreshock was of the high angle, normal type.

The results of my study are shown in Figures 1.19 through 1.25. My work has been combined with the work of Ward and Gregersen (1973), Endo and Rogers (1978) and Rogers (1978), in Figure 1.26. My data show general south to southeastern compression along the Kilauea south

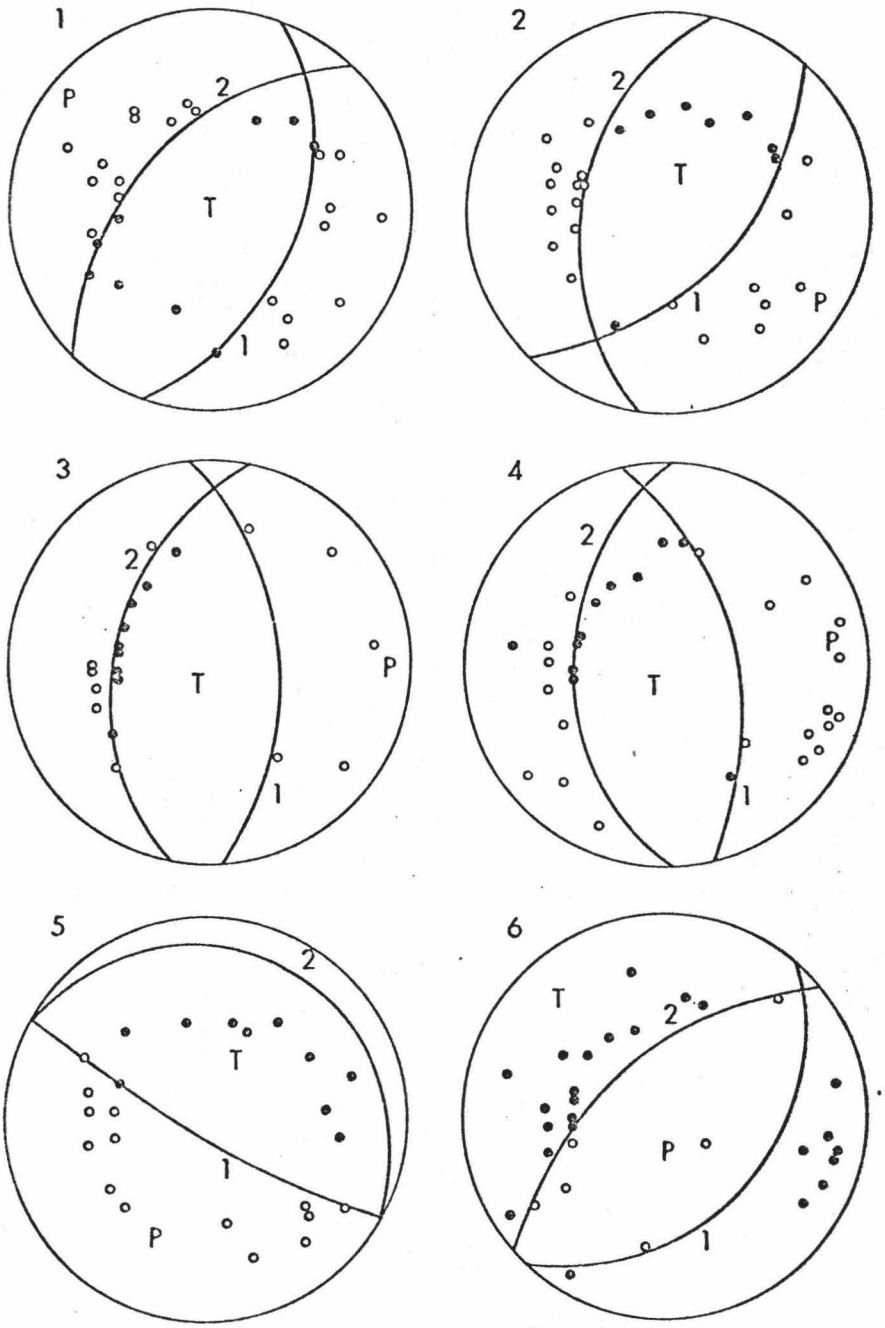

Figure 1.19 Lower hemisphere equal area projections for events 1 through 6 from Table 1.3.

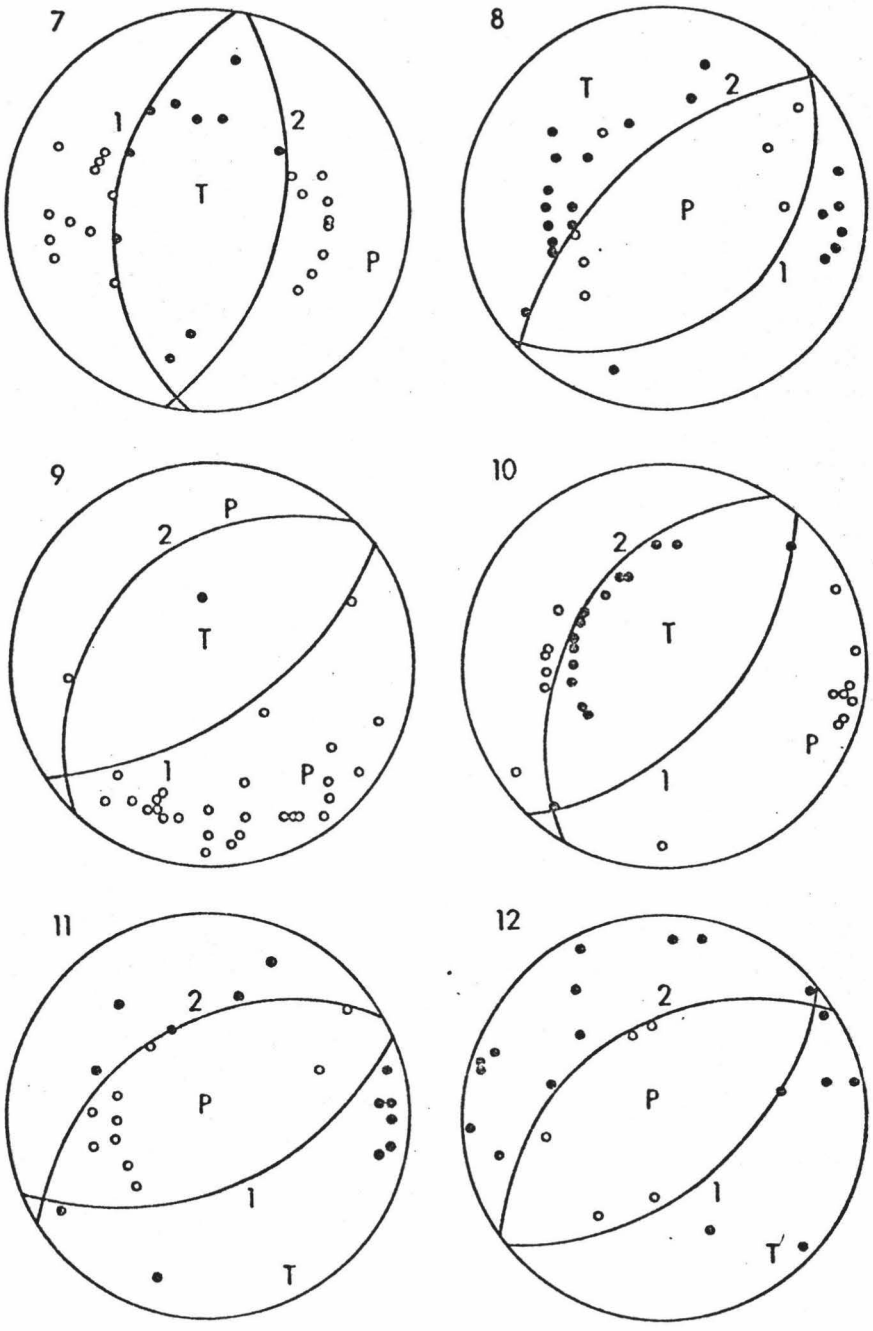

Figure 1.20 Lower hemisphere equal area projections for events 7 through 12 from Table 1.3.

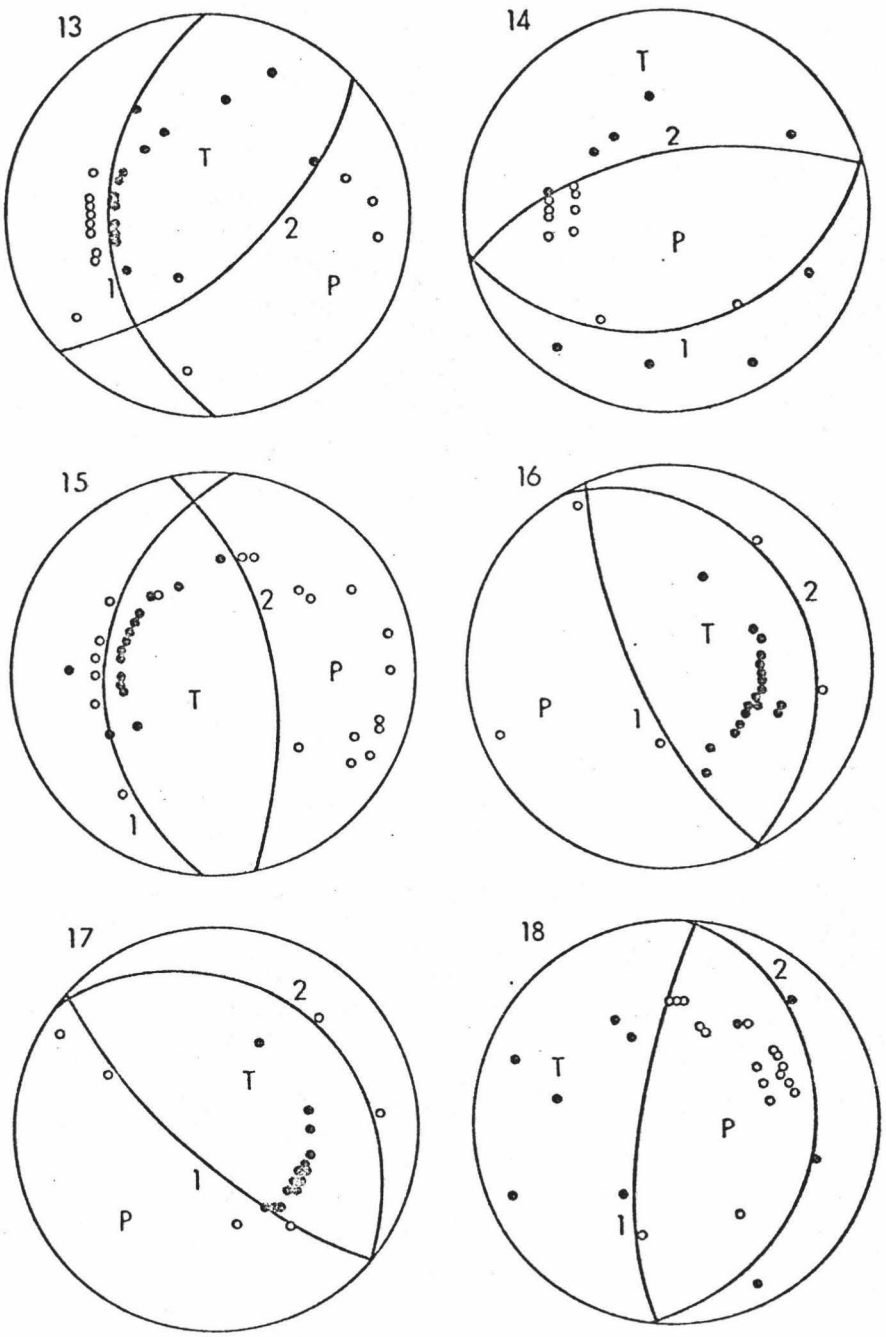

Figure 1.21 Lower hemisphere equal area projections for events 13 through 18 from Table 1.3.

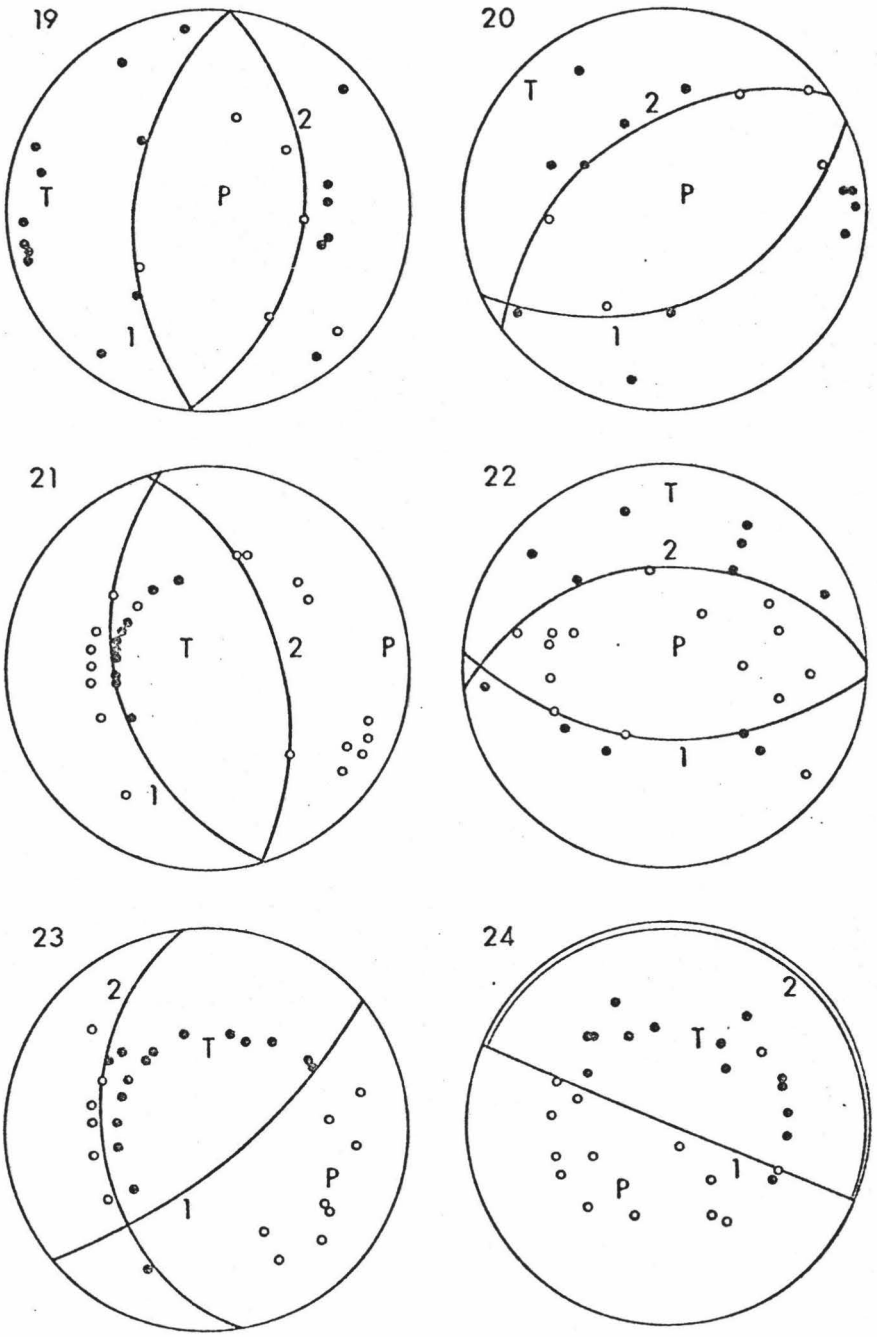

Figure 1.22 Lower hemisphere equal area projections for events 19 through 24 from Table 1.3.

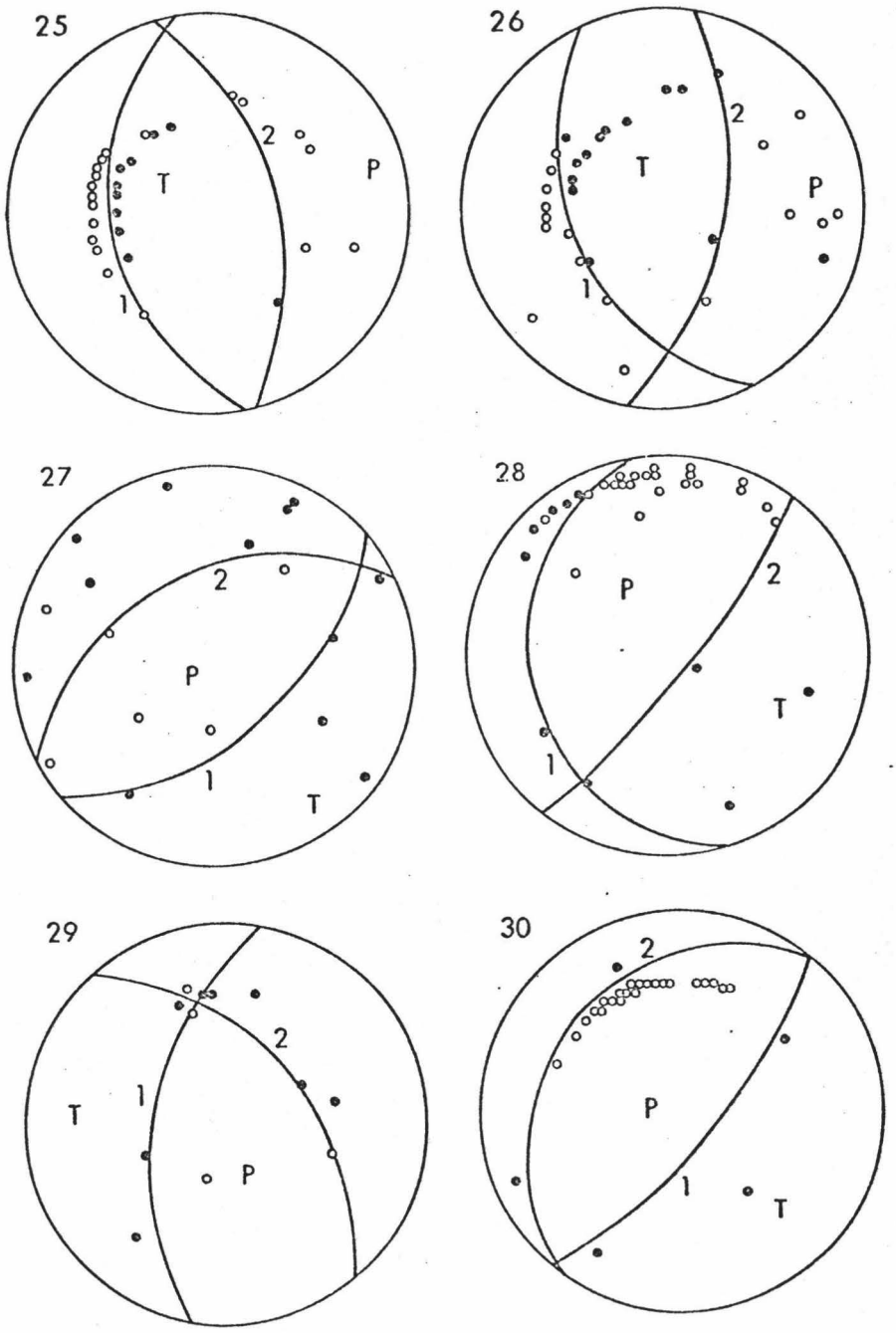

Figure 1.23 Lower hemisphere equal area projections for events 25 through 30 from Table 1.3.

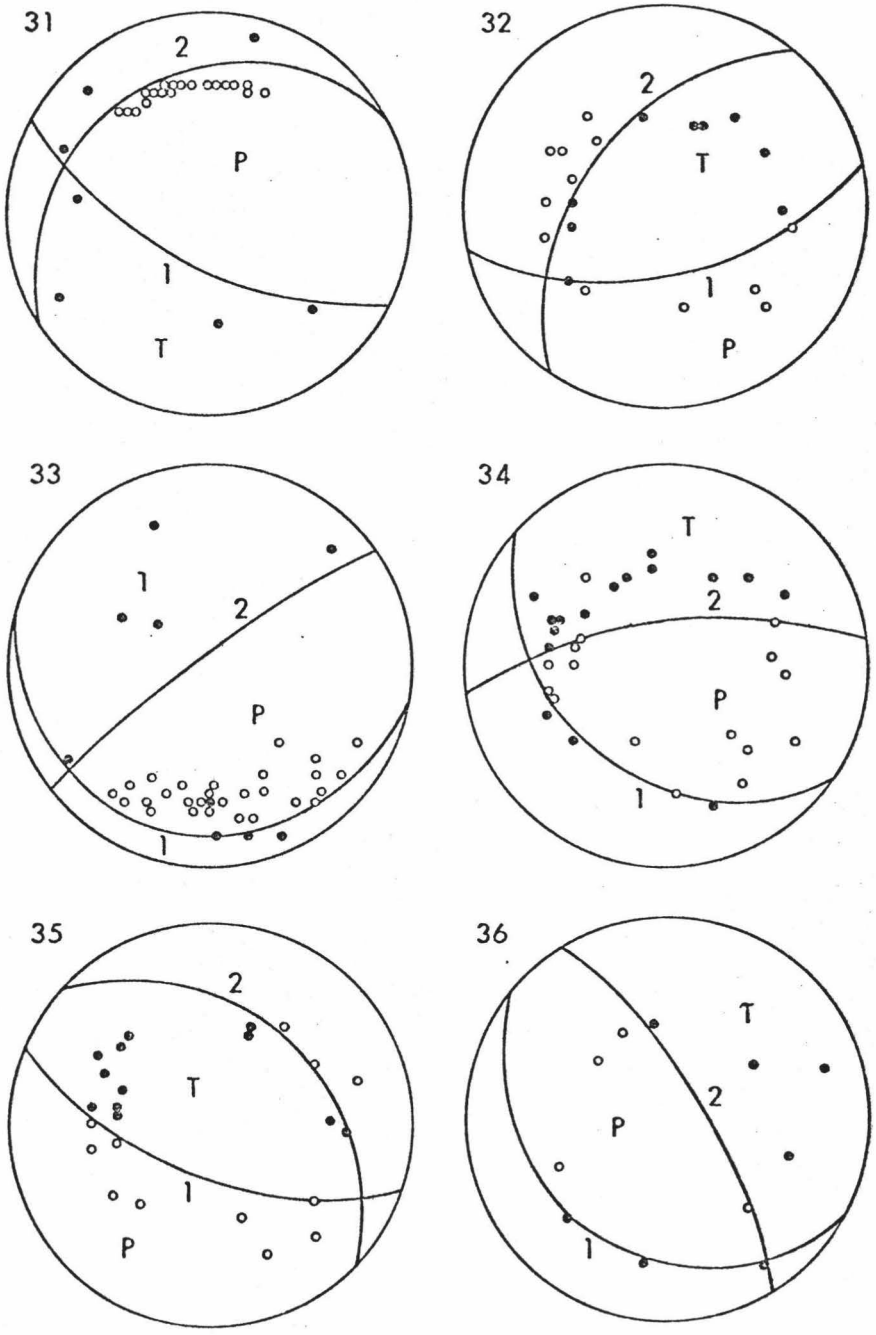

Figure 1.24 Lower hemisphere equal area projections for events 31 through 36 from Table 1.3.

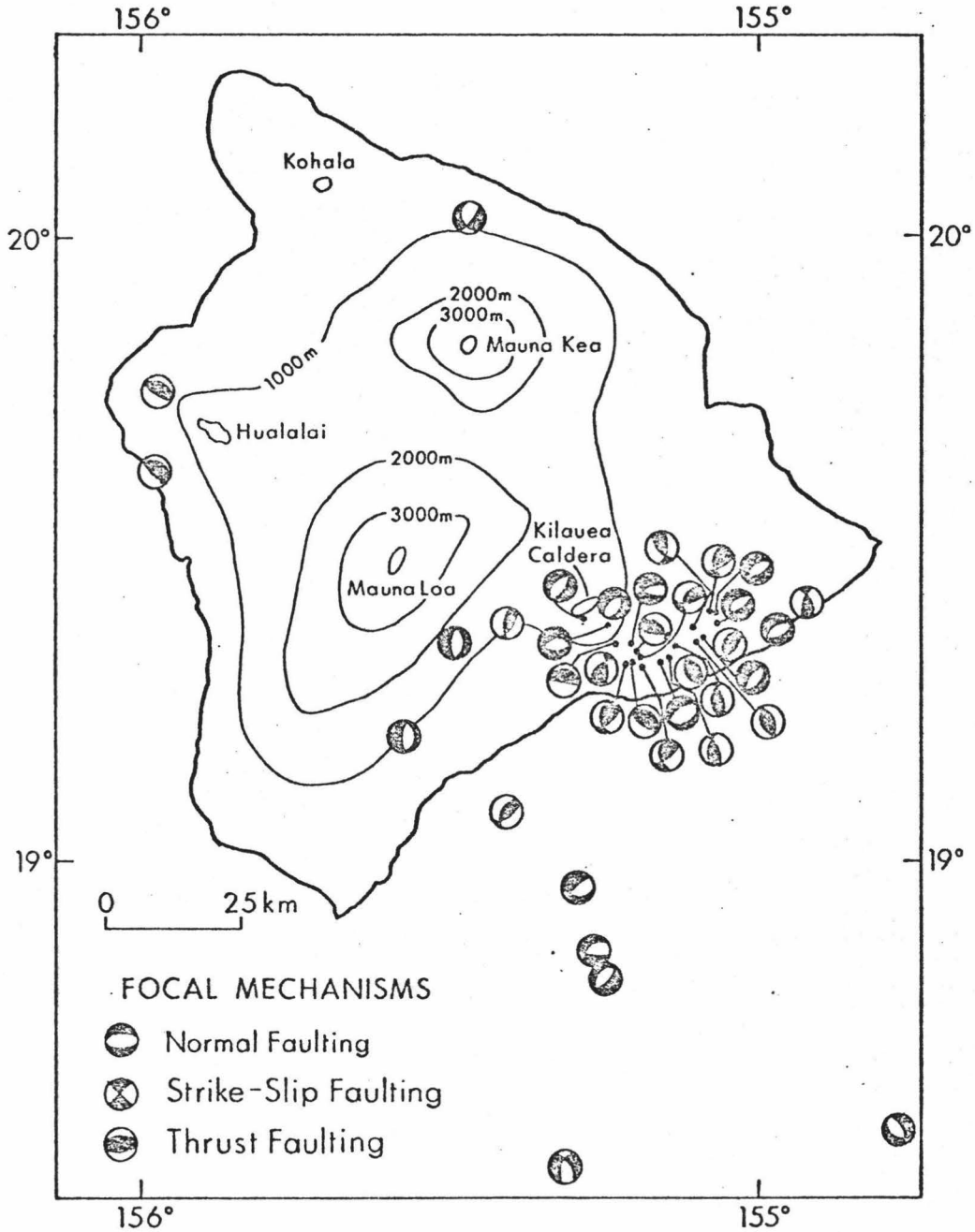

Figure 1.25 Focal mechanisms from Hawaiian Ridge study using OBS and land seismograph arrays. The focal mechanisms are equal area, lower hemisphere projections with the solid area representing the compressional quadrant and the open area the dilatational quadrant.

Figure 1.26 Summary comparison of focal mechanisms studies in Hawaii. Maximum and minimum compressive stress axes correspond to dark and open circles respectively. Numbers near upper right corner of focal areas A through H represent data sources: (1) Ward and Gregersen (1973); (2) Endo and Rogers (1978); (3) Rogers (1978); (4) Rogers (1978), Kalapana aftershocks through December 31, 1975; (5) this dissertation.

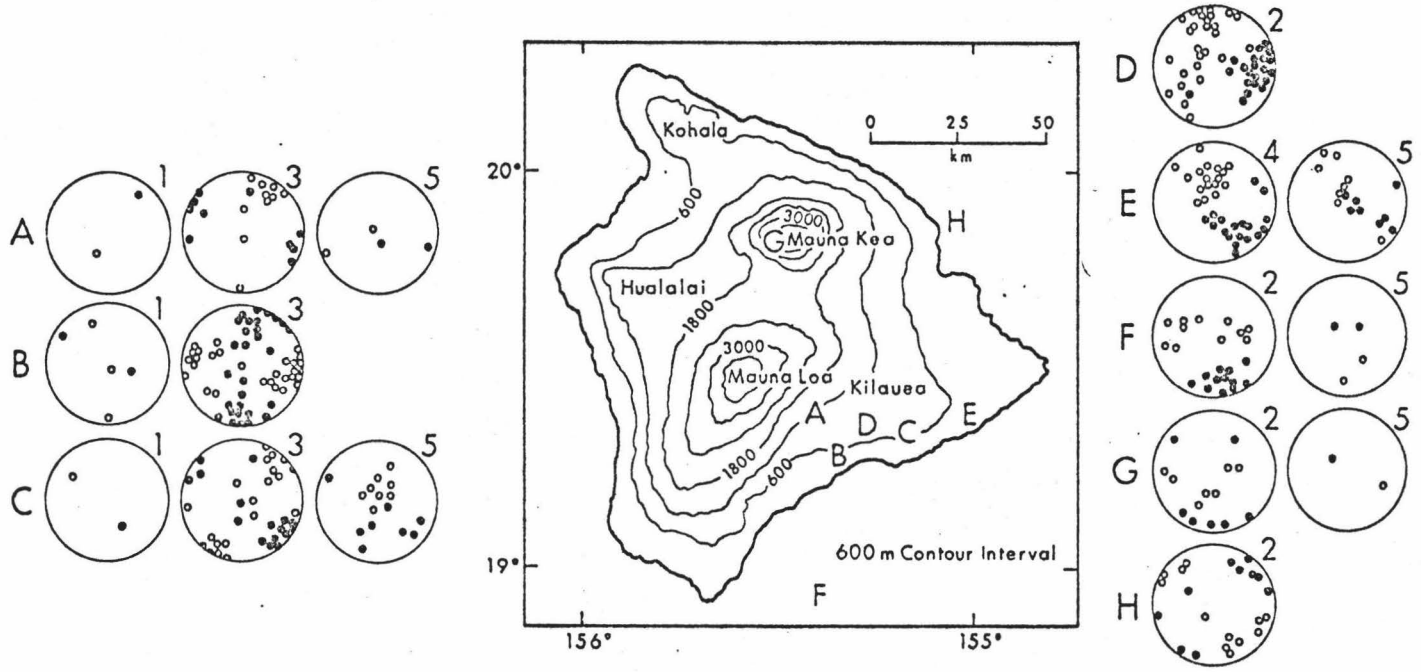
A
B
C
1
3
5
Kohala
0 25 50
km
20°
600
3000
Mauna Kea
H
Hualalai
1800
3000
Mauna Loa
Kilauea
A
D
C
E
B
1800
600
600 m Contour Interval
F
19°
156°
155°
D
E
F
G
H
2
4
5

flank and also significant vertical compression as evidenced by both high angle normal and low angle reverse faulting on the south flank of Kilauea. Also, focal mechanisms determined using both the OBS and land arrays, indicate near vertical pressure axes and horizontal tension axes for offshore upper mantle events, especially near Loihi Seamount.

1.7 B-Values and Strain Energy

In order to determine the stress distribution at depth for the southeastern Hawaiian Ridge, b-values were calculated for the entire Hawaiian Ridge and for three seismically active areas using various depth sampling intervals. B-value, the slope of $\log_{10}$ (number of events) plotted versus magnitude, is inversely related to stress, as shown by Mogi (1963) and Scholz (1968). My determinations of b-value used the cumulative method, that is, an unweighted least squares fit to the graph of $\log_{10}$ (number of earthquakes above a certain magnitude) versus magnitude. A sample population of at least 25 events was used for each b-value determination to minimize the errors in magnitude and unequal weighting of the data. The three areas chosen represent the majority of seismic activity in Hawaii: (1) Mauna Loa volcano; (2) Kilauea Volcano; (3) Kilauea East Rift Zone. A depth sampling interval of 1 km was used unless the number of events in the depth interval was less than 25. Larger sampling intervals, 2.5 km and 5.0 km, were used for the depth intervals with fewer events in the 1 km intervals.

The frequency-magnitude distributions for earthquakes along the entire Hawaiian Ridge with local magnitudes greater than 2.5 are shown in Figure 1.27 using both cumulative and differential distributions. Differential distributions use the number of earthquakes in a particular magnitude interval method versus magnitude for b-value determinations. The differential distribution is more unstable than the cumulative distribution since the number of events in a magnitude interval is dependent on interval size. Possible errors in the distributions could be caused by: (1) use of several different magnitude scales; (2) different detection thresholds at various stations; (3) instrument nonlinearity (Klein et al. (1977)). Nevertheless, the cumulative, N(M), and differential, n(m), distributions are approximately linear above a detection magnitude of 2.5 with an average b-value of 0.93 ± .10 for the entire Hawaiian Ridge.

B-value and strain energy variations with depth are plotted in Figure 1.28 for the Mauna Loa, Kilauea and Kilauea East Rift regions. B-values are difficult to interpret although b-values are generally considered to be inversely proportioned to stress. That is, the higher the stress, the lower the b-value. This is complicated by the fact that low b-values may be associated with low stress-drop events in high ambient stress regions and with events distributed over a wide source areas (Gibowicz (1973)).

As seen in section 1.5 of the hypocenter cross sections for Hawaii, there appears to be a major concentration of earthquakes between 25 and 40 km beneath Kilauea and the south flank of Hawaii.

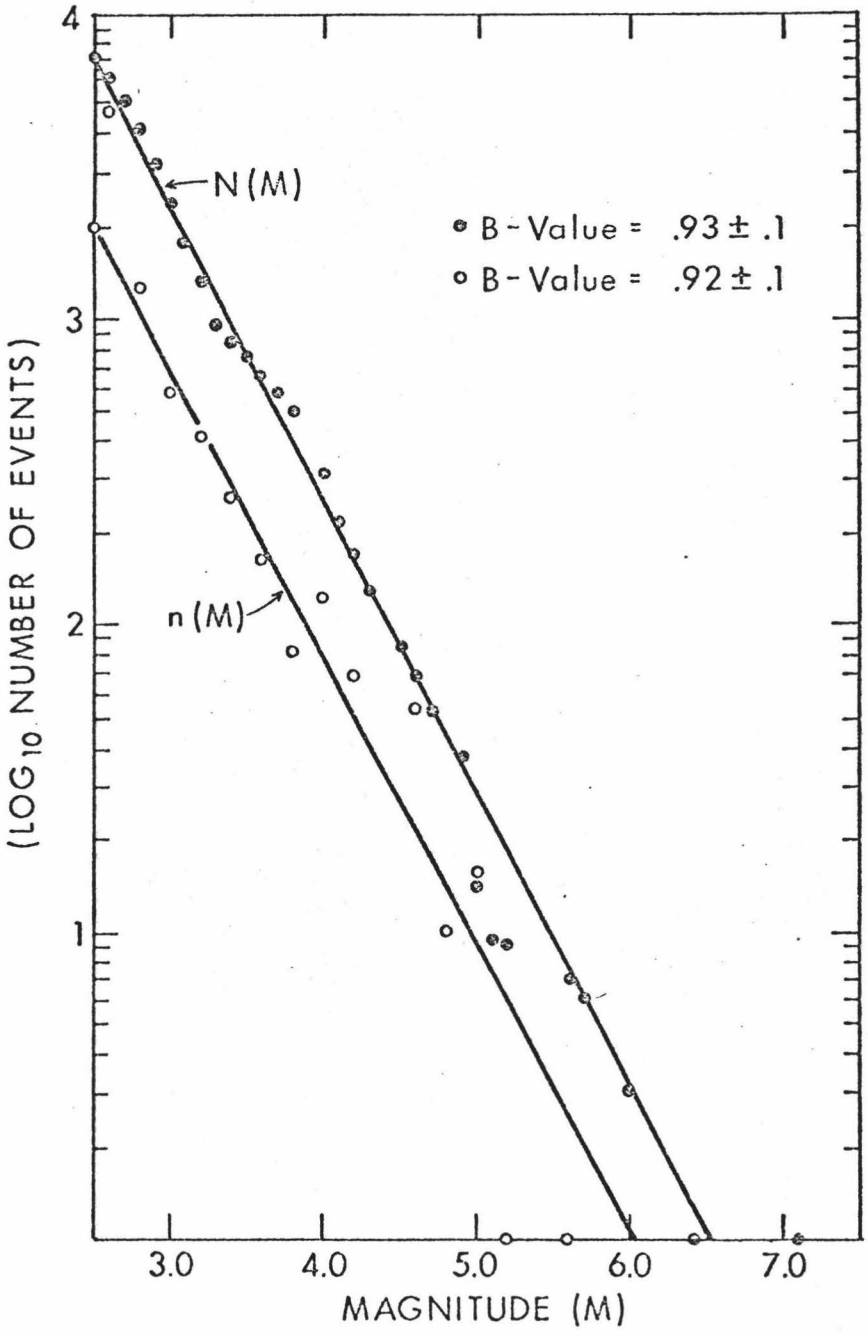

Figure 1.27 Frequency-magnitude distribution for earthquakes along the entire southeastern Hawaiian Ridge with $M_L \geq 2.5$. N(M) is the cumulative distribution and n(M) is the differential distribution.

Figure 1.28 Variation of cumulative b-value and strain energy with depth along the southeastern coast of Hawaii. All events within area of boxes used for b-value and strain energy determinations.

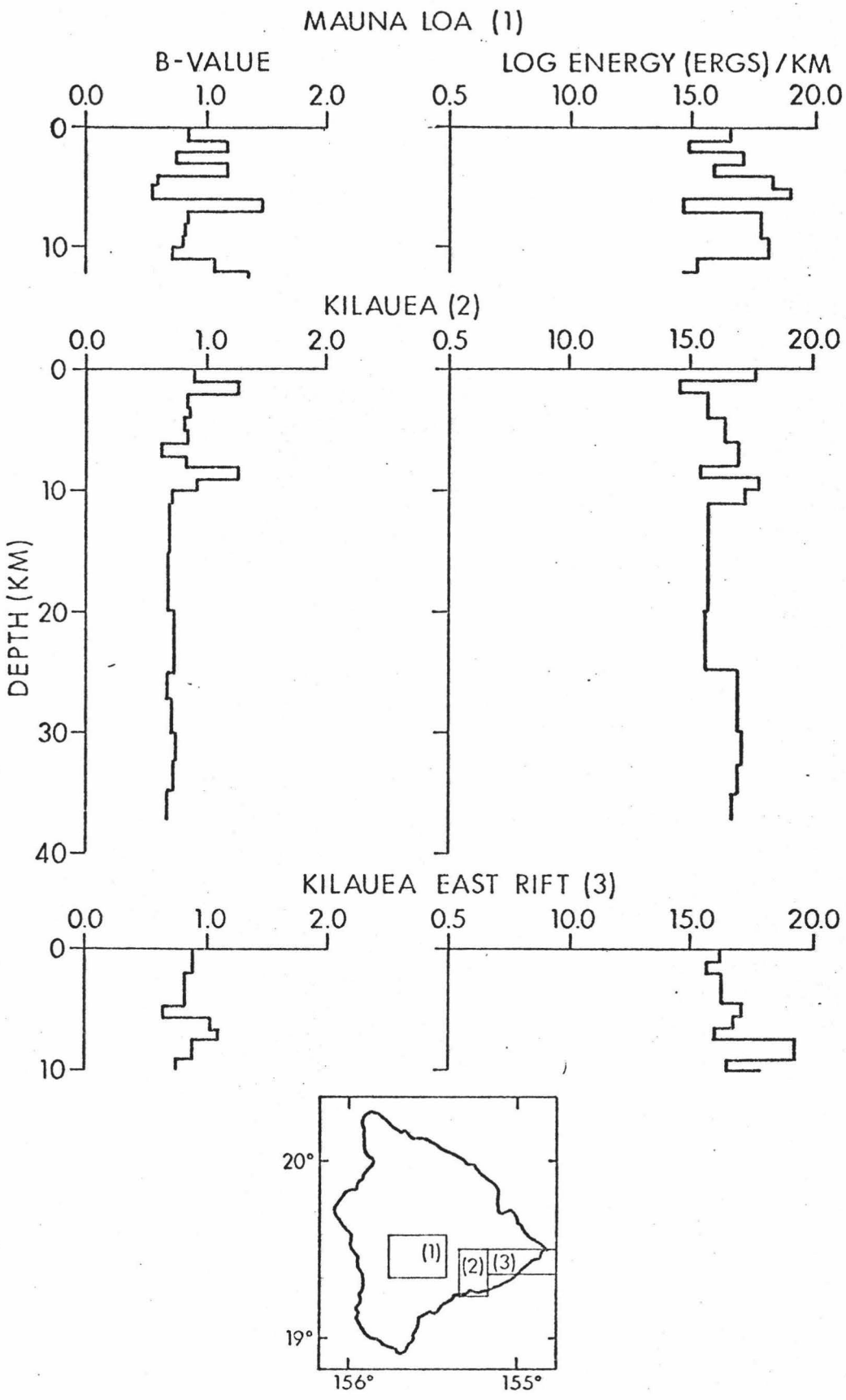
MAUNA LOA (1)
B-VALUE
LOG ENERGY (ERGS)/KM
0.0
1.0
2.0
0.5
10.0
15.0
20.0
0
10
KILAUEA (2)
0.0
1.0
2.0
0.5
10.0
15.0
20.0
0
10
20
30
40
DEPTH (KM)
KILAUEA EAST RIFT (3)
0.0
1.0
2.0
0.5
10.0
15.0
20.0
0
10
20°
19°
156°
155°
(1)
(2)
(3)

Evidence for high stress in this region is shown in Figure 1.28 by the increase in energy between 25 and 40 km in the Kilauea (2) plot, yet the b-value is not significantly different. The region of high seismicity on island hypocenter cross sections between 8 and 12 km depth is seen in Figure 1.28 energy plots. Note that the increase in energy is marked by a similar increase in b-value for Kilauea (2), indicating an increase in the number of smaller events compared to larger magnitude earthquakes.

The b-value data from this study are difficult to interpret. Further, the accuracy of the b-values is in question since the number of events in each determination varied from 25 to 300 events. Also, b-values in volcanic regions may be unrepresentative of stress values since "tectonic" earthquakes may have different b-values than either thermal or magma transport earthquakes. Decker (1978) indicates that steep thermal gradients related to injection or cooling of magma and the increase or decrease in volume of magma chambers could be responsible for stress accumulations leading to shear failure beneath active volcanoes. Extension failure caused by dike injection as suggested by Robson et al. (1968) could be another mechanism separate from low b-value shear failure.

1.8 Discussion and Conclusions

The seismotectonic evidence from this study indicates a southward migration of seismicity at depth beneath Kilauea, and southeastern crustal slumping and uplift. Most seismic activity along rift zones is generally confined to the crust and is probably not

related to deeper stresses. Hawaiian volcanic rifts vary greatly in depth and orientation but are partly influenced by stresses induced by nearby volcanic edifices (Jackson and Shaw, 1975). Eaton and Murata (1960) noted that in general each volcano has two principal rift zones that meet in the summit region at angles of 130° to 180°. If rift zones have tectonic origins then seismic activity along older rift zones might be expected, yet no such activity can be correlated with rift zones associated with Mauna Kea, Hualalai or Kohala. From the data presented (Fig. 1.9) there is some evidence that a seismically active north-trending rift zone exists on Loihi seamount, but it may be purely coincidental to a northwest-southeast regional stress pattern. The seismic data do not support the hypothesis of "pre-stressed" environment in which the favored direction of dike or rift propagation is determined before magma is injected laterally. Also, the major flank eruptions on Mauna Loa and Kilauea are in contrast to the proposed dominant influence of volcano shape.

I believe that gravitational stresses and crustal magma migration paths are the most important factors in rift formation and orientation. Crosson and Rogers (1978) state that large-scale, low-stress block movement in response to rift zone development may be an important factor in volcano evolution for the south flank of Hawaii. R. Koyanagi (personal communication) indicates that the volcanic stress system is presumably developed by the magma forcefully rising at a steep angle from the mantle. Localized stress patterns develop

where the flow of magma is temporarily disrupted and stored beneath the summit of the volcano. Shallow displacements from magmatism take place near and above the interface of the volcanic pile and crust, and the orientation of rift zones appears to be dictated by the gravitational stress field and buttressing created by earlier volcanics (as suggested by the asymmetry of crustal earthquake distribution along the east rift zone of Kilauea). Thus secondarily, peripheral earthquakes in the crust and mantle occur in response to long-term differential loading. Although it seems that there should be no regional tectonic feature that dictates volcanic activity in Hawaii, a few probably coincidental alignments of epicenters are striking, like the concentration of crustal earthquakes that form an east-west band from offshore Kealakekua to the east cape of Hawaii. Also, in looking at small increments of volcanic and seismic activities, it appears relatively straightforward that the seismic activity sets the momentum for increasing buildup of stress that ultimately results in a major seismic event such as that on November 29, 1975. Such large events could reverse the initial "cause and effect" pattern whereby the major displacement along the rift zones would allow magma to passively flow through. So in long-term processes there would be a more sympathetic "give and take" arrangement of earthquakes and volcanism.

Most important, I do not believe that a plate-wide stress field or a deep-seated fracture system in the Pacific lithosphere controls Hawaiian Ridge volcano formation and growth. The major concentration

of seismicity at depth lies beneath southern Kilauea, not directly along the rift zones. Scattered seismicity extends down to 60 km although the variation of b-value with depth indicates decreasing stress below 40 km. No indication of a propagating fracture was observed for offshore Hawaii.

I believe that the episodic magmatic inflation and deflation of the Hawaiian volcanoes are responsible for the Kilauea southwestern compression and extensional features. Further, I feel that due to the large surface separation of the eruptive sites and similarities of tholeiitic volcanics, a primary source of magma exists at depths greater than 60 km, with multiple migration paths and secondary magma reservoirs at intermediate depths. The only obvious reservoir in the upper mantle from the seismicity is below Kilauea, although others may be present below Loihi seamount and farther to the south. Ellsworth (1978) has used an iterative three-dimensional velocity modeling technique using 144 teleseismic events to interpret a low velocity zone in the asthenosphere 100 km to the east of Hawaii in line with the axis of the older islands of the Hawaiian Ridge. Our study indicates that this region is not associated with any overlying volcanism or significant earthquake activity. A second low velocity zone (Ellsworth, 1978) located about 100 km south of Kilauea also shows little seismic activity.

Several essential factors discussed in this paper must be accounted for in proposing a hypothesis for the evolution of the Hawaiian Ridge: (1) the concentration of seismicity along the rift

zones and at depth beneath south Kilauea; (2) the fresh pillow basalts of nearby seamounts; and (3) the historic eruptions along the ridge. I believe that a melting anomaly below the lithosphere (hot spot) could produce each of these features. The problem raised by Jackson et al. (1972) of why the Hawaiian Ridge is not a single continuous volcanic ridge remains unsolved, but perhaps the hot spot melting anomaly is large enough to generate a broad region of secondary magma reservoirs. The large volume of Hawaii compared to the other major Hawaiian islands seems to indicate: (1) an increase in volcanism in the last 0.5 my; and (2) a slowdown and/or change in the direction of the Pacific plate motion from northwest to north relative to the melting anomaly.

Two ideas that need further research are the relation of the duration of volcanism to magma source depth and the possible migration of magma due to overload pressure. If the duration of volcanism and the frequency of eruptions, or both, increase with time then this may imply a systematic decrease in magma source depth as the hot spot burns itself out or becomes shallower with age, expending energy in more frequent eruptions of shorter duration, forming larger islands.

The data presented in this paper indicate a continued southeastern evolution of the Hawaiian Ridge by formation of seamounts through the oceanic crust. Locally, the seismicity indicates a concentration of activity to the south-southwest of Kilauea near Loihi seamount. The pillow basalts photographed by Moore (1964, 1969) at Bushnell Seamount indicate that it may be an active volcano; however, seismicity indicates that no shallow connection exists

between Kilauea and Bushnell Seamount. A plume hypothesis modified from Morgan (1971, 1972a, 1972b) seems to account for the evolution of the Hawaiian Ridge and its present growth to the southeast. A fundamental question regarding the nature of magma intruding from a deep source to a shallow magma chamber or the surface, is whether the magma produces its own path upward or follows a fracture system caused by external stresses (Decker, unpublished text, 1978). Hawaiian ridge seismicity data (Fig. 1.29) seem to indicate no large regional or tectonic concentrated external stresses at depth other than dispersed island loading faulting in the lithosphere. The majority of events beneath Hawaii in the upper mantle are related to magma movement, deflation and inflation episodes. The high stress region and large concentration of earthquakes 25 to 40 km beneath Kilauea represents a major magma intrusion zone beneath Hawaii. Shallow magma chambers and rift zones are probably fed from this 25- to 40-km sub-Kilauea zone, and low stress events below this zone probably represent primary feeding to the 25- to 40-km zone.

1.9 Future Work

Results from this dissertation indicate that dredging, underwater photography (if possible), and OBS seismicity programs are needed in the offshore areas of Loihi and Bushnell Seamounts. Presently all earthquakes offshore are located entirely by onshore stations from a one-sided array. OBS surveys would be ideally suited for epicenter locations and focal mechanism studies in these small active regions. Questions that need clarification are: (1) location and

Figure 1.29 Hypocenter cross section for all events along south-eastern Hawaiian Ridge. All events are projected along A-A' plane.

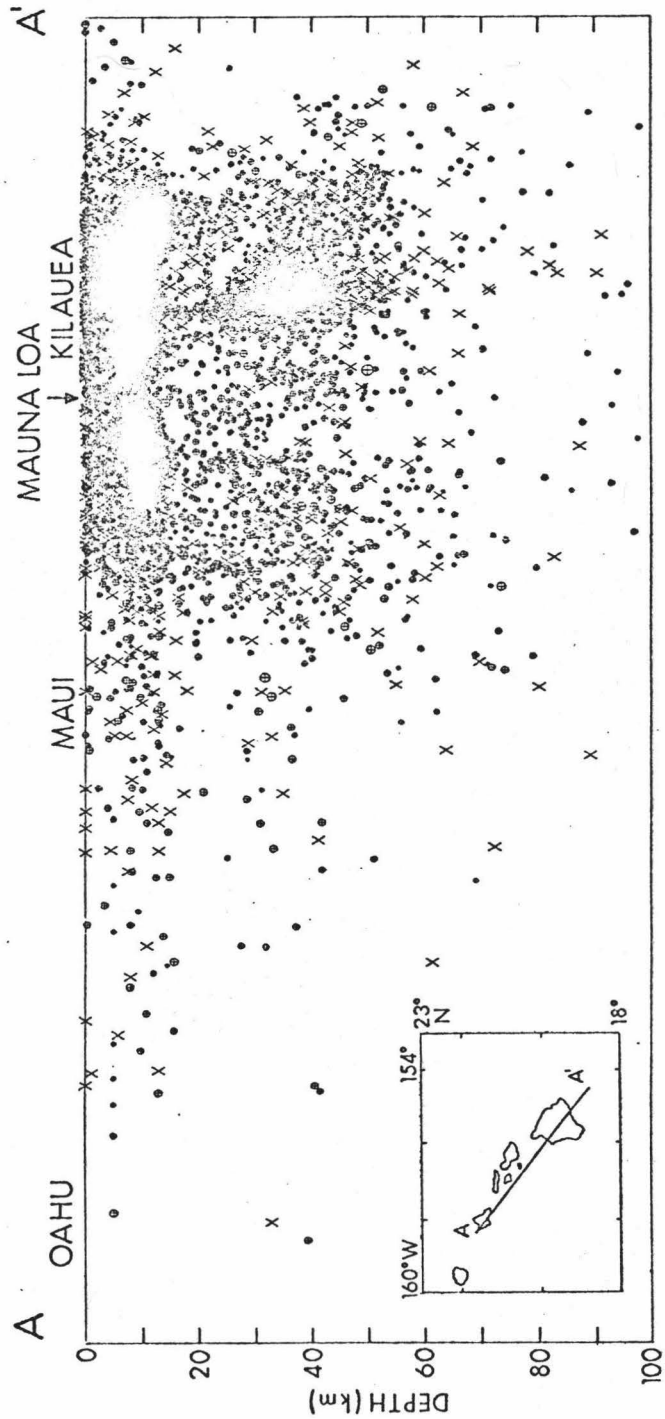
A
A'
OAHU
MAUI
MAUNA LOA
KILAUEA
DEPTH (km)
0
20
40
60
80
100
160°W
154°
23° N
18°

depth of events on offshore seamounts; (2) focal mechanisms; (3) the association of this local seismicity with possible submarine volcanism; (4) the presence of undetected low magnitude events offshore Hawaii, detectable only by OBS deployments; (5) the migration of upper mantle or crustal magma reservoirs offshore due to hot spot migration, evidenced by surface dredging and underwater photos.

2. VELOCITY STRUCTURE OF THE SOUTHEASTERN HAWAIIAN RIDGE USING TAU INVERSION

2.1 Introduction

In an attempt to determine an adequate velocity model with limits for epicenter location and velocity structure along the Hawaiian Ridge, the Tau Inversion method was applied to Hawaiian Ridge earthquake travel time data. The Hawaiian Ridge is instrumented by seismograph stations (Fig. 1.2) of the Hawaii Volcano Observatory (HVO), Honolulu Tsunami Observatory (HTO) and Hawaii Institute of Geophysics (HIG). Using these seismometer arrays and Hawaiian earthquakes (Estill and Odegard, 1978), travel time sampling of the crust and upper mantle were obtained.

Previous studies of the velocity structure of the island of Hawaii by Eaton (1962), Ryall and Bennett (1968), Hill (1969), Ward and Gregersen (1973) and Ellsworth and Koyanagi (1977) are shown in Figure 2.1. Important findings of the previous studies applicable to Tau Inversion results are: (1) higher P-wave velocities along volcano summit and rift zones than in the shield areas due to the presence of denser igneous intrusives; (2) greater velocity variation in the crust than in the mantle under Hawaii (Hill, 1969), and (3) no large P-wave low velocity zones caused by magma reservoirs in the upper mantle, but either an extensive magma conduit system or narrow magma pathways at depth (> 40 km) (Ellsworth and Koyanagi, 1977). Offshore refraction profiles along the Hawaiian Ridge discussed by Furumoto et al. (1973) indicate mantle depths between 12 km and 20 km for the

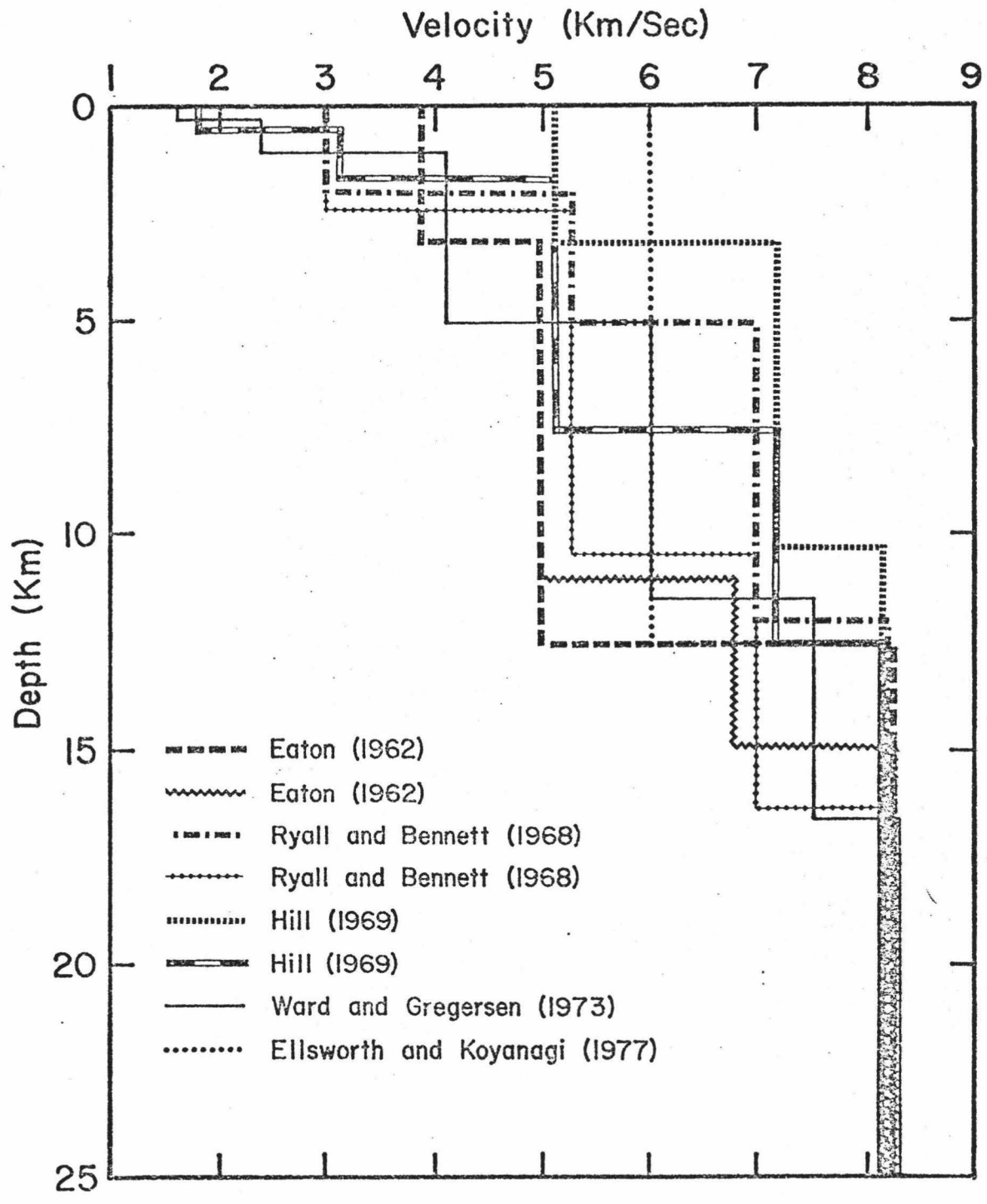

Figure 2.1 Velocity-depth profiles for southeastern Hawaiian Ridge.

major islands of the Hawaiian chain and some evidence for systematic increase of Moho depth with island age.

2.2 Data Analysis

Travel times to seismograph stations were determined from 65 earthquakes occurring along the Hawaiian Ridge during the period July 20, 1976 to March 30, 1977. These events were relocated by use of arrival times at seismographs located along the Hawaiian Ridge (Estill and Odegard, 1978). Travel times were corrected to sea level using an assumed velocity of 5.5 km/sec. The assumed velocity may bias surface velocity determinations but will not significantly affect deeper determinations. The travel times, shown in Figure 2.2, are plotted versus distance with a reducing velocity of 7.0 km/sec. Travel times with distances out to 120 km are Hawaii Island and nearshore events, whereas greater distances correspond to travel times to Maui and Oahu seismographs stations from events on Hawaii. In order to determine velocity-depth limits from this data, the Tau method (Bessonova et al., 1974) was used for inversion.

The Tau inversion process consists of three main steps. First, Tau versus distance data are plotted using the intercept time and a set of assumed ray parameters where Tau is the intercept time for a given distance and ray parameter. The limits on the maximum Tau are determined for each ray parameter and gave Tau as a function of the ray parameter. A plot of Tau versus distance for Hawaiian Ridge travel time data for a ray parameter of 920 sec/km is shown in Figure 2.3. Because of the scatter, ~~this~~ these data ~~was~~ were filtered by means

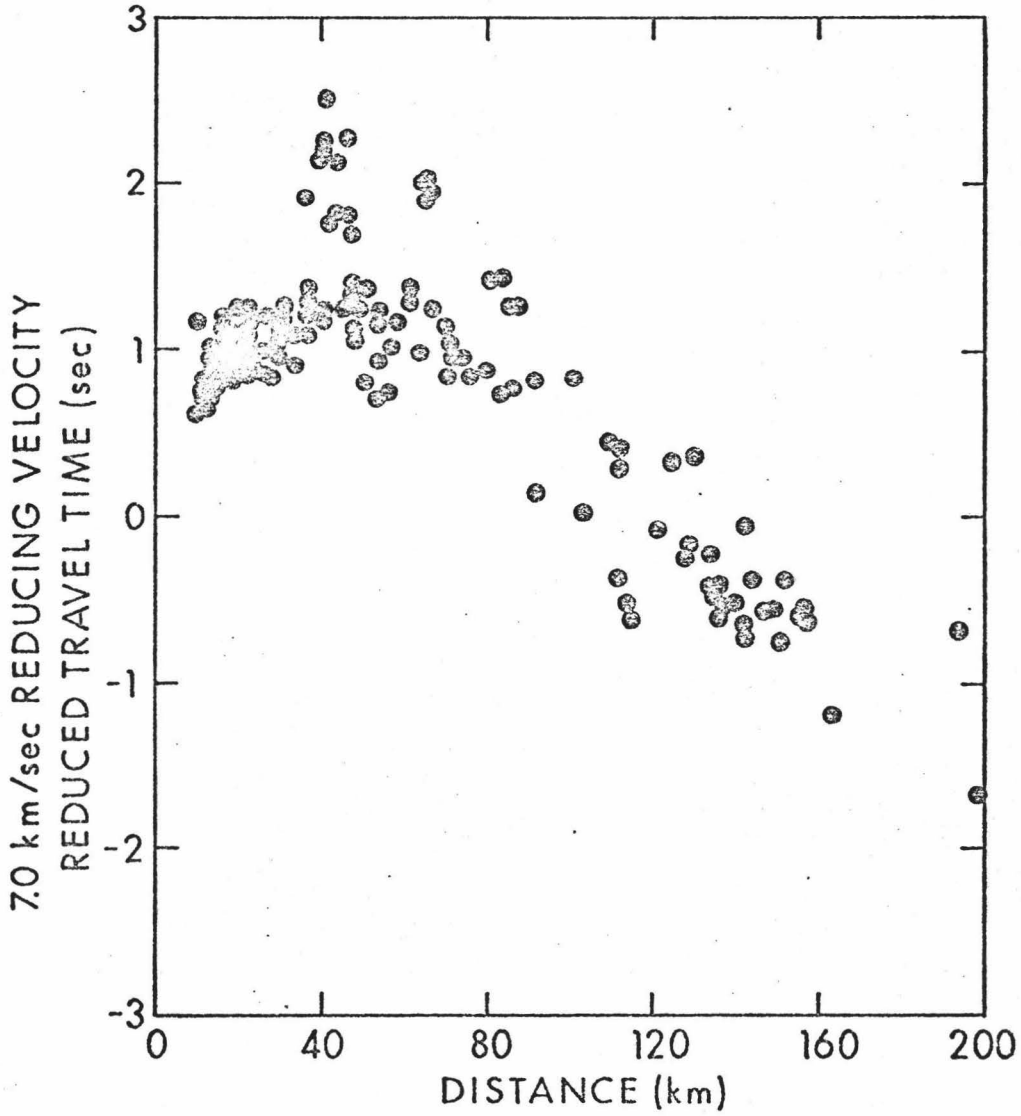

Figure 2.2 Plot of reduced Hawaiian Ridge travel time data used for inversion. Reducing velocity equals 7.0 km/sec.

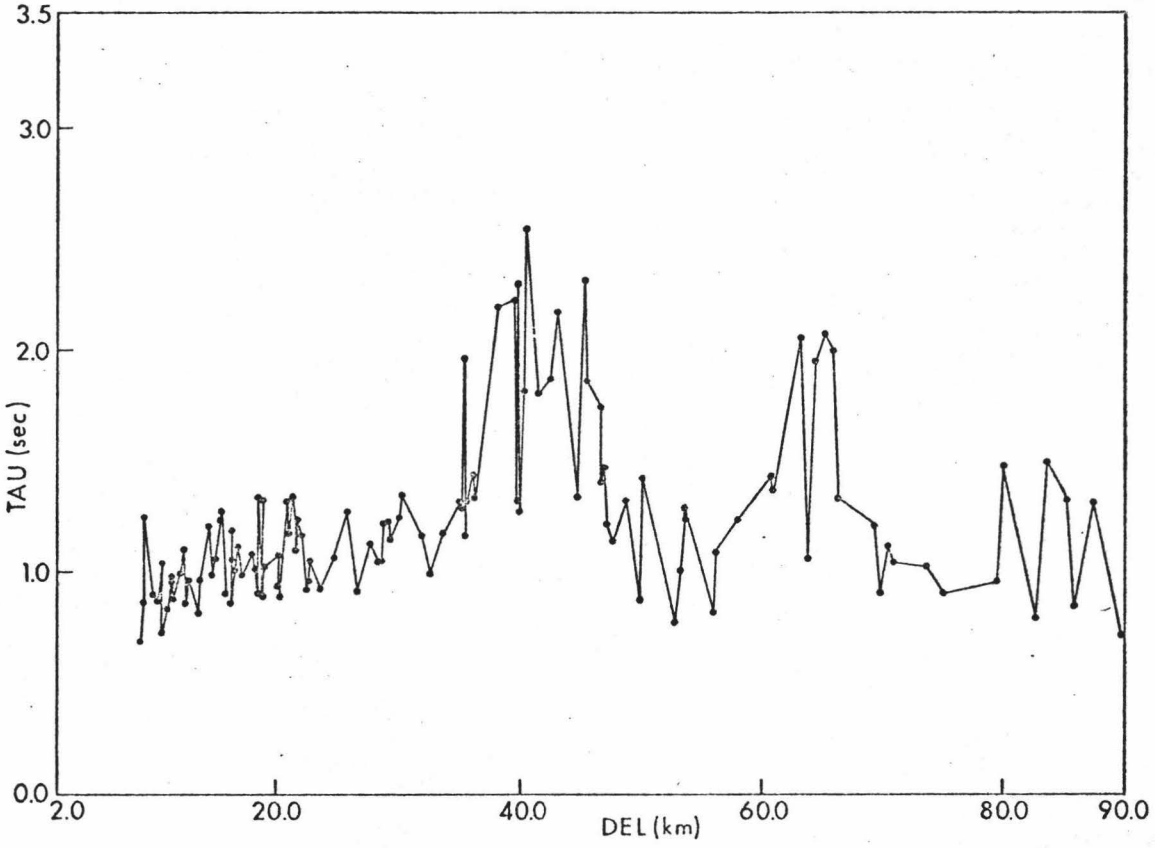

Figure 2.3 Tau versus distance plot for a ray parameter of 920 sec/km where Tau can be represented as the time intercept of the travel time-distance data. Note large Tau anomalies centered at 43, 65 and 85 km corresponding to Kilauea, Mauna Loa and Mauna Kea.

of a center-weighted moving average filter as shown in Figure 2.4. The large peaks at 43 and 65 km and the less distinct peak at 85 km correspond to distances for events with ray paths that passed beneath three major volcanoes of the island of Hawaii: Kilauea, Mauna Loa and Mauna Kea. Since Tau is the intercept time for a given distance and ray parameter, these peaks indicate that there is a time delay caused by the structure beneath the three volcanoes.

The second part of the Tau method involves construction of an envelope of the Tau versus ray parameter values found in the first part. The extent of scatter in the data was considered and the time delays associated with the three volcanoes were eliminated. The third operation in the Tau process is integration of the Tau integrals to determine limits of the velocity depth function consistent with the travel time data. These integrations were performed by means of an averaging interval over the ray parameter that was consistent with the scatter in the data. The best averaging interval is the one that minimizes the differences between an average model and the velocity-depth limits and varies for different portions of the velocity depth function.

The computer program used to invert the data first calculates an average model by means of Herglotz-Wiechert inversions and the Tau-ray parameter envelope. The limits are then calculated for various averaging intervals, as shown in Figure 2.5, essentially contouring the limits. All models consistent with the travel time data are contained within the limit contours closest to the average model.

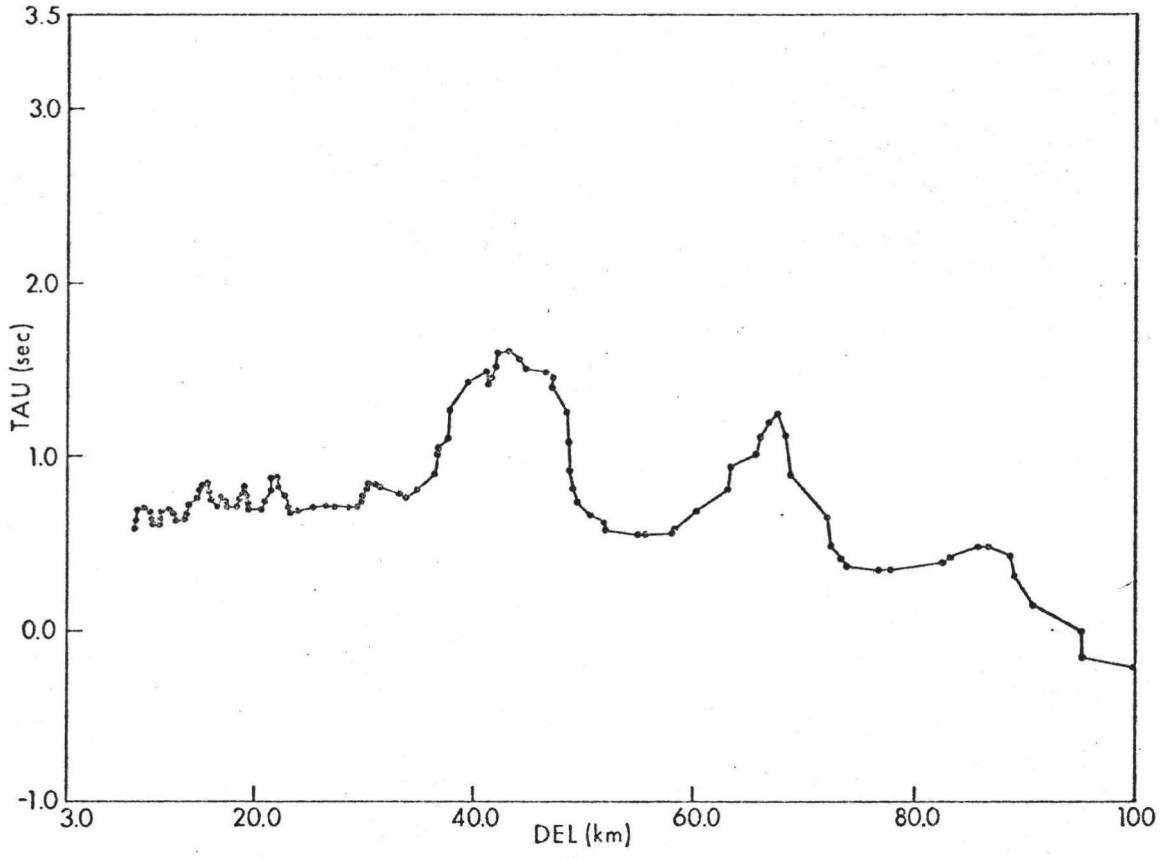

Figure 2.4 Filtered Tau data from Figure 2.3 using center weighted moving average filter.

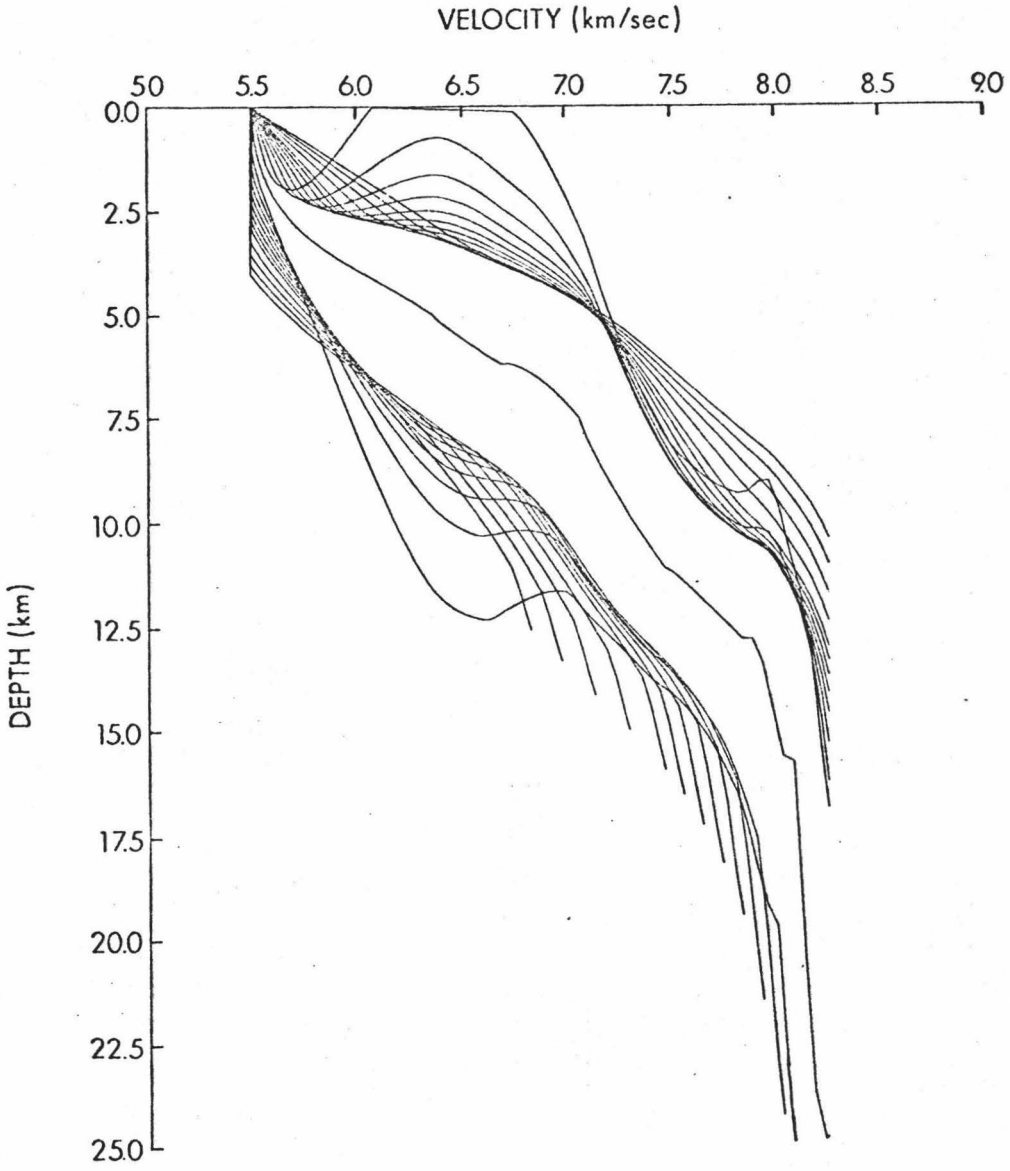

Figure 2.5 Velocity-depth function for Hawaiian Ridge showing extremal bounds and contour plot of limits around average model. Any model consistent with the travel time data are contained within the limit contours closest to the average model.

2.3 Discussion and Conclusion

Three large delay times are noted for epicentral regions corresponding to three major volcanoes on Hawaii: Kilauea, Mauna Loa and Mauna Kea. Because they are so large, the delays must be caused in part by errors in hypocenters and topography corrections. Furthermore the size of the three time delays should not be taken as direct evidence of magma or partial melt at shallow depths, but as partly due to lower velocity shield volcanics lying above higher velocity igneous intrusives. Ellsworth and Koyanagi (1977) and Hill (1969) also note that the mean crustal P-wave velocities within summit and rift areas of Kilauea are substantially higher than shield area velocities, because of possible differences in structure. Applying the techniques described in this paper to a more detailed P- and S-wave study could help to determine limits on contrasting crustal velocities for shield and rift areas as a possible explanation of the observed time delays.

Velocity depth model and extremal limits resulting from the Tau inversion procedure are shown in Figure 2.5 and Table 2.1. Physically, the average velocity-depth model for the Hawaiian Ridge shows the assumed velocity of 5.5 km/sec near the surface, a change in velocity from 5.9 km/sec to 7.2 km/sec between 4 km and 7.5 km and then a gradual increase to 7.5 km/sec at 11-km depth. Between 11 km and 12.5 km the velocity increases rapidly to 7.9 km/sec. Moho velocity of 8.0 km/sec is reached between 12.5- and 15-km depth, and the velocity is essentially constant at 8.1 km/sec below 15 km.

TABLE 2.1

VELOCITY-DEPTH VALUES FOR AVERAGE MODEL

Depth (km)	Velocity (km/sec)
0.772	5.511
1.335	5.535
1.721	5.558
2.033	5.583
2.302	5.607
2.541	5.631
2.758	5.656
2.958	5.681
3.144	5.707
3.318	5.732
3.483	5.758
3.639	5.784
3.787	5.810
3.929	5.837
4.065	5.837
4.065	5.863
4.195	5.890
4.320	5.918
4.441	5.945
4.557	5.973
4.669	6.001
4.778	6.029
4.883	6.058
4.985	6.087
5.084	6.116
5.180	6.145
5.273	6.175
5.364	6.205
5.451	6.235
5.537	6.266
5.620	6.297
5.701	6.328
5.779	6.360
5.856	6.392
5.930	6.424
6.003	6.456
6.073	6.489
6.142	6.522
6.209	6.556
6.274	6.590
6.337	6.624
6.398	6.658
6.458	6.693
6.358	6.729

TABLE 2.1 (Continued)
VELOCITY-DEPTH VALUES FOR AVERAGE MODEL

Depth (km)	Velocity (km/sec)
6.352	6.765
6.375	6.801
6.421	6.837
6.492	6.874
6.586	6.911
6.707	6.949
6.856	6.987
7.034	7.025
7.243	7.064
7.722	7.103
8.123	7.142
8.498	7.182
8.863	7.223
9.222	7.263
9.575	7.305
9.922	7.347
10.262	7.389
10.593	7.432
10.914	7.475
11.063	7.519
11.293	7.563
11.552	7.608
11.830	7.654
12.126	7.700
12.440	7.746
12.773	7.793
13.125	7.841
13.459	7.889
14.031	7.938
14.815	7.987
15.591	8.036
15.489	8.087
22.679	8.130

The velocity depth function determined by the Tau inversion procedure agrees in its major features with the more recent Hawaiian crustal refraction studies shown in Figure 2.1. The models with significant lower velocities at depth fall outside the limits of the Tau model, indicating possible effects from the areas that caused the Tau delays shown in Figure 2.4. Further, the average Moho depth of 12.5 to 15 km from the Tau model is significantly less than the depths of greater than 18 km given by Furumoto et al. (1968) for some sections of the Hawaiian Ridge. Thus there is no apparent thickening of layer 3 and the amount of lithospheric flexural deflection should be considerably less than that assumed by Walcott (1970) and Watts and Cochran (1974). The Tau model is, however, in closer agreement with the 2- to 3-km deflection inferred by Woollard (1970) and Suyenaga (1978) using the 2- layer 3 boundary.

The Tau method has been shown to be a useful inversion technique for determining velocity-depth limits on travel time data. Also, the Tau-distance-ray parameter diagrams are useful in delineating heterogeneous structures. Further work, which should include more detailed P-wave and S-wave travel times from Hawaii, should indicate how important the assumption of lateral homogeneity is to the Tau method.

3. COMPUTER PROGRAMS FOR SEISMICITY STUDIES

3.1 Introduction

This chapter was written for the purpose of providing documentation for computer programs used in OBS data reduction, specifically seismicity studies. Earthquake research at HIG has generally been limited to exploration seismology and to the use of published reports for earthquake information. The programs described in this report will enable HIG researchers to independently determine seismicity information from OBS cassette tapes. Some background in earthquake seismology is assumed and a section of useful programs for earthquake studies is provided as a boot-strap guide.

The programs described in this report will serve as HIG's operational software for OBS seismicity studies (Table 3.1). Preliminary seismicity studies from the Hawaiian Ridge study should be very useful in determining program requirements in terms of array dimensions, minimum number of OBS's and threshold earthquake magnitude required for epicenter determinations. It is hoped that OBS's will provide greater accuracy in epicenter/hypocenter determinations and make microseismicity studies of the ocean floor routine. As a final note it should be emphasized that as better and more numerous OBS data become available, improvements in epicenter resolution will be observed.

TABLE 3.1

OBS SEISMICITY DATA REDUCTION FLOW CHART

OBS
Cassette Tape

Visicorder
Record

Dubbed Tape
of Events of Interest

Expanded Playback
of Events

Pick arrival times,
signal amplitude/duration,
first motion, etc.

Input to HYPO71:
Velocity Model
Station Locations
Datum Corrections
Solutions Parameters Desired
Station Arrival Times
First Motion
Signal Amplitude/Duration

Output of HYPO71:
Epicenter
Hypocenter
Magnitude
Solution Error Estimates
P and S Wave Travel-Time Residuals
Focal Mechanisms

CROSEC QUAKE B-VALVE

3.2 Earthquake Location Program: HYPO71

HYPO71 is a computer program for determining epicenter, hypocenter, magnitude and first motion pattern of local earthquakes. This program was designed for world-wide usage and a user's manual was released as an open-file report of the U. S. Geological Survey by the program authors (Lee and Lahr, 1972). Documentation for HYPO71 (Revised) is 114 pages in length and therefore will not be reproduced here. A computer listing of HYPO71 (Revised) with minor changes, for use on the IBM 370 at the University of Hawaii, is available from the author of this dissertation.

3.3 Epicenter Plotting Program: QUAKE

Program QUAKE written by the author takes HYPO71 epicenter output cards and plots epicenters on a mercator projection. Earthquakes may be sorted by location, date, depth and magnitude before plotting. A (Cal-Comp-Harris) plot routine plots each event according to location and magnitude with reference points also plotted to properly align epicenter plot on geological map. Plot parameters are listed on output along with a listing of earthquakes and reference points. If the numbering of events option is chosen (Table 3.2), each plotted event will have a specific number plotted beside it and be listed on output in sequential order.

TABLE 3.2

PROGRAM QUAKE INPUT

Input:

No. Cards	Format	Description
1	4F10.2, I3, 2X, 3F5.1, I1	CMER = Central Meridian degrees
		XMAX = number of inches of plot in x-direction
		XMAX = number of inches of plot in y-direction
		HEI = height of number symbol in inches
		NN = number of reference points
		MAGC = magnitude cut-off value
		DEPTHB = depth in km of lower depth limit
		DEPTHT = depth in km of upper depth limit
		NUMNUT = set equal to 2 if no numbers next to epicenter required or event listing
1	5F10.2	XBLAD,XBLAM = latitude in degrees and minutes of epicenter map origin
		XBLOND,XBLONM = longitude in degrees and minutes of epicenter map origin
		SCALE = map scale (number of km on ground to number of inches on epicenter map)
	2I10	BDATE = beginning date desired EDATE = ending date desired

TABLE 3.2 (Continued) PROGRAM QUAKE INPUT

No. Cards	Format	Description
1	4F10.2	RLADLH,RLAMLH,RLODLH, RLOMLH = latitude and longitude in degrees and minutes of upper left point of sorting box
1	4F10.2	RLADLL,RLAMLL,RLODLL, RLOMLL = latitude and longitude in degrees and minutes of lower left point of sorting box
1	4F10.2	RLADRH,RLAMRH,RLODRH, RLOMPH = latitude and longitude in degrees and minutes of upper right point of sorting box
1	4F10.2	RLADRL,RLAMRL,RLODRL, RLOMRL = latitude and longitude in degrees and minutes of lower right point of sorting box
1-N card	HYP071 output epicenter cards	
1	I6	999999
1-NN	4F10.2	REFLAD,REFLAM,REFLOD, REFLOM = latitude and longitude in degrees and minutes of reference points

```
C**  EPICENTER PLOT******
     DIMENSION REFLAD(100),REFLAM(100),REFLOD(100),REFLOM(100)
     INTEGER DATE,ORGHM,GAP,BDATE,EDATE
     REAL LATNM,LONGWM,MAG,MAGC
     CALL MODE(0,1200,0,0)
      CALL PLOTS(0,0,0)
     READ(5,1) CMER,XMAX,YMAX,HEI,NN,MAGC,DEPTHB,DEPTHT,NUMNUT
   1 FORMAT(4F10.2,I3,2X,3F5.1,I1)
     READ(5,18) XBLAD,XBLAM,XBLOND,XBLONM,SCALE,BDATE,EDATE
  18 FORMAT(5F10.2,I10,I10)
     CALL UTMC(XBLAD,XBLAM,XBLOND,XBLONM,YB,XB,CMER)
     WRITE(6,61) CMER,XMAX,YMAX,HEI,NN
  61 FORMAT(/1X,'CMER= ',F10.3,5X,'XMAX= ',F10.3,5X,'YMAX= ',F10.3,5X,
    *'NUMBER HEIGHT= ',F10.3,5X,'NUMBER OF REFERENCE POINTS= ',I3)
     WRITE(6,62) SCALE,XBLAD,XBLAM,XBLOND,XBLONM
  62 FORMAT(/1X,'SCALE= ',F10.5,5X,'LATITUDE= ',2F10.3,5X,'LONGITUDE= '
    *,2F10.3,5X,'--- EPICENTER MAP ORIGIN')
     WRITE(6,63) MAGC,DEPTHB,DEPTHT,NUMNUT,BDATE,EDATE
  63 FORMAT(/1X,'MAG CUT-OFF= ',F5.1,5X,'DEPTH RANGE=',F5.1,2X,'TO',2X,
    *F5.1,5X,'NUMNUTS=',I1,5X,'BDATE=',I10,5X,'EDATE=',I10)
     READ(5,41) RLADLH,RLAMLH,RLODLH,RLOMLH
     CALL UTMC(RLADLH,RLAMLH,RLODLH,RLOMLH,YC,XC,CMER)
     READ(5,41) RLADLL,RLAMLL,RLODLL,RLOMLL
     CALL UTMC(RLADLL,RLAMLL,RLODLL,RLOMLL,YD,XD,CMER)
     READ(5,41) RLADRH,RLAMRH,RLODRH,RLOMRH
     CALL UTMC(RLADRH,RLAMRH,RLODRH,RLOMRH,YE,XE,CMER)
     READ(5,41) RLADRL,RLAMRL,RLODRL,RLOMRL
     CALL UTMC(RLADRL,RLAMRL,RLODRL,RLOMRL,YF,XF,CMER)
  41 FORMAT(4F10.2)
     CALL PLOT(7.0,5.0,-3)
     I=0
  10 I=I+1
     READ(10,2) DATE,ORGHM,ORGS,LATND,LATNM,LONGWD,LONGWM,DEPTH,MAG,NO,
    *GAP,DMIN,RMS,ERH,ERZ,Q,M
   2 FORMAT(I6,1X,I4,1X,F5.2,1X,I2,1X,F5.2,1X,I3,1X,F5.2,2X,F5.2,3X,F4.
    *2,1X,I2,1X,I3,F5.1,3F5.2,1X,A1,I1)
  12 IF(DATE.EQ.999999) GO TO 46
  51 SLAD=FLOAT(LATND)
     SLND=FLOAT(LONGWD)
     CALL UTMC(SLAD,LATNM,SLND,LONGWM,YM,XM,CMER)
     IF(XM.LT.XC.OR.XM.GT.XF) GO TO 10
     IF(YM.GT.YC.OR.YM.LT.YF) GO TO 10
     IF(MAG.LT.MAGC) GO TO 10
     IF(DEPTH.GT.DEPTHB.OR.DEPTH.LT.DEPTHT) GO TO 10
     IF(DATE.LT.BDATE.OR.DATE.GT.EDATE) GO TO 10
     XM=(XM-XB)/SCALE
     YM=(YM-YB)/SCALE
     MAG=MAG/40.
     IF(MAG.LE.0.007) GO TO 30
     CALL SYMBOL(XM,YM,MAG,30,0.0,-2)
     MAG=(MAG*40.0)
     IF(NUMNUT.EQ.2) GO TO 10
     WRITE(6,5) I,DATE,ORGHM,ORGS,LATND,LATNM,LONGWD,LONGWM,DEPTH,MAG
   5 FORMAT(/1X,I5,2X,I6,2X,I4,2X,F5.2,2X,I2,2X,F5.2,2X,I3,2X,F5.2,2X,F
    *6.2,2X,F5.2)
     GO TO 31
  30 CALL SYMBOL(XM,YM,HEI,24,0.0,-2)
     MAG=(MAG*40.0)
     IF(NUMNUT.EQ.2) GO TO 10
     WRITE(6,9) I,DATE,ORGHM,ORGS,LATND,LATNM,LONGWD,LONGWM,DEPTH,MAG
   9 FORMAT(/1X,I5,2X,I6,2X,I4,2X,F5.2,2X,I2,2X,F5.2,2X,I3,2X,F5.2,2X,F
```

```
     *6.2,2X,F5.2)
   31 XM=XM
      IF(NUMNUT.EQ.2) GO TO 10
      CALL NUMBER(XM,YM,.07,FLOAT(I),0.0,-1)
      GO TO 10
   46 CONTINUE
      WRITE(6,8)
    8 FORMAT(/1X,'REFERENCE POINTS')
      DO 7 I=1,NN
      READ(5,6) REFLAD(I),REFLAM(I),REFLOD(I),REFLOM(I)
    6 FORMAT(4F10.2)
      WRITE(6,28) REFLAD(I),REFLAM(I),REFLOD(I),REFLOM(I),I
   28 FORMAT(/1X,'LATITUDE= ',2F10.3,10X,'LONGITUDE= ',2F10.3,5X,'REF-PT
     * NO.',I2)
      CALL UTMC(REFLAD(I),REFLAM(I),REFLOD(I),REFLOM(I),YM,XM,CMER)
      CALL CNVERT(XM,YM,XB,YB,SCALE)
      CALL SYMBOL(XM,YM,HEI,31,0.0,-2)
      XM=XM-1.2*HEI
      YM=YM-1.2*HEI
      CALL NUMBER(XM,YM,.07,FLOAT(I),0.0,-1)
    7 CONTINUE
      CALL SYMBOL(0.0,0.0,HEI,43,0.0,-2)
      CALL PLOT(0.0,0.0,999)
      STOP
      END
      SUBROUTINE CNVERT(XM,YM,XB,YB,SCALE)
      XM=(XM-XB)/SCALE
      YM=(YM-YB)/SCALE
      RETURN
      END
      SUBROUTINE UTMC(SLATD,SLATM,SLOND,SLONM,YS,XS,CMER)
C *** THIS SUBROUTINE CONVERTS THE LATITUDE AND LONGITUDE OF A POINT TO
C *** THE EQUIVALENT UNIVERSAL TRANSVERSE MERCATOR COORDINATES. LATITUDE
C *** AND LONGITUDE ARE GIVEN IN DEGREES AND MINUTES (SLATD AND SLATM,
C *** (SLOND AND SLONM) AND THE ANSWERS ARE GIVEN IN KILOMETERS (YS AND
C *** XS). WHERE YS IS THE NORTHING AND XS IS THE EASTING.  CMER IS THE
C *** ZONE CENTRAL MERIDIAN IN DEGREES.
     0CONSF(A)=(SIN (A)*.255239323E-8*(1.-.6768658E-2*SIN (A)**2)**2)/
     1 (3600.*COS (A))
      SLAT=SLATD+SLATM*1.666667E-2
      SLON=SLOND+SLONM*1.666667E-2
      DEGRAD = 0.174532925E-1
      RLAT=SLAT*DEGRAD
      ALOND=SLON-CMER
      ALON=ABS(ALOND)*3600.0
     EN=.63782064E7/SQRT (1.-.6768658E-2*SIN (RLAT)**2)
     S1=EN*COS(RLAT)*0.484813681E-5*(ALON-(ALON**3)*(3.9174E-12))
      SM=S1+S1**3/(6.0*EN*EN)
     SC=0.9996*SM
      SM=SM*SM
      P1=SLAT+CONSF(RLAT)*SM
      P2=SLAT+CONSF(P1*DEGRAD)*SM
      P3=SLAT+CONSF(P2*DEGRAD)*SM
      P3R=P3*DEGRAD                                                    UTM1230
         YS=((0.11113209E6*P3)-(0.16216944E5+SIN (2.0*P3R))+           UTM1240
     1(0.1720937E2*SIN (4.0*P3R)-(0.2273E-1*SIN (6.0*P3R))+            UTM1250
     2(0.33E-4*SIN (8.0*P3R))))*0.9996E-3                              UTM1260
      PRIMX=SC+SC**3*(1.0-.6768658E-2*SIN (RLAT)**2)**2/.2424369E15    UTM1270
      CONTINUE                                                         UTM1280
      IF(ALOND) 1,2,2                                                  UTM1290
    1 XS=(500000. + PRIMX)/1000.0                                      UTM1300
      RETURN                                                           UTM1310
```

```
      2 XS=(500000. - PRIMX)/1000.0                                    UTH1320
      3 RETURN                                                         UTH1330
        END                                                            UTH1340
```

EPPLOT BY ESTILL PRINTED 25 JUL 78 14:19:26

```
157.      20.       10.       0.1         4  3.0  200.0 00. 1
20.       00.       156.      30.       80.000          761010    771230
23.       00.       160.      00.
17.       00.       160.      00.
23.       00.       153.      00.
17.       00.       153.      00.
23.       00.       160.      00.
17.       00.       160.      00.
23.       00.       153.      00.
17.       00.       153.      00.
```

INPUT BY ESTILL PRINTED 25 JUL 78 14:19:26

```
$JOB EARTH 1514HRSO EZ TI=3600 LI=10000 PR=4
$AS 5=INPUT
$AS 10=HAWEQ
$$XEPPLOT
$$*BIGPLOT.P
$EOJ
```

EQJOB BY ESTILL PRINTED 25 JUL 78 14:19:26

3.4 Hypocenter Plotting Program: CROSEC

CROSEC is a program for plotting earthquake cross sections (Estill, M.S. Thesis). This program will sort earthquakes according to magnitude, location, depth, date and root-mean-square (RMS) solution criteria. This means that once an earthquake data file is established in HYPO71 output format, CROSEC can be used to sort events of interest from the earthquake file leaving the original file intact.

Using output from HYPO71, CROSEC sorts out earthquakes within a specified box, projects them along a line through the middle of that sorting box and plots a cross section. The location cards are read in only once but several sorts and cross sections can be made (Table 3.3). CROSEC can also be used as a sorting routine without cross section plots. Earthquake magnitudes are plotted with circles of increasing radius. An "X" is plotted when no magnitude is punched on the location card or when Mag = 0.0.

3.5 B-Value, Strain Energy and Seismic Moment Program: BVALVE

BVALVE is a Harris program written by the author for calculating B-values, strain energy and seismic moment. This program sorts earthquakes according to depth, magnitude, location and date before calculating b-value, energy and moment (Table 3.4). Using output location card format from HYPO71, BVALVE also lists number of events in each 0.1 magnitude range and calculates both cumulative b-value and b-value based on differential magnitude averaging increments.

TABLE 3.3

PROGRAM CROSEC INPUT

Input:

No. Cards	Format	Description
1	F5.1	Zone Central Merdian
1 through N card	HYPO-71 Output Cards	Earthquake Summary Cards
1	Blank Card	
1 (Parameter Card #1)	F5.1	Scale 1 = horizontal plot scale, KM/IN
	F5.1	Scale 2 = vertical plot scale, KM/IN
	F5.1	Width = of sorting box in (KM)
	F5.3	ACC = skips events with RMS>ACC
	F5.2	Size = usually 1.0, changes or magnitude scale size
	I1	I1 = set = 1 for plotting sequence numbers and event listing
	I1	I2 = set = 1 for sort only, no plot
	I1	I3 = set = 1 for sort only, no plot
	I1	I4 = set = 1 for sort and project, no plot
	I6	I5-I10 = no present meaning
	4X, F5.1	CMAG = magnitude cut-off

TABLE 3.3 (Continued) PROGRAM CROSEC INPUT

No. Cards	Format	Description
	4X, I6	BDATE = beginning date desired
	4X, I6	EDATE = ending date desired
	5X, F5.1	BDEPTH = bottom depth of earthquakes of interest in km
	1X, F5.1	TDEPTH = top depth of earthquakes of interest in km
1 (Parameter Card #2)	F5.2	LLAD = left point latitude, degrees
	F5.2	LLAM = left point latitude, minutes
	F5.2	LLOD = left point longitude, degrees
	F5.2	LLOM = left point longitude, minutes
	F5.2	RLAD = right point latitude, degrees
	F5.2	RLAM = right point latitude, minutes
	F5.2	RLOD = right point longitude, degrees
	F5.2	RLOM = right point longitude, minutes

TABLE 3.3 (Continued) PROGRAM CROSEC INPUT

1 Continuation Card -		leave blank and begin again with parameter card #1 to do an additional sort, or 999 in columns 1-3 will end program
Output options	:	Listing of Sorted Events
		Punched Cards of Sorted Events
		Cross-Section Plot
		Sorts according to magnitude, location, date and RMS

```
C *** CROSEC ***
      SPECIAL COMMON LOCTN,CONT
      COMMON/LOCTN/DATE(12000),ORCHM(12000),ORCS(12000),LATND(12000),
     1LATNM(12000),LONGWD(12000),LONGWM(12000),DEPTH(12000),AMAG(12000),
     2XM(12000),YM(12000)
      COMMON/PARA/SCALE1,SCALE2,WIDTH,I1,I2,I3,I4,I5,I6,I7,I8,I9,I10,CMA
     1G,BDATE,EDATE,SIZE,ACC,CMER,BDEPTH,TDEPTH
      COMMON/DIMG/X1,X2,Y1,Y2
      COMMON/CONT/NO(12000),IMAX,JMAX
      COMMON/LTH/AA
      COMMON/SURF/LLAD,LLAM,LLOD,LLOM,RLAD,RLAM,RLOD,RLOM
      REAL LLAD,LLAM,LLOD,LLOM
      INTEGER BDATE,EDATE
      CALL READEQ
   10 CALL INPUT
      CALL SORTEQ
      IF(I3.EQ.1) GO TO 30
      CALL PROJT
      IF(I4.EQ.1) GO TO 30
      CALL XSECT
   30 READ(5,40) IFLAG
   40 FORMAT(I3)
      IF(IFLAG.EQ.999) GO TO 50
      GO TO 10
   50 STOP
      END
      SUBROUTINE READEQ
      SPECIAL COMMON LOCTN,CONT
      COMMON/LOCTN/DATE(12000),ORCHM(12000),ORCS(12000),LATND(12000),
     1LATNM(12000),LONGWD(12000),LONGWM(12000),DEPTH(12000),AMAG(12000),
     2XM(12000),YM(12000)
      COMMON/PARA/SCALE1,SCALE2,WIDTH,I1,I2,I3,I4,I5,I6,I7,I8,I9,I10,CMA
     1G,BDATE,EDATE,SIZE,ACC,CMER,BDEPTH,TDEPTH
      COMMON/DIMG/X1,X2,Y1,Y2
      COMMON/CONT/NO(12000),IMAX,JMAX
      COMMON/SURF/LLAD,LLAM,LLOD,LLOM,RLAD,RLAM,RLOD,RLOM
      INTEGER DATE,ORCHM
      REAL ORCS,LATNM,LONGWM
      REAL LLAD,LLAM,LLOD,LLOM
      INTEGER BDATE,EDATE
      READ(5,11) CMER
   11 FORMAT(F5.1)
      I = 1
   21 CONTINUE
      READ(10,31) DATE(I),ORCHM(I),ORCS(I),LATND(I),LATNM(I),LONGWD(I),
     1LONGWM(I),DEPTH(I),AMAG(I)
   31 FORMAT(I6,1X,I4,1X,F5.2,1X,I2,1X,F5.2,1X,I3,1X,F5.2,2X,F5.2,3X,F4.
     12)
      IF(DATE(I).EQ.999999) GO TO 41
      SLAD = FLOAT(LATND(I))
      SLAM = LATNM(I)
      SLND = FLOAT(LONGWD(I))
      SLNM = LONGWM(I)
      CALL UTMC(SLAD,SLAM,SLND,SLNM,Y,X,CMER)
      XM(I) = X
      YM(I) = Y
      I=I+1
      GO TO 21
   41 IMAX = I-1
      RETURN
      END
```

```
      SUBROUTINE INPUT
      SPECIAL COMMON LOCTN,CONT
      COMMON/LOCTN/DATE(12000),ORGHM(12000),ORGS(12000),LATND(12000),
     1LATNM(12000),LONGWD(12000),LONGWM(12000),DEPTH(12000),AMAG(12000),
     2XM(12000),YM(12000)
      COMMON/PARA/SCALE1,SCALE2,WIDTH,I1,I2,I3,I4,I5,I6,I7,I8,I9,I10,CMA
     1G,BDATE,EDATE,SIZE,ACC,CMER,BDEPTH,TDEPTH
      COMMON/DING/X1,X2,Y1,Y2
      COMMON/CONT/NO(12000),IMAX,JMAX
      COMMON/SURF/LLAD,LLAM,LLOD,LLOM,RLAD,RLAM,RLOD,RLOM
      REAL LLAD,LLAM,LLOD,LLOM
      INTEGER BDATE,EDATE
      READ(5,12) SCALE1,SCALE2,WIDTH,ACC,SIZE,I1,I2,I3,I4,I5,I6,I7,I8,I9
     1,I10,CMAG,BDATE,EDATE,BDEPTH,TDEPTH
   12 FORMAT(3F5.1,F5.3,F5.2,10I1,4X,F5.1,4X,I6,4X,I6,5X,F5.1,1X,F5.1)
      READ(5,22) LLAD,LLAM,LLOD,LLOM,RLAD,RLAM,RLOD,RLOM
   22 FORMAT(8F5.2)
      CALL UTMC(LLAD,LLAM,LLOD,LLOM,Y1,X1,CMER)
      CALL UTMC(RLAD,RLAM,RLOD,RLOM,Y2,X2,CMER)
      WRITE(6,32) SCALE1,SCALE2,CMER,WIDTH,ACC,SIZE,I1,I2,I3,I4,I5,I6,I7
     1,I8,I9,I10,CMAG,BDATE,EDATE,BDEPTH,TDEPTH
   32 FORMAT(1H1,1X,'MAP SCALE = ',F5.1,'KM/IN ',5X,'DEPTH SCALE = ',
     1F5.1,'KM/IN ',5X,'CMER = ',F5.1,3X,'WIDTH = ',F5.1,3X,'RMS LT ',
     2F5.3,3X,/,1H ,' SIZE = ',F5.1,3X,'OPTIONS = ',10I1,3X,'CMAG= ',F5.
     11,3X,'BDATE= ',I6,3X,'EDATE= ',I6,3X,'BDEPTH= ',F5.1,3X,'TDEPTH= '
     2,F5.1)
      WRITE(6,42) LLAD,LLAM,LLOD,LLOM,Y1,X1,RLAD,RLAM,RLOD,RLOM,Y2,X2
   42 FORMAT(1H ,'LEFT POINT  = ',F4.0,F5.2,3X,F5.0,F5.2,2X,'OR ',F9.4,
     12X,F9.4,/,1H ,'RIGHT POINT = ',F4.0,F5.2,3X,F5.0,F5.2,2X,'OR ',
     2F9.4,2X,F9.4)
      RETURN
      END
      SUBROUTINE SORTEQ
      SPECIAL COMMON LOCTN,CONT
      COMMON/LOCTN/DATE(12000),ORGHM(12000),ORGS(12000),LATND(12000),
     1LATNM(12000),LONGWD(12000),LONGWM(12000),DEPTH(12000),AMAG(12000),
     1XM(12000),YM(12000)
      COMMON/PARA/SCALE1,SCALE2,WIDTH,I1,I2,I3,I4,I5,I6,I7,I8,I9,I10,CMA
     1G,BDATE,EDATE,SIZE,ACC,CMER,BDEPTH,TDEPTH
      COMMON/DING/X1,X2,Y1,Y2
      COMMON/CONT/NO(12000),IMAX,JMAX
      COMMON/SURF/LLAD,LLAM,LLOD,LLOM,RLAD,RLAM,RLOD,RLOM
      REAL LLAD,LLAM,LLOD,LLOM
      INTEGER DATE,ORGHM,BDATE,EDATE
      REAL ORGS,LATNM,LONGWM
      H=SQRT((Y2-Y1)**2)+((X2-X1)**2))
      CS=(X2-X1)/H
      SN=(Y2-Y1)/H
      XE=CS*X2+SN*Y2
      XB=CS*X1+SN*Y1
      YE=CS*Y2-SN*X2+WIDTH/2.
      YB=CS*Y1-SN*X1-WIDTH/2.
      WRITE(6,13)
   13 FORMAT(5X,'DATE',8X,'ORIGIN',7X,'LATITUDE',5X,'LONGITUDE',7X,'UTM-
     1N',9X,'UTM-E',7X,'DEPTH',5X,'MAG',6X,'RMS',6X,'ERZ')
      J=0
      DO 53 I=1,IMAX
      IF(DEPTH(I).LT.TDEPTH.OR.DEPTH(I).GT.BDEPTH) GO TO 53
      IF(AMAG(I).LT.CMAG) GO TO 53
      IF(DATE(I).LT.BDATE.OR.DATE(I).GT.EDATE) GO TO 53
      XSORT=CS*XM(I)+SN*YM(I)
      YSORT=CS*YM(I)-SN*XM(I)
```

```
      IF(XSORT.GT.XE.OR.XSORT.LT.XB) GO TO 53
      IF(YSORT.GT.YE.OR.YSORT.LT.YB) GO TO 53
   23 J =J+1
      DEPTH(J) = DEPTH(I)
      XM(J) = XM(I)
      YM(J) = YM(I)
      AMAG(J) = AMAG(I)
      NO(J)=I
      IF(I1.NE.1) GO TO 53
      WRITE(6,33)NO(J),DATE(I),ORGHM(I),ORGS(I),LATND(I),LATNM(I),
     1LONGWD(I),LONGWM(I),YM(I),XM(I),DEPTH(I),AMAG(I)
   33 FORMAT(1X,I5,1X,I6,5X,I4,1X,F5.2,5X,I2,1X,F5.2,5X,I3,1X,F5.2,
     13X,F9.4,5X,F9.4,5X,F5.2,5X,F4.2)
   53 CONTINUE
      JMAX = J
      RETURN
      END
      SUBROUTINE PROJT
      SPECIAL COMMON LOCTN,CONT
      COMMON/LOCTN/DATE(12000),ORGHM(12000),ORGS(12000),LATND(12000),
     1LATNM(12000),LONGWD(12000),LONGWM(12000),DEPTH(12000),AMAG(12000),
     2XM(12000),YM(12000)
      COMMON/PARA/SCALE1,SCALE2,WIDTH,I1,I2,I3,I4,I5,I6,I7,I8,I9,I10,CMA
     1G,BDATE,EDATE,SIZE,ACC,CMER,BDEPTH,TDEPTH
      COMMON/DING/X1,X2,Y1,Y2
      COMMON/CONT/NO(12000),IMAX,JMAX
      COMMON/SURF/LLAD,LLAM,LLOD,LLOM,RLAD,RLAM,RLOD,RLOM
      COMMON/LTH/AA
      REAL LLAD,LLAM,LLOD,LLOM
      INTEGER BDATE,EDATE
      WRITE(6,4)
    4 FORMAT(1X,'NO',5X,'DEPTH',10X,'UTM-N',9X,'UTM-E',5X,'PROJECTION DI
     1ST',7X,'DIST')
      SLOPE = (Y1-Y2)/(X1-X2)
      DO 24 I = 1, JMAX
      A = SLOPE/(1+(SLOPE)**2)
      X4 = A*(X1*SLOPE+XM(I)/SLOPE+YM(I)-Y1)
      Y4 = SLOPE*(X4-X1) + Y1
      PDIST = SQRT((X4-XM(I))**2+(Y4-YM(I))**2)
      DIST = SQRT((X4-X1)**2+(Y4-Y1)**2)
      XM(I)=DIST/SCALE1
      YM(I)=DEPTH(I)/SCALE2
   24 CONTINUE
      AA = SQRT((X1-X2)**2+(Y1-Y2)**2)
      AA = AA/SCALE1
      RETURN
      END
      SUBROUTINE XSECT
      SPECIAL COMMON LOCTN,CONT
      COMMON/LOCTN/DATE(12000),ORGHM(12000),ORGS(12000),LATND(12000),
     1LATNM(12000),LONGWD(12000),LONGWM(12000),DEPTH(12000),AMAG(12000),
     2XM(12000),YM(12000)
      COMMON/PARA/SCALE1,SCALE2,WIDTH,I1,I2,I3,I4,I5,I6,I7,I8,I9,I10,CMA
     1G,BDATE,EDATE,SIZE,ACC,CMER,BDEPTH,TDEPTH
      COMMON/DING/X1,X2,Y1,Y2
      COMMON/CONT/NO(12000),IMAX,JMAX
      COMMON/SURF/LLAD,LLAM,LLOD,LLOM,RLAD,RLAM,RLOD,RLOM
      COMMON/LTH/AA
      REAL LLAD,LLAM,LLOD,LLOM
      INTEGER BDATE,EDATE
      HEI = 0.15
       CALL MODE(0,1200,0,0)
```

```
      CALL PLOTS(0,0,0)
      CALL FACTOR(.6)
      CALL PLOT(1.0,15.,-3)
      CALL AXIS(0.,0.,'DEPTH(KM)',-9,10.,270.,0.0,SCALE2)
      CALL PLOT(0.,0.,3)
      CALL AXIS(0.0,0.0,'CROSS-SECTIONAL DISTANCE (KM)',29,AA,0.,0.0,SCA
     1LE1)
      CALL AXIS(AA,0.,'DEPTH(KM)',9,10.,270.,0.0,SCALE2)
      CALL PLOT(AA,-10.,3)
      CALL PLOT(0.,-10.,2)
      CALL PLOT(0.,0.,3)
      CALL NUMBER(0.,.5,.2,LLAD,0.,0)
      CALL NUMBER(1.2,.5,.2,LLAM,0.,2)
      CALL SYMBOL(2.4,.5,.2,'N',0.,1)
      CALL NUMBER(0.,.8,.2,LLOD,0.,0)
      CALL NUMBER(1.2,.8,.2,LLOM,0.,2)
      CALL SYMBOL(2.4,.8,.2,'W',0.,1)
      CALL PLOT(0.,0.,3)
      CALL NUMBER(AA,.5,.2,RLAD,0.,0)
      CALL NUMBER(AA+1.2,.5,.2,RLAM,0.,2)
      CALL SYMBOL(AA+2.4,.5,.2,'N',0.,1)
      CALL NUMBER(AA,.8,.2,RLOD,0.,0)
      CALL NUMBER(AA+1.2,.8,.2,RLOM,0.,2)
      CALL SYMBOL(AA+2.4,.8,.2,'W',0.,1)
      CALL PLOT(0.0,0.0,3)
      DO 26 I = 1, JMAX
      IF(AMAG(I).LT.0.00001.AND.AMAG(I).GT.-0.00001) GO TO 6
      AMAG(I)=(AMAG(I)/20.0)*SIZE
      CALL SYMBOL(XM(I),-YM(I),AMAG(I),30,0.0,-2)
      GO TO 16
    6 CALL SYMBOL(XM(I),-YM(I),0.21,24,0.0,-2)
C *** PLOTS INDEX NUMBERS
   16 IF(I1.NE.1) GO TO 26
      X = XM(I)+(HEI*1.3)
      Y = YM(I)+(HEI/3)
      FI=FLOAT(NO(I))
      CALL NUMBER(XM(I),-YM(I),0.08,FI,0.0,-1)
   26 CONTINUE
      CALL PLOT(0.0,0.0,999)
      RETURN
      END
      SUBROUTINE UTMC(SLATD,SLATM,SLOND,SLONM,YS,XS,CMER)
C *** THIS SUBROUTINE CONVERTS THE LATITUDE AND LONGITUDE OF A POINT TO
C *** THE EQUIVALENT UNIVERSAL TRANSVERSE MERCATOR COORDINATES. LATITUDE
C *** AND LONGITUDE ARE GIVEN IN DEGREES AND MINUTES (SLATD AND SLATM),
C *** (SLOND AND SLONM) AND THE ANSWERS ARE GIVEN IN KILOMETERS (YS AND
C *** XS). WHERE YS IS THE NORTHING AND XS IS THE EASTING.  CMER IS THE
C *** ZONE CENTRAL MERIDIAN IN DEGREES.
     @CONSF(A)=(SIN (A)*.255239823E-8*(1.-.6768658E-2*SIN (A)**2)**2)/
     1 (3600.*COS (A))
      SLAT=SLATD+SLATM*1.666667E-2
      SLON=SLOND+SLONM*1.666667E-2
      DEGRAD = 0.174532925E-1
      RLAT=SLAT*DEGRAD
      ALOND=SLON-CMER
      ALON=ABS(ALOND)*3600.0
     EN=.63782064E7/SQRT (1.-.6768658E-2*SIN (RLAT)**2)
     S1=EN*COS(RLAT)*0.484813681E-5*(ALON-(ALON**3)*(3.9174E-12))
      SH=S1+S1**3/(6.0*EN*EN)
     SC=0.9996*SM
      SM=SH*SM
      P1=SLAT+CONSF(RLAT)*SM
```

```
      P2=SLAT+CONSF(P1*DEGRAD)*SM
      P3=SLAT+CONSF(P2*DEGRAD)*SM
      P3R=P3*DEGRAD                                                    UTM1230
         YS=((0.11113209E6*P3)-(0.16216942E5+SIN (2.0*P3R))+           UTM1240
     1(0.1720937E2*SIN (4.0*P3R)-(0.2273E-1*SIN (6.0*P3R))+            UTM1250
     2(0.38E-4*SIN (8.0*P3R)))*0.9996E-3                               UTM1260
      PRIMX=SC+SC**3*(1.0-.6768658E-2*SIN (RLAT)**2)**2/.2424369E15    UTM1270
      CONTINUE                                                         UTM1280
      IF(ALOND)1,2,2                                                   UTM1290
    1 XS=(500000. + PRIMX)/1000.0                                      UTM1300
      RETURN                                                           UTM1310
    2 XS=(500000. - PRIMX)/1000.0                                      UTM1320
    3 RETURN                                                           UTM1330
      END                                                              UTM1340

CROSEC      BY ESTILL          PRINTED 25 JUL 78 14:19:26
```

```
157.
20.0  10.0 500.  0.5  1. 0000000000      0.0    010101    771212     200.0 0.00
21.0045.00158.015.0017.0000.00153.000.00
999

INPUTA      BY ESTILL          PRINTED 25 JUL 78 14:19:26
```

```
$JOB EARTHA 1514HRS0 EZ TI=7200 LI=15000 PR=4
$AS 5=INPUTA
$AS 10=HAWEQ
$$XCROSEC
$$*B1CPLOT.P
$EOJ

EQJOBA      BY ESTILL          PRINTED 25 JUL 78 14:19:26
```

TABLE 3.4

PROGRAM BVALVE INPUT

Input:

No. Cards	Format	Description
1	F5.1	CMER = Central meridian of area concerned in degrees
	F5.1	MAGC = magnitude cut-off
	F5.1	DEPTHB = lower hypocentral depth of interest
	F5.1	DEPTHT = upper hypocentral depth of interest
	I10	BDATE = beginning date
	I10	EDATE = ending date
	F10.2	DEC = magnitude averaging increment
1	4F10.2	RLADLH = upper left latitude, degrees
		RLAMLH = upper left latitude, minutes
		RLODLH = upper left longitude, degrees
		RLOMLH = upper left longitude, minutes
1	4F10.2	RLADLL = lower left latitude, degrees
		RLAMLL = lower left latitude, minutes
		RLODLL = lower left longitude, degrees
		RLOMLL = lower left longitude, minutes

TABLE 3.4 (Continued) PROGRAM BVALVE INPUT

No. Cards	Format	Description
1	4F10.2	RLADRH = upper right latitude, degrees
		RLAMRH = upper right latitude, minutes
		RLODRH = upper right longitude, degrees
		RLOMRH = upper right longitude, minutes
1	4F10.2	RLADRL = lower right latitude, degrees
		RLAMRL = lower right latitude, minutes
		RLODRL = lower right longitude, degrees
		RLOMRL = lower right longitude, minutes

Convention of left to right as one would read topographic map.

```
C **********  PROGRAM BVALVE(B-VALUES ,STRAIN ENERGY AND SEISMIC MOMENTS)
C
      DIMENSION RMAG(100),XLG(100),TNX(100),SUM(100)
      DIMENSION X(100),Y(100),A(100),B(100),C(100),D(100)
      DIMENSION TIT(100),CX(100),DY(100),CY(100),CA(100)
      DIMENSION CB(100),CC(100),CD(100)
      INTEGER DATE,ORGHM,GAP,BDATE,EDATE
      REAL LATNM,LONGWM,MAG,MAGC,MAGCC
      READ(5,1) CMER,MAGC,DEPTHB,DEPTHT,BDATE,EDATE,DEC
    1 FORMAT(4F5.1,2I10,F10.2)
      WRITE(6,63) MAGC,DEPTHB,DEPTHT,BDATE,EDATE,DEC
   63 FORMAT(/1X,'MAG CUT-OFF= ',F5.1,5X,'DEPTH RANGE= ',F5.1,' TO ',
     *2X,F5.1,5X,'BEGINNING DATE= ',I6,4X,'ENDING DATE= ',I6,5X,
     *'DEC= ',F10.2)
C
C **********  INPUT REFERENCE CORNERS OF SORTING BOX IN THIS ORDER
C **********  TOP LEFT,BOTTOM LEFT,TOP RIGHT,BOTTOM RIGHT IN MANNER
C **********  ONE WOULD READ TOPOGRAPHIC MAP(HI-MOM)
C
      READ(5,41) RLADLH,RLAMLH,RLODLH,RLOMLH
      WRITE(6,28) RLADLH,RLAMLH,RLODLH,RLOMLH
      CALL UTMC(RLADLH,RLAMLH,RLODLH,RLOMLH,YC,XC,CMER)
      READ(5,41) RLADLL,RLAMLL,RLODLL,RLOMLL
      WRITE(6,28) RLADLL,RLAMLL,RLODLL,RLOMLL
      CALL UTMC(RLADLL,RLAMLL,RLODLL,RLOMLL,YD,XD,CMER)
      READ(5,41) RLADRH,RLAMRH,RLODRH,RLOMRH
      WRITE(6,28) RLADRH,RLAMRH,RLODRH,RLOMRH
      CALL UTMC(RLADRH,RLAMRH,RLODRH,RLOMRH,YE,XE,CMER)
      READ(5,41) RLADRL,RLAMRL,RLODRL,RLOMRL
      WRITE(6,28) RLADRL,RLAMRL,RLODRL,RLOMRL
      CALL UTMC(RLADRL,RLAMRL,RLODRL,RLOMRL,YF,XF,CMER)
   41 FORMAT(4F10.2)
   28 FORMAT(/1X,'LATITUDE= ',2F10.3,10X,'LONGITUDE= ',2F10.3)
      JMAX=100
      DO 98 K=1,JMAX
      TNX(K)=0.0
   98 CONTINUE
      I=0
   10 I=I+1
      READ(10,2)DATE,ORGHM,ORGS,LATND,LATNM,LONGWD,LONGWM,DEPTH,MAG,NO,
     *GAP,DMIN,RMS,ERH,ERZ,Q,M
    2 FORMAT(I6,1X,I4,1X,F5.2,1X,I2,1X,F5.2,1X,I3,1X,F5.2,2X,F5.2,3X,F4.
     *2,1X,I2,1X,I3,F5.1,3F5.2,1X,A1,I1)
   12 IF(DATE.EQ.999999) GO TO 46
   51 SLAD=FLOAT(LATND)
      SLND=FLOAT(LONGWD)
      CALL UTMC(SLAD,LATNM,SLND,LONGWM,YM,XM,CMER)
      IF(XM.LT.XC.OR.XM.GT.XF) GO TO 10
      IF(YM.GT.YC.OR.YM.LT.YF) GO TO 10
      IF(MAG.LT.MAGC) GO TO 10
      IF(DEPTH.GT.DEPTHB.OR.DEPTH.LT.DEPTHT) GO TO 10
      IF(DATE.LT.BDATE.OR.DATE.GT.EDATE) GO TO 10
      MAGCC=MAGC-0.1
      RL=(MAG-MAGCC)/(0.1)
      L=IFIX(RL)
      TNX(L)=TNX(L)+1.0
C     WRITE(6,5) I,DATE,ORGHM,ORGS,LATND,LATNM,LONGWD,LONGWM,DEPTH,MAG
C    5 FORMAT(/1X,I4,2X,I6,2X,I4,2X,F5.2,2X,I2,2X,F5.2,2X,I3,2X,F5.2,2X,F
C     *6.2,2X,F5.2)
      GO TO 10
   46 CONTINUE
```

```
      WRITE(6,73)
   73 FORMAT(/,5X,'MAGNITUDE',10X,'NUMBER OF EVENTS',10X,'LOG NUMBER OF'
     *'EVENTS',10X,'LOG ENERGY(ERGS)',10X,'LOG SEISMIC MOMENT(DYNE-CM)')
      WRITE(6,74)
   74 FORMAT(//)
      IMAX=0
      DO 75 J=1,JMAX
      IF(TNX(J).LT.1.0) GO TO 77
      IMAX=IMAX+1
      XJ=FLOAT(J)
      TNX(IMAX)=TNX(J)
      RMAG(IMAX)=MAGCC+(0.1*XJ)
      XLG(IMAX)=ALOG10(TNX(IMAX))
      SLGEN=5.8+((2.4)*(RMAG(IMAX)))
      SLGSM=15.1+((1.7)*(RMAG(IMAX)-0.2))
      SLGEN=SLGEN+XLG(IMAX)
      SLGSM=SLGSM+XLG(IMAX)
      TOTSUM=TOTSUM+TNX(IMAX)
      TIT(IMAX)=TOTSUM
      TSLGEN=TSLGEN+(10.**SLGEN)
      TSLGSM=TSLGSM+(10.**SLGSM)
      WRITE(6,76) RMAG(IMAX),TNX(IMAX),XLG(IMAX),SLGEN,SLGSM
   76 FORMAT(5X,F10.2,10X,F10.2,10X,F10.2,25X,F10.2,15X,F10.2)
   77 IMAX=IMAX
   75 CONTINUE
      WRITE(6,101)
  101 FORMAT(//)
      TSLGEN=ALOG10(TSLGEN)
      TSLGSM=ALOG10(TSLGSM)
      WRITE(6,102) TSLGEN,TSLGSM
  102 FORMAT(/,5X,'TOTAL LOG ENERGY(ERGS) =',F10.2,10X,
     *'TOTAL LOG SEISMIC MOMENT(DYNE-CM)=',F10.2)
      WRITE(6,82)
   82 FORMAT(1H1,5X,'MAGNITUDE',10X,'CUMULATIVE NUMBER OF EVEMTS > M',
     *10X,'LOG CUMULATIVE NUMBER OF EVENTS > M')
      WRITE(6,83)
   83 FORMAT(//)
      DO 84 JM=1,IMAX
      CX(JM)=RMAG(JM)
      DY(JM)=TOTSUM-TIT(JM)
      IF(DY(JM).LT.1.00) GO TO 104
      CY(JM)=ALOG10(DY(JM))
  104 WRITE(6,103) CX(JM),DY(JM),CY(JM)
  103 FORMAT(5X,F10.2,15X,F10.2,35X,F10.2)
   84 CONTINUE
      DO 85 M=1,IMAX
      CA(M)=CX(M)*CY(M)
      CB(M)=CX(M)
      CC(M)=CY(M)
      CD(M)=CX(M)*CX(M)
      TOTCA=CA(M)+TOTCA
      TOTCB=CB(M)+TOTCB
      TOTCC=CC(M)+TOTCC
      TOTCD=CD(M)+TOTCD
   85 CONTINUE
      TOTCE=(TOTCB**2.0)/(IMAX)
      SLOPD=(TOTCA-((TOTCB*TOTCC)/IMAX))/(TOTCD-TOTCE)
      RINTD=(TOTCC/IMAX)-(SLOPD)*((TOTCB)/IMAX)
      YINTD=(SLOPD*MAGC)+RINTD
      XINTD=(-RINTD/SLOPD)
      DO 110 MJ=1,IMAX
      SUNY=((CY(MJ)-((SLOPD*CX(MJ))+RINTD))**2.0)+SUNY
```

```
  110 CONTINUE
      SDE=SQRT(SUNY/IMAX)
      WRITE(6,112) SLOPD,SDE
  112 FORMAT(//,5X,'CUMULATIVE B-VALUE=',F10.2,5X,
     * 'STANDARD ERROR = + OR -',F5.2)
      WRITE(6,113) YINTD,XINTD
  113 FORMAT(//,5X,'Y-INTERCEPT=',F10.2,5X,'X-INTERCEPT=',F10.2)
C     CALL MODE(0,1200,0,0)
C     CALL PLOTS(0,0,0)
      KMAX=0
      TOTALN=0.0
      TRLGEN=0.0
      TRLGSM=0.0
      WRITE(6,205)
  205 FORMAT(1H1,5X,'MAGNITUDE',10X,'NUMBER OF EVENTS',10X,
     *'LOG NUMBER EVENTS',10X,'LOG ENERGY(ERGS)',10X,
     *'LOG SEISMIC MOMENT(DYNE-CM)')
      WRITE(6,206)
  206 FORMAT(/)
      DO 201 L=1,JMAX
      RLMAG=MAGC+(FLOAT(L-1)*DEC)
      IF(RLMAG.EQ.RHMAG) RLMAG=RLMAG+0.01
      RHMAG=MAGC+(FLOAT(L)*DEC)
      IF(RHMAG.GT.7.5) GO TO 201
      DO 202 I=1,IMAX
      IF(RMAG(I).LT.RLMAG.OR.RMAG(I).GT.RHMAG) GO TO 202
      SUMM=SUMM+TNX(I)
      YY=ALOG10(SUMM)
      XX=(RLMAG+RHMAG)/(2.0)
  202 CONTINUE
      IF(SUMM.LT.1.0) GO TO 201
      KMAX=KMAX+1
      SUM(KMAX)=SUMM
      Y(KMAX)=YY
      X(KMAX)=XX
      RLGEN=5.8+((2.4)*(X(KMAX)))
      RLGSM=15.1+((1.7)*(X(KMAX)-0.2))
      RLGEN=RLGEN+Y(KMAX)
      RLGSM=RLGSM+Y(KMAX)
      TRLGEN=TRLGEN+(10.**RLGEN)
      TRLGSM=TRLGSM+(10.**RLGSM)
      WRITE(6,207) RLMAG,RHMAG,SUM(KMAX),Y(KMAX),RLGEN,RLGSM
  207 FORMAT(2X,F5.2,2X,'TO',F5.2,10X,F10.2,10X,F10.2,20X,F10.2,20X,
     *F10.2)
      SUMM=0.0
      YY=0.0
      XX=0.0
  201 CONTINUE
      TRLGEN=ALOG10(TRLGEN)
      TRLGSM=ALOG10(TRLGSM)
C **********LEAST SQUARES WITH VARIANCE ESTIMATE NOW PERFORMED**********
      IMAX=KMAX
      DO 86 J=1,IMAX
      A(J)=X(J)*Y(J)
      B(J)=X(J)
      C(J)=Y(J)
      D(J)=X(J)*X(J)
      TOTALA=A(J)+TOTALA
      TOTALB=B(J)+TOTALB
      TOTALC=C(J)+TOTALC
      TOTALD=D(J)+TOTALD
   86 CONTINUE
```

```
      TOTALE=(TOTALB**2.0)/(IMAX)
      SLOPE=(TOTALA-((TOTALB*TOTALC)/IMAX))/(TOTALD-TOTALE)
      RINTEC=(TOTALC/IMAX)-(SLOPE)*((TOTALB)/IMAX)
      YINTEC=(SLOPE*MAGC)+RINTEC
      XINTEC=(-RINTEC/SLOPE)
      DO 210 LJ=1,KMAX
      SUMY=((Y(LJ)-((SLOPE*X(LJ))+RINTEC))**2.0)+SUMY
  210 CONTINUE
      SE=SQRT((SUMY/KMAX))
      WRITE(6,92) SLOPE,SE
   92 FORMAT(///,5X,'B-VALUE = ',F10.2,5X,'STANDARD ERROR = + OR -',
     *F5.2)
      WRITE(6,93) YINTEC,XINTEC
   93 FORMAT(//,5X,'Y-INTERCEPT=',F10.2,5X,'X-INTERCEPT=',F10.2)
      WRITE(6,209) TRLGEN,TRLGSM
  209 FORMAT(//,5X,'TOTAL LOG ENERGY= ',F10.2,2X,'ERGS',5X,'TOTAL LOG OF
     * SEISMIC MOMENT= ',F10.2,2X,'DYNE-CM')
C **********NOW PLOT IT**** BRAH **********************
      STOP
      END
      SUBROUTINE UTMC(SLATD,SLATM,SLOND,SLONM,YS,XS,CMER)
C *** THIS SUBROUTINE CONVERTS THE LATITUDE AND LONGITUDE OF A POINT TO
C *** THE EQUIVALENT UNIVERSAL TRANSVERSE MERCATOR COORDINATES. LATITUDE
C *** AND LONGITUDE ARE GIVEN IN DEGREES AND MINUTES (SLATD AND SLATMD,
C *** (SLOND AND SLONMD AND THE ANSWERS ARE GIVEN IN KILOMETERS (YS AND
C *** XS). WHERE YS IS THE NORTHING AND XS IS THE EASTING. CMER IS THE
C *** ZONE CENTRAL MERIDIAN IN DEGREES.
     0CONSF(A)=(SIN(A)*.255239323E-8*(1.-.6768658E-2*SIN(A)**2)**2)/
     1 (3600.*COS(A))
      SLAT=SLATD+SLATM*1.666667E-2
      SLON=SLOND+SLONM*1.666667E-2
      DEGRAD=0.174532925E-1
      RLAT=SLAT*DEGRAD
      ALOND=SLON-CMER
      ALON=ABS(ALOND)*3600.0
     EN=.63782064E7/SQRT(1.-.6768658E-2*SIN (RLAT)**2)
     S1=EN*COS(RLAT)*0.484813681E-5*(ALON-(ALON**3)*(3.9174E-12))
      SM=S1+S1**3/(6.0*EN*EN)
     SC=0.9996*SM
      SM=SM*SM
      P1=SLAT+CONSF(RLAT)*SM
      P2=SLAT+CONSF(P1*DEGRAD)*SM
      P3=SLAT+CONSF(P2*DEGRAD)*SM
      P3R=P3*DEGRAD
         YS=((0.11113209E6*P3)-(0.162169442E5+SIN (2.0*P3R))+
     1(0.1720937E2*SIN (4.0*P3R)-(0.2273E-1*SIN (6.0*P3R))+
     2(0.33E-4*SIN (8.0*P3R))))*0.9996E-3
     PRIMX=SC+SC**3*(1.0-.6768658E-2*SIN (RLAT)**2)**2/.2424369E15
      CONTINUE
      IF(ALOND)1,2,2
    1 XS=(500000.+PRIMX)/1000.0
      RETURN
    2 XS=(500000.-PRIMX)/1000.0
    3 RETURN
      END
```

```
155.    2.0 42.5 37.5     010101     771231        0.1
          19.        30.       155.        20.
          19.        15.       155.        20.
          19.        30.       155.        10.
          19.        15.       155.        10.

INPUTB       PRINTED BY ESTILL            21 FEB 79 21:15:24


$JOB EARTHB 1514HRS0 EZ TI=7200 LI=15000 PR=15
$AS 5=INPUTB
$AS 10=HAWEQ
$$XBVALVE
$EOJ

EQJOBB       PRINTED BY ESTILL            21 FEB 79 21:15:24
```

BIBLIOGRAPHY

Anderson, D. L., Chemical plumes in the mantle, Geol. Soc. Am. Bull., 86, 1593-1600, 1975.

Ando, M. A., Source model of the M = 7.2 Kalapana earthquake of November 29, 1975, EOS Trans. Am. Geophy. Un., 57, 954, 1976.

Bessonova, E. N., V. M., Fishman, V. Z. Ryaboyi and G. A. Sitnikova, The Tau method for inversion of travel times--I. Deep seismic sounding data, Geophys. J. R. Astr. Soc., 36, 377-398, 1974.

Crosson, R. S., Velocity structure below the island of Hawaii from earthquake modeling, EOS Trans. Am. Geophy, Un., 57, 961, 1976.

Crosson, R. S. and D. B. Rogers, The Hawaii earthquake of November 29, 1975: Large scale horizontal block movement on a weak layer at depth?, 73 An. Meet. SSA (abs.); in Earthquake Notes, 49, 1, p. 37, 1978.

Decker, R. W., (unpublished text), Volcano Geophysics, 1978.

Dewey, J. F., Plate tectonics, Continents Adrift and Continents Aground, p. 34-35, 1976.

Dieterich, J. H. and R. W. Decker, Finite element modeling of surface deformation associated with volcanism, J. Geophy. Res., 80, 4094-4102, 1975.

Eaton, J. P., Crustal structure and volcanism in Hawaii, in The Crust of the Pacific Basin, Geophys. Monograph 6, pp. 13-29 American Geophysical Union, Washington, D. C., 1962.

Eaton, J. P., and J. Murata, How volcanoes grow, Science, 132, 925-938, 1960.

Ellsworth, W. L. and R. Y. Koyanagi, Three-dimensional crust and upper mantle structure of Kilauea Volcano, Hawaii, J. Geophys. Res., 82, 5379-5394, 1977.

Ellsworth, W. L., Mantle structure beneath the island of Hawaii: Evidence for a hot spot, 73 An. Meet. SSA (abs.); in Earthquake Notes, 49, 1, p. 68-69, 1978.

Endo, E. T., Focal mechanisms for the May 15-18, 1970, shallow Kilauea earthquake swarm, M. S. Thesis, San Jose State College, California, 1971.

Endo, E. T., and D. B. Rogers, Focal mechanisms for upper mantle earthquakes and flexure of the lithosphere near Hawaii, Bull. Seism. Soc. Am., in press, 1978.

Estill, R. E., Temporal variations of P-wave travel times and lateral velocity structure across the Wasatch Front, Utah, M. S. Thesis, University of Utah, 1976.

Estill, R. E. and M. E. Odegard, Hawaiian Ridge seismicity from the Makapuu ocean bottom seismograph, Geophys. Res. Lett., 5, 485-486, 1978.

Estill, R. E. and M. E. Odegard, Velocity structure of the southeastern Hawaiian Ridge using Tau inversion, J. Geophys. Res. (in press), 1978.

Furumoto, A. S., G. P. Woollard, J. F. Campbell, and D. M. Hussong, Variation in the thickness of the crust in the Hawaiian archipelago, in The Crust and Upper Mantle in the Pacific Area, Geophys. Monog. Ser., 12, ed., L. Knopoff, C. L. Drake and P. J. Hart, 94-111, AGU, Washington, D. C., 1968.

Furumoto, A. S., W. A. Wiebenga, J. P. Webb, and G. H. Sutton, Crustal structure of the Hawaiian archipelago, Northern Melanesia, and the Central Pacific basin by seismic refraction methods, Tectonophysics, 20, 153-164, 1973.

Furumoto, A. S., Prospects for geothermal energy on the island of Oahu, Hawaii, Geothermal Energy Magazine, vol. 4, no. 6, 7-25, 1976.

Gibowicz, S. J., Stress drop and aftershocks, Bull. Seism. Soc. Am., 63, 1433-1446, 1973.

Hill, D. P., Crustal structure of the island of Hawaii from seismic refraction measurements, Bull. Seism. Soc. Am., 59, 101-130, 1969.

Jackson, E. D., E. A. Silver, and G. B. Dalrymple, Hawaiian-Emperor chain and its relation to Cenozoic circum-Pacific tectonics, Geol. Soc. Am. Bull., 83, 601-617, 1972.

Jackson, E. D. and H. R. Shaw, Stress fields in central portions of the Pacific plate: Delineated in time by linear volcanic chains, J. Geophys. Res., 80, 1861-1874, 1975.

Jarrard, R. D. and D. A. Clague, Implications of Pacific island and seamount ages for the origin of volcanic chains, Rev. Geophys. Space Phys., 15, 57-76, 1977.

Klein, F. W., P. Einarsson, and M. Wyss, The Reykjanes Peninsula, Iceland, earthquake swarm of September 1972 and its tectonic significance, J. Geophys. Res., 82, 865-888, 1977.

Koyanagi, R. Y., H. L. Krivoy, and A. T. Okamura, The 1962 Kaoiki, Hawaii, earthquake and its aftershocks, Bull. Seism. Soc. Am., 56, 1317-1335, 1966.

Koyanagi, R. Y., Earthquakes from common sources beneath Kilauea and Mauna Loa volcanoes in Hawaii from 1962 to 1965, U. S. Geol. Survey Prof. Paper 600C, C120-C125, 1968.

Koyanagi, R. Y., and E. T. Endo, Hawaiian seismic events during 1969, U. S. Geol. Surv. Prof. Pap. 750-C, C158-C164, 1971.

Koyanagi, R. Y., Swanson, D. A., and E. T. Endo, Distribution of earthquakes related to mobility of the south flank of Kilauea volcano, Hawaii, U. S. Geol. Survey Prof. Paper 800-C, D89-D97, 1972.

Koyanagi, R. Y., E. T. Endo, and P. L. Ward, Seismic activity on the island of Hawaii, 1970 to 1973, in Geophysics of the Pacific Basin and its Margin, Geophys. Monog. Ser., 19, ed. by G. H. Sutton, M. H. Manghnani and R. Moberly, AGU, Washington, D. C., 1976.

Kroenke, L. W., Seismic reflection studies of sediment thickness around the Hawaiian Ridge, Pacific Sci., 19, 335-338, 1965.

Lee, W. H. K. and J. C. Lahr, HYP071: A computer program for determining hypocenter, magnitude, and first motion pattern of local earthquakes, open file report, U. S. Geol. Surv., Menlo Park, California, 1972.

Macdonald, G. A. and C. K. Wentworth, The Kona earthquake of August 21, 1951, and its aftershocks, Pacific Sci., 6, 269-287, 1952.

Macdonald, G. A., The south Hawaii earthquake of March and April, 1952, Volcano Letter, 515, 1-8, 1952.

Macdonald, G. A., The activity of Hawaiian volcanoes during the years 1951-1956, Bulletin Volcanologique, 22, 3-70, 1959.

Macdonald, G. A. and A. T. Abbott, Volcanoes in the Sea, The Geology of Hawaii, The University Press of Hawaii, p. 50, 380-408, 1970.

Macelwane, J. B. and F. W. Sohon, Theoretical Seismology, vol. I, p. 286, 1932.

McDougall, I., Volcanic island chains and sea-floor spreading, Nature Phys. Sci., 231, 141-144, 1971.

McKenzie, D. P. and N. O. Weiss, Speculations on the thermal and tectonic history of the earth, Geophys. J. Roy. Astron. Soc., 42, 131-174, 1975.

Menard, H. W., Marine Geology of the Pacific, 271 p., McGraw-Hill, New York, 1964.

Mogi, K., Some discussions on aftershocks, foreshocks, and earthquake swarms--the fracture of a semi-infinite body caused by an inner stress origin and its relation to the earthquake phenomena (3rd Paper), Bull. Earthquake Res. Inst. Tokyo Univ., 41, 615-658, 1963.

Moore, J. G. and P. K. Reed, Pillow structure of submarine basalts east of Hawaii, U. S. Geol. Survey Prof. Paper, 475-B, p. B153-157, 1963.

Moore, J. G., Giant submarine landslides on the Hawaiian Ridge, U. S. Geol. Survey Prof. Paper, 501-D, p. D95-D98, 1964.

Moore, J. G., Petrology of deep-sea basalt near Hawaii, Am. Jour. Sci., 263, 40-52, 1965.

Moore, J. G. and R. S. Fiske, Volcanic substructure inferred from dredge samples and ocean bottom photographs, Hawaii, Geol. Soc. Am. Bull., 800, 1191-1202, 1969.

Morgan, W. J., Convection plumes in the lower mantle, Nature, 320, 42-43, 1971.

Morgan, W. J., Plate motion and deep mantle convection, Geol. Soc. Am. Mem. 132, 7-22, 1972a.

Morgan, W. J., Deep mantle convection plumes and plate motion, Am. Assoc. Petrol. Geol. Bull. 56, 203-213, 1972b.

Parmentier, E. M., D. L. Turcotte, and K. E. Torrance, Numerical experiments on the structure of mantle plumes, J. Geophys. Res., 80, 4417-4425, 1975.

Pho, H. T. and L. Behe, Extended distances and angles of incidence of P waves, Bull. Seism. Soc. Am., 62, 885-902, 1972.

Richter, F. M., Convection and large scale circulation in the mantle, J. Geophys. Res., 78, 8735-8745, 1973.

Richter, F. M., and P. Parsons, On the interaction of two scales of convection in the mantle, J. Geophys. Res., 80, 2529-2541, 1975.

Ringwood, A. E., Composition and petrology of the Earth's mantle, 618 p., McGraw-Hill, New York, 1975.

Robson, G. R., K. G. Barr, and L. C. Luna, Extension failure: an earthquake mechanism, Nature, 218, 28-32, 1968.

Rogers, D. B., The Hawaii earthquake of November 29, 1975: Focal mechanism of associated events, M. S. Thesis, Univ. of Washington, 1978.

Ryall, A. and D. L. Bennett, Crustal structure of southern Hawaii related to volcanic processes in the upper mantle, J. Geophys. Res., 73, 4561-4582, 1968.

Scholz, C. H., The frequency-magnitude relation of microfracturing in rock and its relation to earthquakes, Bull. Seism. Soc. Am., 58, 399-415, 1968.

Shaw, H. R. and E. D. Jackson, Linear island chains in the Pacific: Result of thermal plumes or gravitational anchors?, J. Geophys. Res., 78, 8634-8652, 1973.

Shimozura, D., K. Kano, and W. T. Kinoshita, Volcanic tremor of Kilauea volcano, Hawaii, during July-December, 1963, Bull. Earthquake Res. Inst., Tokyo, 44, 1093-1133, 1966.

Stearns, H. T. and G. A. Macdonald, Geology and ground water resources of the island of Hawaii, 363 p., Hawaii Div. Hydrog., Bull., 9, Honolulu, 1946.

Sutton, G. H., Kasahara, J., Ichinose, W. N., and D. A. Byrne, Ocean bottom seismograph development at Hawaii Institute of Geophysics, Marine Geophys. Res., 3, 152-177, 1977.

Suyenaga, W., Isostasy and flexure of the lithosphere under the Hawaiian Islands, J. Geophys. Res., in press, 1978.

Swanson, D. A., Duffield, W. A., and R. S. Fiske, Displacement of the south flank of Kilauea Volcano: The result of forceful intrusion of magma into the rift zones, U. S. Geol. Survey Prof. Pap. 963, 39 p., 1976.

Turcotte, D. L. and E. R. Oxburgh, Mid-plate tectonics, Nature, 244, 337-339, 1973.

Unger, J. D. and P. L. Ward, Travel time delays and tectonic stress from a subcrustal Hawaiian earthquake (abs.), EOS Trans. Am. Geophys. Un., 56, 1150, 1974.

Walcott, R. I., Flexure of the lithosphere at Hawaii, Tectonophysics, 9, 435-446, 1970.

Walcott, R. I., Lithospheric flexure, analysis of gravity anomalies and the propagation of seamount chains, in Geophysics of the Pacific Basin and its Margin, Geophys. Monog. Ser., 19, ed. by G. P. Woollard, G. H. Sutton, M. H. Manghnani and R. Moberly, AGU, Washington, D. C., 1976.

Ward, P. L. and S. Gregersen, Comparison of earthquake locations determined with data from a network of stations and small tripartite arrays on Kilauea volcano, Hawaii, Bull. Seism. Soc. Am., 63, 679-711, 1973.

Watts, A. B. and J. R. Cochran, Gravity anomalies and flexure of the lithosphere along the Hawaiian-Emperor seamount chain, Geophys. J. R. Astr. Soc., 38, 119-141, 1974.

Wilson, J. T., A possible origin of the Hawaiian islands, Can. J. Phys., 41, 863-870, 1963.

Wood, H. O., On the earthquake of 1868 in Hawaii, Bull. Seism. Soc. Am., 4, 169-203, 1914.

Woollard, G. P., Evaluation of the isostatic mechanism and the role of mineralogic transformation from seismic and gravity data, Phys. Earth Planet. Interiors, 3, 484-498, 1970.